FLEXURAL BEHAVIOUR OF HIGH STRENGTH STEEL FIBRE NORMAL AND LIGHTWEIGHT CONCRETE BEAMS

by

©Mohamed Abdulhakim Zurgani, B.Sc.

A thesis submitted to the

School of Graduate Studies

in partial fulfillment of the requirement for the degree of

Master of Engineering

Faculty of Engineering & Applied Science

Memorial University of Newfoundland

May 2018

St. John's Newfoundland Canada

Abstract

An experimental study was conducted to investigate the flexural behaviour of high strength normal and lightweight reinforced concrete beams with steel fibres. Three different mixtures were developed for each type of concrete with three different steel fibre volume ratios. The target compressive strength was 85 MPa. Material and structural experimental programs were performed. In the material investigation, twenty four prisms with dimensions of 100 mm × 100 mm × 400 mm and one hundred and twenty cylinders with dimensions of 100 mm × 200 mm were cast, cured and tested to determine the mechanical properties for all different mixtures. The investigated mechanical properties included the compressive strength, splitting tensile strength, modulus of rupture and flexural toughness.

In the structural investigation, a series of six high strength lightweight aggregate (LWAC) concrete reinforced beams and six high strength normal weight (NWC) reinforced concrete beams were cast and tested. The beams were 200 mm × 400 mm × 3200 mm and were simply supported on a clear span of 2900 mm. The main variables in this study were the concrete type (normal weight concrete and light weight aggregate concrete), steel fibre volume ratio, (0 %, 0.375%, 0.75%), and the longitudinal reinforcement ratio, (0.85%, 1.50%). The structural behaviour of the test beams was examined in terms of load-deflection behaviour, steel reinforcement strain, concrete strain, crack pattern, crack width, crack spacing, mode of failure and ultimate moment capacity.

The test results revealed that the addition of steel fibres to high strength lightweight or normal weight concrete improved the mechanical properties. The compressive strength, splitting tensile strength and the modulus of rupture of fibrous LWAC and NWC concrete increased compared to the plain concrete.

Adding steel fibre to both high strength normal and lightweight concrete increased both cracked and un-cracked stiffness in addition to increasing the ultimate flexural capacity. The steel fibres also enhanced the cracking behaviour for both NWC and LWAC beams, reduced the crack widths and increased the number of the cracks for both type of concrete. The LWAC beams developed more cracks but less cracks width compared to their identical NWC beams. The ductility indexes of fibrous and non-fibrous NWC beams were higher than the ductility indexes measured for the corresponding LWAC beams.

For all fibre reinforced NWC and LWAC beams, CSA A23.3-14, ACI 318-08, EC2-04, and EC2-91 codes overestimated the maximum crack width due to the fact that these models do not consider the presence of steel fibres. The Rilem TC162-TDF was found to accurately predict the maximum crack width of fibrous NWC beams. However, the model was seen to be conservative when predicting the maximum crack width for fibrous LWAC beams.

Acknowledgement

I am deeply indebted to my thesis supervisor and research advisor Dr. Amgad Hussein, Head of Department of Civil Engineering at Memorial University of Newfoundland; grateful acknowledgment is due for his sincere support, valuable guidance, fruitful discussions, and comments throughout the courses of this study. I would like to thank him for giving me this great opportunity; it was a rewarding experience, both professionally and personally.

I would also like to thank the technical staff at the Civil Department Laboratory, especially Mrs. Shawn organ and Jason Murphy, who helped me a lot, made my work easier, and added pleasant moments in my work. I would also to like all my colleagues who helped me in the lab work.

Finally, my deepest appreciation goes to my family especially my mother for her continuous and unconditional support.

I dedicate this thesis to the memory of my late father; Engineer Abdulhakim Zurgani, who supported and encouraged me throughout his life and passed away while I was writing my thesis; I will miss you so much. You will be in my heart forever.

Table of Contents

List of Figures

List of Tables

Abbreviations

a/d	Shear span to depth ratio
A_{ceff}	Effective tension area, mm^2
As	Area of the steel reinforcement, mm^2
$A_{s,min}$	Minimum area of steel, mm^2
b_w	Minimum effective web width, mm
c	Depth of the neutral axis, mm
d	Effective depth, mm
d_b	Diameter of the steel bar, mm
d_f	Fibre diameter, mm
e	Distance from the extreme compression fibre to the top of the tensile stress block of fibrous concrete
E_c	Modulus of elasticity of concrete, MPa
f_c'	Concrete compressive strength, MPa
f_{ck}	Characteristic compressive cylinder strength
f_{ctm}	Mean value of axial tensile strength of concrete, MPa
f_s	Stress in the longitudinal reinforcement
f_r	Modulus of rupture, MPa
f_{sp}	Splitting tensile strength, MPa
f_y	Yield strength of the bars, MPa
F_{be}	Bond efficiency of steel fibres, MPa
G_m	Shear modulus of concrete matrix, MPa
h	Depth of the beam, mm
I_g	Cross sectional moment of inertia, mm^4
I_e	Average effective second moment of area, mm^4
k_1	A factor accounting for the bond characteristics
k_2	A Factor related to the strain shape in a concrete member
k_f	A factor accounting for fibre effectiveness due to the fibre aspect

	ratio
K_{cr}	Cracked stiffness, kN/mm
K_t	Un-cracked stiffness, kN/mm
l_f	Fibre length, mm
M_a	Applied moment, kN.m
M_{cr}	Cracking moment, kN.m
M_n	Ultimate moment capacity, kN.m
P_u	Ultimate applied capacity, kN
P_{cr}	First crack load, kN
r_f	Radius of fibres, mm
s_{avg}	Experimental average crack spacing between cracks, mm
s_{max}	Experimental maximum crack spacing between cracks, mm
s_m	Theoretical average crack spacing between cracks, mm
s_{min}	Experimental minimum crack spacing between cracks, mm
V	Fibre Volume Ratio, %
w	Factor to account for concrete density
w_{avg}	Average crack width, mm
w_{max}	Maximum crack width, mm
y_t	Distance from centroid to extreme tension fibre, mm
α_0	Orientation factor of steel fibres
α_1	Length efficiency factor of steel fibre
α_b	Bond efficiency factor of steel Fibres
α_f	Fibre aspect ratio
β	Factor for fibre shape and concrete type
ρ'	Compression steel reinforcement ratio
ρ_b	Balanced reinforcement ratio

$\rho_{s,eff}$	Effective reinforcement ratio of conventional reinforcement
σ_s	Stress in the tensile reinforcement calculated based on cracked section, MPa
σ_{sr}	Stress in tensile reinforcement under the first crack, MPa
σ_t	Post cracking tensile Resistance of fibres reinforced concrete, MPa
ε	Steel strain at stress f_s
ε_{cm}	Mean strain in concrete between cracks
ε_u	Concrete strain at ultimate load
$\varepsilon_s\left(fibres\right)$	Tensile strain for fibres
ε_{sm}	Mean strain in the reinforcement
φ_m	Mean moment-curvature
η_1	Reduction factor for lightweight concrete
ACI	American concrete institute
CEB-FIP	European committee for concrete
CSA	Canadian standard association
EC2	European code
RILEM TC 162-TDF	Test and design methods for steel fibre reinforced concrete
LVDT	Linear variable differential transformer

Chapter 1

Introduction

1.1 General

The definition of high strength concrete (HSC) is always changing due to the rapid development in concrete technology. Concrete that was known in the past 50 years as high strength is considered now as low strength . In the 1950s, concrete with a compressive strength of 30 MPa was considered as high strength concrete. By the end of the 1980s, concrete with a compressive strength of 100 MPa was produced and used in some practical constructions (Rashid and Mansur, 2009). The ACI committee 211 defines HSC as concrete that possesses a specified compressive strength of 42 MPa or higher. Other codes such FIP-CIB Model Code describes HSC concrete as the concrete that has a compressive strength of 60 MPa.

In terms of its high strength, many advantages can result from using HSC compared to conventional concrete. The use of HSC would result in reduced dimensions of compressed members such as columns and piles thus increasing usable floor space. Also, the use of HSC in buildings would cause reduced both the self-weight of the structure due to the reduction in both floor thickness and supporting members sections.

High strength concrete has a steeper descending stress-strain curve compared to normal strength concrete due to the quick drop in the compressive strength in the post-

peak load region leading to brittle mode of failure (Palmquist et al., 2001). Such a problem might affect the ductility of the high strength concrete.

In addition to the compressive strength, High Strength Concrete (HSC) has excellent durability characteristics in terms, of its low permeability, absorption, chloride ion permeability (RCPT), and high abrasion resistance, which makes it suitable for use in harsh environments. Hence, HSC is also referred to as High Performance Concrete (HPC). For the past four decades, HSC has been successfully used on a commercial scale in the construction of tall buildings, long span bridges, and marine and offshore structures.

Commercial demand for lighter weight concrete has increased in recent years. This is due to its inherent economy and advantages over conventional concrete in large structures. Light weight aggregate concrete (LWAC) reduces the dead weight of the structure and the strength-to-weight ratio compared to conventional normal weight concrete is advantageous. As a result of reduced weight of structure, the inertia force is decreased in seismic regions. Moreover, the use of LWAC has become economically feasible and provides advantages for offshore structures, floating offshore structures and temporary floating ground-based structures such as liquefied natural gas (LNG) terminals.

Other advantages of LWAC are improved durability properties, fire resistance and lower thermal conductivity compared to normal weight concrete. The major disadvantage of LWAC is increased brittleness compared to normal density concrete. On the structural

level, the use of LWAC will generally result in larger cracks, deformations, and lower ductility under similar loading conditions.

Due to the considerable improvement in concrete technology in recent years, the production of high strength light weight concrete with a compressive strength of more than 70 MPa has become practically possible. ACI committee 213R considers lightweight concrete to be high strength when the compressive strength is greater than 40 MPa. To produce different levels of high strength lightweight concrete, pozzolans such as (fly ash, silica fume, metakaolin, calcined clays, and shales) are used.

The design of reinforced concrete structures should meet the ultimate and serviceability limit states criteria. The ultimate limit state requires that a structure function without damage under the normal expected loads, and under abnormal (but probable overloads), including earthquake or extreme winds, the likelihood of collapse should be minimal. The serviceability limit states requires that under expected loads the structure perform satisfactorily with regard to its intended use, without discomfort to the user due to excessive deflection, dynamic effects (vibration, acceleration), or other similar ill effects.

In addition to meeting the limit states criteria, a structural engineer should also insure that the members exhibit adequate ductility under overload conditions. Ductility refers to the ability of structural members to withstand large deformation after the yielding of tensile reinforcement. The ductility of individual structural members, as well as that of an entire structure, becomes a major design consideration in earthquake regions.

Another serviceability criterion for a satisfactory structural design is to limit the cracks that form in concrete members to an acceptable width. The definition of what is acceptable depends on the intended use of the structure, the anticipated loading, and the environment to which it is exposed. In general, for a water-retaining concrete vessel or a foundation wall protecting a dry basement space, 0.5 mm cracks that allow water to seep through are not acceptable. However, the same cracks in a non-exposed beam within a building envelope may be permissible. Engineering judgment, durability requirements and experience should lead to a decision on the level of crack control that is necessary. On the other hand, satisfying the crack width and crack spacing requirements could be the dominant governing criteria in some structures such as marine and offshore structures. Guidelines are given by codes of practice for crack width and crack spacing requirements.

The known brittleness of LWAC compared to normal density concrete has limited the use of the material. Demands for energy dissipation and/or a controlled behaviour after failure may exclude LWAC as a preferred material. In addition, the use of high strength concrete in exposed structures is required to meet durability requirements.

The addition of steel fibres to high strength normal and light weight concrete is an attractive alternative that has been found to improve the performance of concrete. The real start in studying the potential of fibres as reinforcement was performed in early 1960s. Since that time, many experimental and theoretical investigations have been conducted to study the influence of different fibre characteristics and types on the behaviour of concrete (ACI committee 544.1R-96).

At the material level, Steel fibres work by increasing the tensile and flexure strength of concrete, and improve the toughness due to the enhancement of the post-crack behaviour. Using fibres also enhances the structural performance by improving the ductility, cracking, and enhancing the fatigue performance of high-strength LWAC. By limiting crack width and thus moisture ingress, the corrosion of the reinforcement and the resulting deterioration of the concrete can be avoided (Shah, 1991).

The addition of steel fibres was found to significantly improve the mechanical properties of high strength lightweight concrete (Jianming Gao et al., 1997). Steel fibres control both cracking and deflection at service loads since they resist the growth and the widening of the cracks through the birding action mechanism (Meda et al., 2012). The addition of steel fibre to reinforced concrete beams appears to increase both flexural and shear strength (Kima et al., 2016).

Fibres are effective in improving crack development of a concrete structural element, causing a higher number of cracks and consequently lower crack spacing values and narrower crack widths compared to the concrete matrix alone. This effect can be exploited to improve the design for durability requirements of concrete structures, especially those exposed to aggressive environments.

The current Canadian Design Codes CSA A23.3-14 do not have any design provisions for steel fibre reinforced concrete. The American Concrete Institute design code ACI 318 does not have any provisions either except for allowing the use of steel fibres as minimum shear reinforcement in normal strength normal weight reinforced

concrete beams. ACI 318-14 allows the use of fibres as minimum shear reinforcement for such beams provided that the beam height is less than 600 mm, the compressive strength is less than 40 MPa and the length-to-diameter ratio of the fibres is at least 50 mm and not exceeding 100 mm.

On the other hand, the European Codes have a more active approach towards developing design provisions for crack width and spacing in steel fibre reinforced concrete structural elements. This includes the recent development of the RILEM TC 162 TDF and the new MC2010. Nonetheless, those provisos were primarily developed for normal strength normal weight concrete. Hence, further validation of these code equations and models by experimental results is still needed especially for different types of concrete.

1.2 Research Scope and Objectives

In the current research, the structural behaviour of high strength steel fibre normal and lightweight aggregate reinforced concrete beams is investigated. To achieve this objective, twelve full scale beams were cast and tested. Three different parameters were under investigation in order to develop and improve current understanding of the effect of steel fibre on the structural behaviour of high strength normal and lightweight aggregate reinforced concrete beams in flexure. These parameters were the concrete type (normal weight concrete NWC and light weight aggregate concrete LWAC), steel fibre volume ratio (0%, 0.375%, 0.75%), and flexure reinforcement ratio (0.85%, 1.50%). Three different concrete mixtures with different steel fibre volume ratios were developed and used for each type of concrete to construct the test beams. For each type of concrete,

the beams were divided into two main groups, each with different reinforcement ratios. The material proportions used to make each concrete mixture were based on different trial mixtures that were first conducted in the concrete lab at Memorial. These trial mixtures covered many different proportion of cement, water, fine aggregate, coarse aggregate, steel fibre, superplasticizer and retarder. The mechanical properties of the chosen concrete mixtures, used to cast the test beams, were evaluated by conducting several tests which including the compressive strength, splitting strength, modulus of elasticity and modulus of rupture. All beams were tested in four loading points. Test data was recorded through a data acquisition system connected to a personal computer. All obtained data and observations were analyzed and then compared to results obtained by applying different code equations and different models presented by previous researchers.

The main objectives of this study are summarized as follows;

1. To investigate the flexural behaviour of steel fibre high strength normal and lightweight aggregate reinforced concrete beams in terms of deflection, ductility, stiffness, strain, and flexural capacity.
2. To assess the serviceability performance of steel fibre high strength normal and lightweight aggregate reinforced concrete beams in terms of cracking (crack width and crack spacing) and deflection behaviour.
3. To examine the design limits of the serviceability limit states for the beams based on the obtained results.

4. To add to the experimental data bank in the literature on steel fibre high strength normal and lightweight reinforced concrete beams, in order to will assist in improving the understanding of the behaviour of such beams.
5. To validate code equations and the models proposed by different committees and researchers for high strength normal and light weight concrete beams.

1.3 Thesis Outline

Chapter 1 presents a brief introduction on the high strength concrete and an overview on the research scope, objectives and outline of this study.

Chapter 2 contains the literature review of previous work on the mechanical and flexural behaviour of high strength normal and lightweight concrete with and without steel fibres. In addition, the current codes provisions available to predict the flexural capacity, crack width and crack spacing of reinforced concrete (RC) beams are presented.

Chapter 3 presents the material proportions, standard testing and mechanical properties of the concrete used to construct the test beams for this study.

Chapter 4 describes the experimental program. Details of the test setup, preparation of test specimens. The instruments used and testing procedure are also presented.

Chapter 5 presents the results and observations obtained from the experiments. These results covers the load-deflection behaviour, concrete and steel strains, flexural capacity, mode of failure, crack width and crack spacing. In this chapter, the experimental results are also compared to the predictions obtained from the codes and expressions identified in the literature in Chapter 2.

Chapter 6 presents the summary and conclusions drawn based on the experimental observation and codes validations.

Chapter 2

Literature Review

2.1 Introduction

This Chapter is divided into two parts: the first part presents a brief review of mechanical properties of steel fibre reinforced concrete, followed by relevant experimental investigations and research on high strength normal weight beams and normal strength light weight concrete beams. There are no studies published in the literature on steel fibre high strength light weight aggregate concrete beams in flexure. Hence, this topic is not covered in this review. The second part of the chapter presents the current codes provisions available in the literature covering the flexural capacity, crack width and crack spacing of flexure members.

2.2 Previous Experimental Investigations

2.2.1 Mechanical Properties of Steel fibre Concrete

2.2.1.1 High Strength Steel Fibre Normal Weight Concrete

The effectiveness of fibre inclusion in improving of mechanical performance of high strength normal and lightweight concrete was investigated by Balendran et al. (2001). The compressive strength of the concrete was varied 90 MPa to 115 MPa. Steel fibres with volume ratio of 1 % were utilized in this study. The test results showed that cylinder splitting tensile strength and modulus of rupture improved significantly with the steel fibre. However, insignificant impact was noticed on the compressive strength. The

enhancement of splitting tensile strength and modulus of rupture was more effective for lightweight aggregate concrete compared to normal weight concrete. Toughness was also investigated based on ASTM C1018. It was observed that the toughness index of lightweight fibre reinforced concrete was not influenced by the specimen size, whereas increasing the specimen size of normal weight concrete resulted in smaller toughness index for normal weight concrete.

Song and Hwang (2004) conducted an experimental study of the mechanical properties of high strength steel fibre reinforced concrete. Four steel fibre volume ratios were applied while holding the aspect ratio constant for all mixes. The fibre volume ratio varied between 0.5 % and 2 %, whereas the aspect ratio of the fibre was chosen to be 64, with fibre length of 35 mm and fibre diameter of 0.55 mm. The compressive strength of the mixes ranged between 85 MPa to 98 MPa. It was concluded that the addition of fibres improved the compressive strength of high strength concrete and reached its maximum effect when the fibre volume ratio was 1.5 % and then started slightly decreasing with additional steel fibre. Moreover, as steel fibre increased, both the splitting tensile strength and modulus of rupture effectively improved.

2.2.1.2 Normal Strength Steel Fibre Lightweight Concrete

Wang et al. (2012) conducted an experiment to evaluate the static and dynamic mechanical properties of steel fibre reinforced lightweight aggregate concrete. The study included five series of fibrous light weight concrete specimens with fibre volume ratios of 0 %, 0.5 %, 1.0 %, 1.5 %, and 2 %. For all mixes, the water cement ratio and the coarse to fine aggregate ratio were maintained consistent and equal to 0.42 and 1.3 respectively.

The addition of steel fibres was observed to slightly enhance the compressive strength of lightweight concrete. However, as the steel fibre volume ratio increased the tensile strength, flexure strength, and flexural toughness improved significantly. The impact resistance of lightweight concrete was also reported and it was evident that the usage of steel fibres improved in the impact strength. In general, the addition of steel fibres significantly improved the strength and fracture toughness of high strength light weight concrete. the authors also deduced that there was a logarithmic relationship between flexural toughness energy and impact energy of fibrous light weight concrete.

Li et al. (2016) investigated the influence of fibre content on the flexural properties of steel fibre lightweight aggregate concrete prisms. Four levels of fibre volume ratios between 0% to 2.5% were used with a constant fibre aspect ratio of 54. The maximum compressive strength reported in this study was 42.6 MPa. Based on the experimental observations, it was concluded that the workability of lightweight concrete was reduced due to the introduction of steel fibres. The addition of fibres seemed to increase the compressive strength and enhance the post cracking ductility of lightweight concrete. Moreover, the width of cracks in the aggregate-paste interface was less than the fibre-paste interface, and increasing steel fibre resulted in more voids between the fibres and the paste. Based on the findings, the authors recommended 2 % fibre content as the most effective in improving the flexural toughness of plain lightweight concrete.

2.2.1.3 High Strength Steel Fibre Lightweight Concrete

Gao et al. (1997) reported and investigated the mechanical properties of fibre high strength lightweight concrete with compressive strength up to 85.4 MPa. Three steel fibre

aspect ratios of 46, 58, and 70 were used. The volume fibre ratios were 0 %, 0.6 %, 1.0 %, 1.5 %, and 2 %. The results of compressive strength, tensile strength, flexural strength, modulus of elasticity and poisson's ratio tests are presented and discussed. The results show that the addition of steel fibres increase the compressive strength of high strength light weight concrete. Also, a significant increase in splitting tensile and flexural strength occurred due to the bridging effect of the steel fibres. The obtained splitting tensile strength ranged from 4.95 MPa to 8.8 MPa, while the flexural strength was rated between 6.2 MPa and 11.8 MPa.

The authors presented Figure 2.1 which shows typical load versus deflection curves for steel fibre high strength lightweight concrete prism with volume fibre ratios of 1 %, and 2 % and fibre aspect ratios of 70 and 58.

A significant increase in the flexural capacity occurred due to the inclusion of steel fibres. An increase of both the fibre volume ratio and the aspect ratio caused the deformation at the ultimate load to increase with a corresponding increase in the ultimate load and flexural fracture toughness.

The effect of steel fibres on the mechanical properties of high strength lightweight aggregate concrete was investigated by Kayali et al. (2003). The tested mechanical properties included compressive strength, indirect tensile strength, modulus of rupture, modulus of elasticity, stress–strain relationship and compression toughness. A total of 8 concrete mixtures with different steel fibre content were developed. The lightweight aggregate consisted of sintered fly ash with three different sizes. All tests were carried out according to ASTM standards. The maximum compressive strength was 72.5 MPa. It was noted that a significant increase in the indirect tensile strength, the modulus of

rupture, and the compression toughness was obtained, when the steel fibres were added. However, the addition of steel fibre appeared to slightly reduce the modulus of elasticity and altered the shape of stress-strain curve to be more curvilinear.

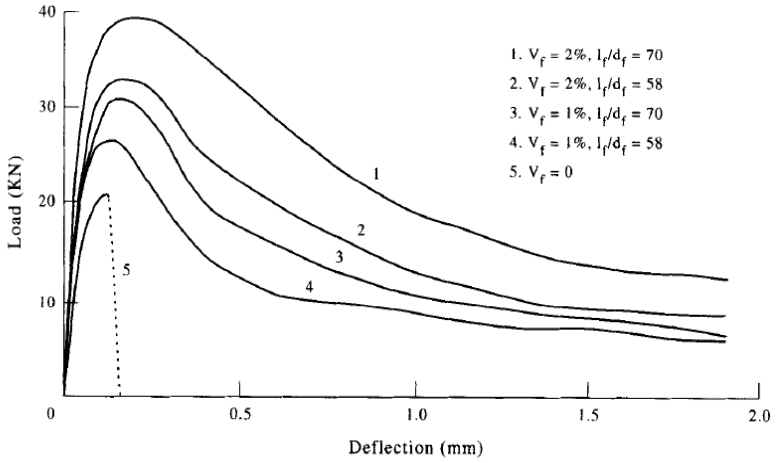

Figure 2.1: Typical Flexural Load-Deflection Curves of Steel Fibre High Strength Lightweight Concrete (Gao et al. 1997).

2.2.2 Flexural Behaviour of High Strength Reinforced Concrete Beams

A study was carried out by Ashour et al. (1998) to investigate the effects of compressive strength and reinforcement ratio on the flexural behaviour of high-strength concrete beams. The authors investigated nine high strength concrete beams with concrete compressive strength ranging from 48 MPa to 102 MPa. Three levels of longitudinal reinforcement ratios were used. It was concluded that the load at which the first crack happened, increased due to an increase in concrete compressive strength. Moreover, the measured cracking moment was compared to the theoretical cracking moment and it was

found that American code (ACI318-98) overestimated the cracking moment of the high strength concrete beams.

The response of high strength concrete beams in flexure was also investigated by Rashid and Mansur (2005). Sixteen beams with a cross section of 250 mm × 400 mm and clear concrete cover of 20 mm were tested. The beams were simply supported over a span of 3400 mm. Four different parameters were investigated. The parameters comprised the concrete compressive strength, longitudinal reinforcement, compressive reinforcement, and stirrup spacing. The concrete compressive strength varied between 42.8 MPa and 126.2 MPa and was the main parameter in this study. To obtain more reliable conclusions, the authors considered the results obtained previously by other investigators. It was concluded that ACI318 code was able to predict the cracking moment of high strength concrete beams. Furthermore, at an assumed service load that was defined as the ultimate load divided by 1.7, the ACI318-05 code underestimated the deflection of the high strength concrete beams. It was also noted that the maximum crack width increased when the compressive strength increased. It was further reported that the ductility of the beams was obtained due to an increase in the concrete compressive strength up to 105 MPa. However, a reduction in the ductility occurred when the compressive strength passed 105 MPa.

2.2.3 Flexural Behaviour of Normal Strength Steel Fibre Reinforced Concrete beams

The flexural behaviour of fibre reinforced concrete beams was investigated by Oh(1992). Nine beams with steel fibre volume ratio of 0 %, 1 %, 2 % were tested. The

steel fibre had a length of 40 mm and a diameter of 0.7 mm and thus the fibre aspect ratio was consistent for all beams and equal to 57. The test beams were categorized into three series, two of which were singly reinforced beams while the third series was of doubly reinforced beams. All beams had the same dimensions of 120 mm × 180 mm × 2000 mm and they were tested under four loading points with a clear span of 1800 mm. The compressive strength of each series were 40.3 MPa, 43 MPa, and 47.8 MPa respectively. It was reported that the ultimate moment capacity increased when the steel fibre volume increased. Moreover, increasing fibre volume enhanced both the ductility and energy absorption and the effect of fibre was more evident in beams with less longitudinal reinforcement. The cracking behaviour was also investigated of this study, and it was noted that the crack width and crack spacing decreased as a result of adding more steel fibres.

The author also suggested a model by which the bending capacity of fibrous singly and doubly reinforced concrete beam can be calculated, this model was as follows:

$$M_n = A_s f_y \left(d - \frac{a}{2}\right) + \frac{\sigma_t b \left(h - c\right)\left(h + c - a\right)}{2} + A_s^{'} \sigma_s^{'} \left(\frac{a}{2} - d'\right) \tag{2.1}$$

The position of neutral axis can be calculated by equating the internal forces shown in Figure 2.2, which would result in the next formula:

$$c = \frac{A_s f_y + \sigma_t b h}{0.85 \beta f_c^{'} b + \sigma_t b} \tag{2.2}$$

The post cracking tensile resistance of fibre reinforced concrete σ_t can be calculated as follows:

$$\sigma_t = 2\alpha_0\alpha_1\alpha_b\rho_f\tau\left(\frac{l_f}{d_f}\right) \tag{2.3}$$

where $\alpha_0\alpha_1\alpha_b$ are orientation factor, length efficiency factor, and bond efficiency factor of steel fibre, respectively. The orientation factor α_0 and the bond efficiency factor α_b are assumed to be roughly 0.41 and 1 respectively, whereas the length efficiency factor can be calculated by:

$$\alpha_1 = \frac{1-\tanh\frac{\beta l_f}{2}}{\frac{\beta l_f}{2}} \tag{2.4}$$

where

$$\beta = \sqrt{\frac{2\pi G_m}{E_f A_f\left(\frac{s}{r_f}\right)}}$$

$$s = 25\sqrt{\frac{l_f}{V_f d_f}}$$

where G_m is the shear modulus of concrete matrix, E_f is the elastic modulus, A_f is the and cross-sectional area of fibre, s is the average spacing of fibre, r_f is the radius of

fibre, V_f is the volume ratio of the fibre, d_f is the diameter of the fibre and l_f is the length of fibre.

Vandewalle (2000) conducted an experimental investigation and theoretical study on the crack behaviour of normal weight concrete beams with different fibre volume ratios and different fibre aspect ratios. Five beams with a concrete compressive strength of 42 MPa and dimensions of 200 mm × 350 mm × 3600 mm were tested. Fibre volume fraction of 0.38 %and 0.56 % with two aspect ratios of, l_f/d_f, 65/35 and 80/50 were utilized in this study. The author concluded that at the assumed service moment, no significant difference in the crack spacing can be found as a result of changing the test parameters. However, when the load exceeded the service load, increasing the aspect ratio decreased the crack spacing. Moreover, the crack width at the service moment was reduced to about 37 % when steel fibres were used. It was also reported that the effect of changing either the aspect ratio on fibre volume ratio had no clear influence on the crack width at the assumed service load. However, when exceeding the assumed service load and at higher moment values, increasing the aspect ratio resulted in a notable reduction in the crack width. Based on the results obtained from the experiment, the author proposed an equation to predictthe crack width for hooked end steel fibre reinforced members, as presented in Eq. 2.7. This formula was constructed and improved based on the EC2-91 code formula which is recommended to predict the crack spacing for members not containing steel fibres.

$$w_m = s_{rm} \cdot \varepsilon_{sm} \tag{2.7}$$

Where

$$s_{rm} = (50 + 0.25 \cdot k_1 \cdot k_2 \cdot d_b / \rho_r) \cdot \frac{50}{(L / d_f)} \qquad with \quad \frac{50}{(L / d_f)} \leq 1$$

$$\varepsilon_{sm} = \frac{\sigma_s}{E_s}\left(1 - \beta_1 \beta_2 \left(\frac{\sigma_{sr}}{\sigma_s}\right)^2\right)$$

where s_{rm} is the average final crack spacing between cracks, ε_{sm} is the mean strain in the tension reinforcement, k_1 is taken as 0.8 for high bond bars, k_2 is equal to 0.5 for a member subjected to pure moment, σ_s is the stress in the reinforcement calculated based on cracked section analysis, σ_{sr} is the stress in the reinforcement at first crack, E_s is the modulus of elasticity of the longitudinal reinforcement, β_1 is a coefficient taken as 1.0 for high bond bars and β_2 is a coefficient related to the loading duration and taken as 1.0.

The steel fibre contribution to the flexural behaviour of seven reinforced concrete beams was investigated by Meda et al. (2012). Beams behaviour at both the ultimate and serviceability limit state was the focus of the study, particularly the effect of fibres on ductility, crack width and tension stiffening. The test beams had a dimensions of 200 mm × 300 mm × 4000 mm with a clear span of 3600 mm. Beams were reinforced against shear failure with leg stirrups distributed outward from the constant moment zone at constant spacing of 100 mm. The cylinder concrete strength varied from 33.5 MPA to 45.5 MPa. Two longitudinal reinforcement ratios of 0.75 % and 1.5 % were considered. Steel fibres with constant aspect ratio of 50 were used and added to mixes in two different quantities 30 kg/m^3 and 60 kg/m^3. All beams were tested under four point loading. The

obtained results showed that the use of fibres influenced the initial failure mode of the beams where steel fibres caused the longitudinal reinforcement to rupture instead of crushing the concrete. In addition, the increase of fibre content reduced the ductility of the beams which was attributed to the strain concentration in the steel bars. The ultimate moment did not show any significant increase due to the usage of fibres. Furthermore, fibrous beams with high longitudinal reinforcement did not undergo any sudden crushing in the concrete. the crack width and crack spacing were not investigated in the study.

Shaoo and Sharma (2014) conducted an experiment on the effect of steel fibre content on the behaviour of concrete beams with and without stirrups. Twelve reinforced concrete beams with steel fibre were tested to study both shear and flexural response under monotonic loadings. Beams had dimensions of 150 mm × 300 mm × 2100 mm over a clear span of 1800 mm. End-hooked steel fibre was used in the this study with fibre aspect ratio of 80 slenderness and volume ratio ranging between 0.0 % and 1.5 %. Three levels of reinforcement ratio were applied, these levels were 0.87 %, 1.15 %, and 1.95 %. The compressive strength of the test beams varied between 19.1 MPa and 32.9 MPa. It was concluded that flexural strength and ductility increased when steel fibres were added. However, when fibre volume fraction exceeded 0.5 %, further increase in flexural strength was not notable.

Deluce et al. (2013) proposed a new model (Eq. 2.8 and Eq. 2.9) for the calculation of crack spacing and crack width in reinforced concrete members with steel fibres. The model was developed to account for the effect of different steel fibre aspect ratios and different tensile reinforcing steel ratios. The author conducted an experimental

program on specimens subjected to direct tension. Results of crack spacing and crack width for 17 plain reinforced concrete and 53 steel fibrous specimens are compared to those predicted by the proposed models. It is concluded that the proposed models are adequate in predicting the crack spacing and crack width for fibre reinforced concrete beams. It is also claimed that the model performance is better than other currently available models. The proposed Eq. 2.8 for average crack spacing calculation was developed based on the CEB-FIP 1978 crack spacing formula.

$$s_m = 2\left(c + \frac{s_b}{10}\right)k_3 + \frac{k_1 k_2}{s_{mi}} \tag{2.8}$$

$$w_{cr,avg} = s_m \cdot \varepsilon_{t,avg} \tag{2.9}$$

where

$$s_b = 0.5\sqrt{\frac{\pi d_b^2}{\rho_{s,eff}}} \le 15 d_p$$

$$s_{mi} = \frac{\rho_{s,eff}}{d_p} + k_f \frac{\alpha_f V_f}{d_f}$$

$$k_3 = 1 - \frac{\min(V_f, 0.015)}{0.015}\left(1 - \frac{1}{k_f}\right)$$

$$k_f = \frac{l_f}{50 \cdot d_f} \ge 1.0$$

where s_m is the average crack spacing, $w_{cr,avg}$ is the average crack width, c is the concrete cover, d_b is the bar diameter, $\rho_{s,eff}$ is the effective reinforcement ratio of conventional reinforcement, k_3 is a fibre content factor, k_1 is a factor accounting for the bond characteristics and is taken as 0.4 for deformed bars, k_2 is a factor related to the strain

shape in a concrete member and is taken as 0.25 in case of uniaxial strain condition, k_f is a factor accounting for fibre effectiveness due to the fibre aspect ratio, α_f is the fibre aspect ratio, l_f is the fibre length and d_f is the fibre diameter.

2.2.4 Flexural Behaviour of High Strength Steel Fibre Reinforced Concrete beams

To account for high strength concrete, Imam et al. (1995) modified the ACI 544 equation, which was developed for predicting the flexure capacity of fibrous reinforced normal strength concrete beams. The verification of the modified ACI544 equation was done by utilizing available experimental data collected by the authors, in addition to the results obtained by testing 16 high strength reinforced concrete beams with compressive strength of 110 MPa. The modified equation was improved by changing the tensile stress of steel fibre concrete coefficient from 0.00772 to 0.002 to account for higher fibre- high strength concrete bond. This new coefficient represents bond strength of 4.15 MPa, whereas the previous coefficient of 0.00772 which is allocated for normal strength concrete represents a bond strength of 2.3 MPa. Figure 2.2 shows the simplified stress diagram along with the strain diagram of fibrous reinforced concrete section presented by the authors.

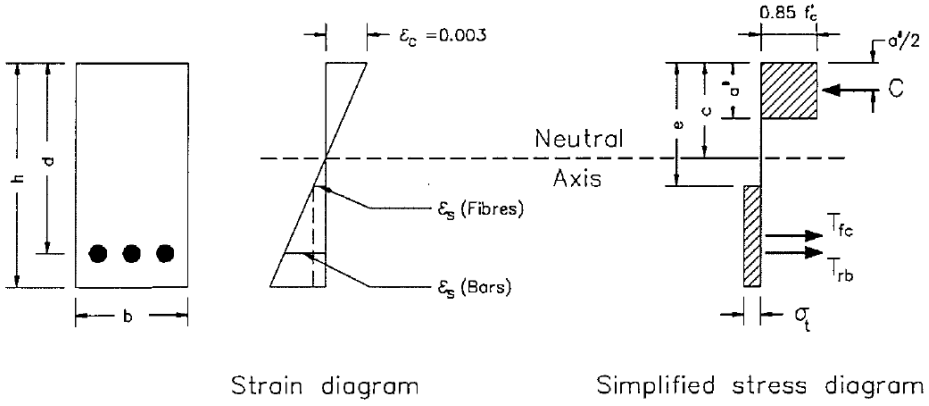

Figure 2.2: Stress and Strain Diagram of Fibrous Reinforced Concrete Section.

The modified equation suggested to calculate the nominal capacity of high strength reinforced concrete beams with a rectangular cross-section was given as follows:

$$M_n = \frac{1}{2}\rho f_y b d^2 (2-\eta) + 0.83 F b d^2 (0.75-\eta)(2.15+\eta) \tag{2.5}$$

where

$$\eta = \frac{a'}{d} = \frac{\rho f_y + 2.32F}{0.85 f_c^{'} + 3.08F}$$

$$\sigma_t = 2.0F$$

$$F = (L_f / D_f) V_f d_f$$

An experimental investigation associated with the effect of steel fibre on the shear resistance of reinforced concrete beams was conducted by Khuntia et al (1999). The next

simplified formula (2.6) was suggested by the authors to be used to calculate the post cracking tensile resistance of steel fibre reinforced concrete σ_t.

$$\sigma_t = 0.28F\sqrt{f_c'} \tag{2.6}$$

Where

$$F = v_f \frac{l_f}{d_f}\beta$$

Where β is the shape factor which is assumed to be 1 for normal weight concrete, and v_f is the volume of fibre in percentage.

Chunxiang et al. (1998) conducted an experiment to evaluate the properties of high-strength steel fibre reinforced concrete beams in bending. Ten beams were fabricated and cast with concrete that had a compressive strength fluctuating between 72.8 MPa to 92.2 MPa. The cross section of the beams was selected to be 120 mm × 150 mm whereas the support length for the beams was 2000 mm. Three different fibre aspect ratios were investigated. The fibre volume ratio was 1 %. The aspect ratios were 38, 45, and 46. Three of the beams were reference specimen without fibres. The authors concluded that the flexural rigidity of the beams increased before the yielding stage due to the addition of steel fibres. Furthermore, the increase in the rigidity mainly depended on the fibre aspect ratios, where the smaller fibre resulted in improving stiffness of the beams. It was also concluded that the displacement of the fibrous beams at failure increased compared to the reference beams.

A study of flexural cracking behaviour of normal strength, and high strength steel fibre concrete beams, using the Digital Image Correlation technique was conducted by Harmrat et al. (2015). The study focused on the crack behaviour of different normal weight concrete types. The authors also evaluated the accuracy of different codes in evaluating the crack width. Nine beams were divided into three groups based on the compressive strength and fibre content. Group one comprised three normal strength concrete beams with a compressive strength of 44 MPa. Group two had three fibre reinforced beams with a high compressive strength of 78 MPa, whereas group three consisted of three beams with high a compressive strength of 85 MPa. Steel fibre with a length of 40mm and an aspect ratio of 80 was added to the mix that was used to cast the second group with steel volume ratio of 0.5 %. Three longitudinal reinforcement areas were used for each group, those areas were 157 mm^2, 226 mm^2, and 308 mm^2. It was concluded that the addition of steel fibres increased the first cracking load by 10 % to 25 % of the ultimate load. Furthermore, a reduction of 35 % to 70 % occurred in final average crack spacing and crack width at assumed service load. The beams were 100 mm × 160 mm × 1500 mm, tested using four points loading over a span of 1300 mm. It was also noted that predicting crack width using BS8110 and Eurocode EC2-04 formulas was found to be acceptable for all beams without steel fibre.. The beams tested in the study are more representative of a material level than a structural one due to the small depth of the specimen. Moreover, there appears to be an error in the load versus crack width plots as they used the actuator load rather than the support reaction. Good predictions were

obtained when applying RILEM TC-162-TDF crack width model to fibrous concrete beams.

2.2.5 The Flexural Behaviour of Normal Strength Reinforced Lightweight Concrete beams

Wu et al. (2011) tested six beams to study the flexural behaviour and size effect of lightweight aggregate concrete beams. The longitudinal reinforced ratio ρ varied between 0.33% to 1.3%. Beams were fabricated and cast with different dimensions and constant concrete compressive strength of 34 MPa. Six beams were tested. Beams had a depth that varied from 400 mm to 700 mm. It was concluded that lightweight concrete beams exhibited similar flexural capacity to their corresponding normal weight concrete beams. Nonetheless, lightweight concrete beams displayed higher deflection compared to normal weight concrete beams. The test results revealed that increasing the depth of the beams from 400 mm to 700 mm resulted in a decrease in the ultimate capacity ratio. That indicates a size effect due to the increase in the beam depth. Moreover, the authors compared the experimental deflection at assumed service load to that calculated using ACI 318 code and indicated that the ACI 318 code underestimates the service deflection for both normal and lightweight concrete.

2.2.6 The Flexural Behaviour of High Strength Reinforced Lightweight Concrete beams

The flexural behaviour of reinforced high strength lightweight concrete beams was investigated by Shuaib and Baker (1991). This study was performed by testing six singly reinforced beams over a length of 3.45 m. The compressive strength of the beams

varied between 39.9 MPa to 75.9 MPa, and the longitudinal reinforcement ratio to balanced reinforcement ratio ρ / ρ_b , ranged from 0.18 to 0.54. All beams were 152.4 mm wide and 304.8 mm deep, the effective depth varied between 228.4 mm and 260.4 mm. It was concluded that for low reinforcement ratio ρ, which was between 0.01 to 0.025, increasing ρ caused a notable reduction in the displacement ductility. However, after exceeding reinforcement ratio of 0.025, the displacement ductility continued to slightly decrease until it became insignificant at higher levels of reinforcement. It was also noted that for reinforcement steel ratio ρ / ρ_b less than 0.5, the increase in compressive strength decreased the displacement ductility index. Moreover, beams with a compressive strength of 75.9 MPa displayed insufficient ductility of less than three, when the reinforcement ratio ρ / ρ_b was 0.24. The author also compared the ultimate moment capacity obtained experimentally to that predicted using the ACI318 code. It was concluded that the code gave a conservative prediction of the ultimate flexural capacity for the lightweight concrete beams with compressive strength not exceeding 75.9 MPa and ρ / ρ_b not greater than 0.54. It was also found that the strain value of 0.003 recommended by the ACI318 code seemed to be acceptable for high strength lightweight concrete with a compressive strength less than 75.9 MPa.

Shuaib and Batts (1991) conducted an experiment to evaluate the flexural behaviour of doubly reinforced high-strength lightweight concrete beams with web reinforcement. Two main variables were investigated in this study, compressive strength and the longitudinal reinforcement ratio to balanced reinforcement ratio, ρ / ρ_b . The

compressive strength varied between 46.2 MPa to 76.3 MPa, whereas the tensile steel ratio, ρ / ρ_b ranged between 0.16 to 0.47. Six doubly reinforced beams with a cross section of 152.4 mm × 304.8 mm and a length of 3.6 m were investigated. It was concluded that when increasing the compressive strength, the displacement ductility index decreased. However, after the ρ / ρ_b ratio exceeded 0.22, it seemed that the compressive strength had no influence on the ductility. It was further reported that the ACI318 rectangular stress block underestimated the flexural capacity for high strength lightweight concrete beams. Hence, it was considered safe to estimate the flexural capacity using ACI318 code. Ultimate compressive strain in the concrete was also investigated. The obtained results indicated that the strain of 0.003 recommended by ACI318 code seemed to be acceptable for doubly reinforced high strength lightweight concrete beams with compressive strength not exceeding 75.9 MPa.

The flexural behaviour of lightweight aggregate concrete (LWAC) beams was investigated by Sin (2011). Eighteen beams with dimensions of 150 mm × 300 mm × 3100 mm were tested. The beams were simply supported over a span of 2.8 m. Three normal weight concrete (NWC) beams were added as reference specimen . Five parameters were examined and the test beams were categorized into five groups. Only one parameter was changed at a time, whereas all other parameters were kept constant. The vareid parameters were compressive strength, longitudinal reinforcement in compression and tension zone, transverse reinforcement and total perimeter of flexural reinforcement. The compressive strength varied from 20 MPA to 80 MPa, whereas the reinforced steel ratios were 0.67 %, 1.02 %, 1.45 %, 1.61 % and 2.22 %. Four levels of

compression reinforcement ratio were used, these levels were 0 %, 0.43 %, 0.73 %, and 1.11 %. In the flexure zone, the authors varied the amount of transverse reinforcement in order to investigate their effect of the confinement of the compression reinforcement on the beams ductility. The spacing between the stirrups ranged from 50 mm to 180 mm. Three different bars with diameters of 13 mm, 16 mm, and 20 mm were used. It was observed that all beams failed in flexure mode where the steel yielded first followed by crushing of the concrete zone.

The authors concluded that the number of cracks of LWAC beams at the assumed service load was higher than the number of cracks in the identical NWC beams. The assumed service load was defined as the ultimate load divided by 1.6. It was also noted that the maximum crack width in LWAC beams is less than that in NWC beams. The deflection of the LWAC beams in comparison with LWAC beams was also studied. It was found that the LWAC beams had higher deflection compared to the NWC beams. However, the test results reveals that LWAC beam with compressive strength of 79 MPa had 9 % lower deflection than its corresponding NWC beams. The moment capacity of the LWAC beams appeared to be identical to the NWC beams. However, LWAC beams showed less curvature ductility than NWC beams.

A study was conducted by Almousawi (2011) to evaluate lightweight concrete beams in flexure. The author tested fourteen lightweight beams with a cross section of 200 mm × 300 mm, and with a length of 3600 mm. Three different parameters were investigated; the compressive strength, flexural reinforcement ratio, and compression steel reinforcement ratio. The concrete compressive strength varied between 50.9 MPa to 68.5 MPa. The conclusion was that the ultimate load capacity of beams increased as a

result of increasing the compressive strength. Moreover, increasing either longitudinal tensile reinforcement ratio, ρ, or compression reinforcement ratio, ρ', resulted in an increase in the ultimate load. The displacement ductility of the beams was also measured It was found that, contrary to the increase in the compression steel reinforcement ratio, the increase in either compressive strength or tensile reinforcement ratio led to a decrease in the ductility of the beams.

Carmo et al. (2012) investigated and reported the influence of both concrete strength and transverse confinement on bending behaviour of reinforced LWAC beams in terms of strength and ductility. The study focused on three issues, mainly on the theoretical pure bending area, and partially on the cracking stage and the plastic stage. The authors tested thirteen LWAC beams with dimension of 120 mm × 270 mm × 3000 mm, these beams were simply supported over a length of 2800 mm. Beams were divided into three different groups in order to investigate the influence of each parameter. The first group was established to study the effect of varying the tensile reinforcement ratio ρ, which was varied between 0.55 % and 2.96 %. The second group was to study the influence of the transverse reinforcement ratio A_{sw}/s at the constant moment zone, this group was composed from six beams. Three different transverse reinforcement ratios A_{sw}/s of 0 %, 0.6 % and 1.68 % were used. The third group that consisted of six beams was used to study the effect of compressive strength, which was varied from 35 MPa to 70 MPa. All beams were failed under bending. It was reported that the ability of LWAC beams to undergo deformation depends on the tensile reinforcement ratio. When increasing the reinforcement ratio, the deformation capacity would decrease.

Furthermore, the increase of compressive strength resulted in an increase in the vertical deformation in addition to increasing curvature specifically when the steel ratio was low. Within the constant moment zone and when there was no transverse reinforcement, the beams exhibited a brittle failure compared to beams with transverse reinforcement particularly for the beams with higher longitudinal tensile reinforcement ratio. It was also found that an increase in compressive strength controlled the mode of failure and changed the mode to tension failure in some cases where the beams were over-reinforced. The stiffness ratio E_I / E_{II} and ductility were measured and it was found that the stiffness ratio E_I / E_{II} was less than 2 and different from the value estimated by EC2-04 code.

2.2.7 Flexural behaviour of Normal Strength Steel Fibre Reinforced Lightweight Concrete

Altun and Aktas (2013) carried out an experiment investigation of fibre on the behaviour of lightweight concrete beams. A total of eighteen beams with dimensions of 300 mm × 300 mm × 2000 mm were tested. Beams were labeled into three series based on the cement content. Each series had three different samples and each sample was repeated twice; in total, each series had six beams. The cement dosages were $350\,kg/m^3$, $400\,kg/m^3$, and $450\,kg/m^3$, and the maximum and minimum compressive strength were 23.75 MPa and 15.5 MPa respectively. The steel fibres were 60 mm in length, 0. 75 mm in diameter with an aspect ratio of 80 and tensile strength of $1050\,N/mm^2$. Steel fibre content ratios for each group were 0 kg/m^3, 30 kg/m^3, $60\,kg/m^3$.The longitudinal reinforcement area was constant for all beams and equal to $400\,mm^2$. To ensure that the

beams would fail in flexure, and to avoid shear failure, stirrups with a diameter of 8 mm were placed throughout the length of the beams. It was concluded that the use of steel fibres increased the energy absorption of the beams. However, no noticeable difference was found when increasing the fibre content from 30 kg/m^3 to 60 kg/m^3. It was also found that the use of fibre generally increased the flexural capacity of the beams when compared to non-fibrous beams. The authors also concluded that when the cement content was 350 kg/m^3, beams with fibre content of 30 kg/m^3 gave 2.22 times the capacity of beams without steel fibres, whereas 2.24 times the capacity of beams without fibre were achieved by beams with fibre content of 60 kg/m^3. However, when the cement content raised to 400 kg/m^3, the increase in capacity was about 6 % as a result of increasing the fibre content from 30 kg/m^3 to 60 kg/m^3 and when the cement content was increased to 450 kg/m^3 the increase in the capacity was 8 %. Also, it was observed that the inclusion of fibres increased the ductility of the beams. This study was more of a material and mechanical properties rather than a full assessment of a structural behaviour of the beams.

2.2.8 Summary of Experimental Findings in the Literature

Based on the literature reviewed in the above sections, it can be stated that there have been no significant studies that address the effect of steel fibres on the flexural behaviour of high strength lightweight aggregate reinforced concrete beams. Also, the investigations on the flexural behaviour of steel fibre high strength normal weight concrete beams are still limited. Therefore, this study will generally add to the present

knowledge of steel fibre high strength normal and lightweight aggregate concrete and specifically will improve the current understanding of the flexural behaviour of steel fibre high strength lightweight aggregate concrete beams on both serviceability and ultimate states of loading. It was also concluded through the work presented in the literature that investigating the serviceability limit state of high strength normal and lightweight aggregate concrete beams are also limited but more adequate high strength LWAC beams.

.

2.3 Codes Provision for Ultimate limit state and Serviceability limit state of Beams.

This section presents empirical and statistical equations for flexural strength, crack width and crack spacing as specified or recommended by different codes and technical reports. The employed codes are the Canadian Code CSA A23.3-14, the European Code EC2-91, the European Code EC2-04, the American Code ACI318-08, the American Code ACI318-14, the Model Code CIB-FIB 1978 and the Model Code CIB-FIB 1990. Whereas the technical reports are those published by ACI committee 544 and RILEM TC 162-TDF.

2.3.1 Prediction of Flexural Strength.

2.3.1.1 Canadian Code [CSA A23.3-14]

The CSA standard A23.3-14 does not account for adding fibre to the concrete matrix in evaluating the flexural capacity. However for elements that contains no steel fibre in the concrete, the CSA standard A23.3-14 assumes that the moment resistance of members have to be evaluated based on strain compatibility and equilibrium of forces. The strain in the longitudinal reinforcement must be calculated according to the distance from the natural axis. The maximum strain at which the compressive fibre of concrete first crushes is assumed to be 0.0035. This specified strain value must be applied by the code regardless of concrete type or concrete strength.

Canadian code A23.3 recommends, as do many other codes, the Equivalent rectangular concrete stress distribution approach in order to evaluate the relationship between the compressive stress and concrete strain. Figure 2.3 shows the strain distribution accompanied by concrete stress block in a rectangular section. The concrete

stress of $\alpha_1\beta_1 f_c^{'}$ has to be assumed to be uniformly distributed over a depth of $a = \beta_1 c$, where c is the distance between the extreme compressive fibre to the natural axis.

The depth of neutral axis, c, can be calculated by equating the internal forces, which would lead to the next formula:

$$c = \frac{Asf_y}{\alpha_1\beta_1 f_c^{'}} \tag{2.10}$$

The factors α_1 and β_1 can be calculated as follows:

$$\alpha_1 = 0.85 - 0.0015 f_c^{'} \leq 0.67 \tag{2.11}$$

$$\beta_1 = 0.97 - 0.0025 f_c^{'} \leq 0.67 \tag{2.12}$$

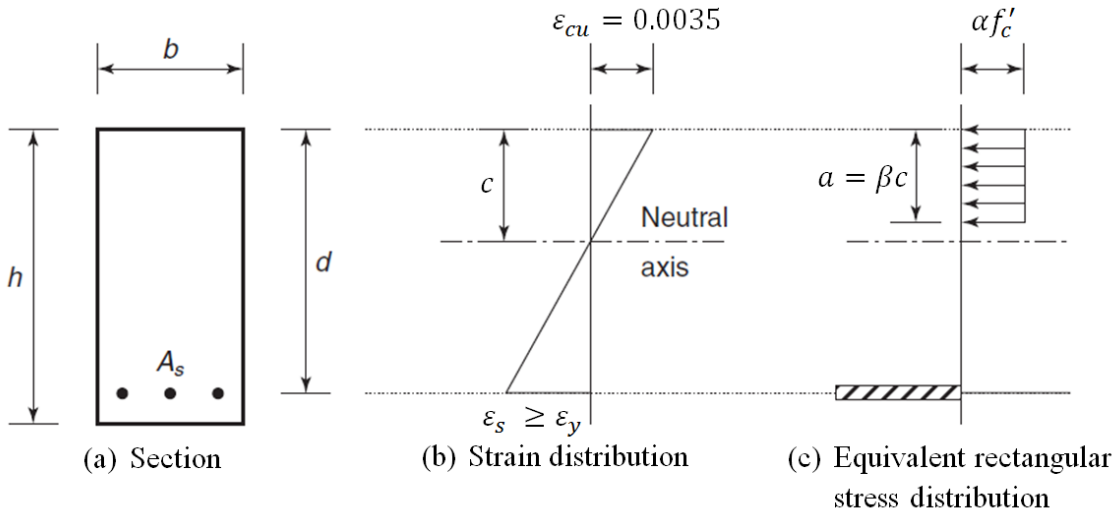

Figure 2.3: Strain Distribution and Concrete Stress Block in a Section with Conventional Reinforcement.

To evaluate the moment resistance, the following equation can be applied.

$$M_n = Asf_y\left(d - \frac{a}{2}\right) = \alpha_1\beta_1 f_c' cb\left(d - \frac{a}{2}\right) \tag{2.13}$$

where M_n is the nominal moment capacity, b and d are width of the beam and the distance from the extreme compression fibre to the centroid of the tension reinforcements respectively, f_c' and f_y are the compressive strength of the concrete and the yield strength of the bars , a is the depth of the rectangular block and A_s is the area of the steel reinforcement.

2.3.1.2 The American Code [ACI 318-14] Provision

According to the American code ACI 318-14, the nominal moment capacity for a flexural reinforced concrete member can be calculated based on Eq.2.14.

$$M_n = A_s f_y\left(d - \frac{a}{2}\right) = \alpha_1\beta_1 f_c' cb\left(d - \frac{a}{2}\right) \tag{2.14}$$

where M_n is the nominal moment capacity, α_1 is a coefficient taken as 0.7 when $f_c' \geq 58$ MPa, β_1 is a coefficient taken as 0.65 when $f_c' \geq 58$ MPa, b and d are width of the beam and the distance from the extreme compression fibre to the centroid of the tension reinforcements respectively, f_c' and f_y are the compressive strength of the concrete and the yield strength of the bars , a is the depth of the rectangular block and A_s is the area of the steel reinforcement. The American code ACI 318-14 recommends the maximum strain in the compressed concrete fibre to be taken as 0.003.

2.3.1.3 The ACI Committee 544.

ACI committee 544 adopted Eq. 2.15 for evaluating the strength of beams reinforced with both bars and steel fibres. This equation was developed by Henager and Doherty (1976), they tested a series of six beams. The ratios of the calculated moments using the proposed model to the actual moments varied between 1.001 and 1.017.

The model was also used by Henager (1977) to evaluate the strength of fibrous lightweight concrete beams and provided good agreement. The approach used to derive the equation is similar to the ACI ultimate strength design method where the tensile strength contributed by steel fibres was added to the tensile strength provided by the longitudinal reinforcement. Figure 2.4 shows the design assumption for analysis of fibrous-singly reinforced beam proposed by Henager and Doherty (1976).

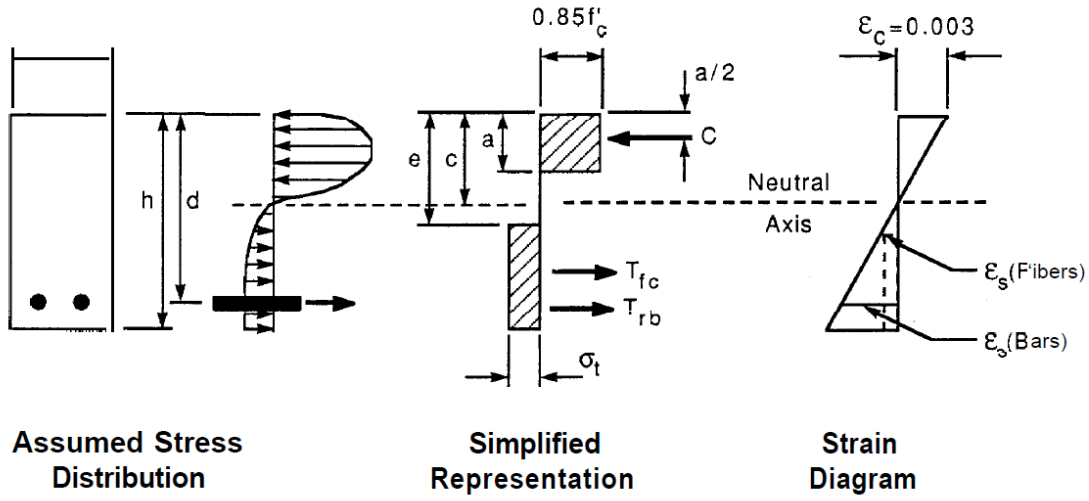

Figure 2.4: Design Assumption for Analysis of Fibrous-Singly Reinforced Beam Proposed by Henager and Doherty in 1976.

$$M_n = A_s f_y \left(d - \frac{a}{2} \right) + \sigma_t b \left(h - e \right) \left(\frac{h}{2} + \frac{e}{2} - \frac{a}{2} \right) \tag{2.15}$$

Where

$$e = \frac{\varepsilon_s \left(fibres \right) + 0.003) c}{0.003}$$

$$\sigma_t = 0.00772 \frac{l}{d_f} \rho_f F_{be}$$

Where l is the fibre length, d_f is the fibre diameter, F_{be} is the bond efficiency of steel fibre which is taken between 1.0 to 1.2 depending upon fibre characteristics, e is the distance from the extreme compression fibre to the top the tensile stress block of fibrous concrete, σ_t is the tensile stress in the fibrous concrete , c is the distance from the extreme compressive fibre to the neutral axis and $\varepsilon_s \left(fibres \right)$ is the tensile strain for fibre which is based on dynamic bond stress of 2.3 MPa.

Herein, it is important to address that the bond stress of 2.3 MPa which was used to derive the coefficient of 0.00772 was meant for normal strength concrete. Therefore, using this coefficient for high strength concrete has to be further investigated due to the higher fibre-concrete bond strength of high strength concrete. The maximum allowable strain to be applied at the extreme compressive concrete fibre is limited to 0.003. However, Some other investigations suggested that the strain of 0.003 is underestimated. Studies performed by Williamson (1973) and by Pearlman (1979) suggested the strain of 0.0033 to be more valid. Larger strain value of 0.0035 was advocated by Swamy and AL-Tan (1981).

2.3.2 Prediction of Cracking Moment

2.3.2.1 Canadian Code [CSA A23.3-14] Provision

The Canadian code provision for cracking moment is based on Eq. 2.16, where M_{cr} is the theoretical cracking moment at which the first flexural cracking occurs.

$$M_{cr} = f_r \frac{I_g}{y_t} \tag{2.16}$$

where f_r is modulus of rupture and shall be taken as $0.62\lambda\sqrt{f_c'}$,λ is a factor accounting for density of the aggregate and is equal to 1 for normal density concrete, 0.85 for semi-low-density concrete in which all the fine aggregate is natural sand, and 0.75 low-density concrete in which none of the fine aggregate is natural sand, I_g is gross moment of inertia of the reinforced concrete section (the steel bars can be ignored) , y_t is the distance from centroid to extreme tension fibre.

2.3.2.2 The American Code [ACI 318-08] Provision

The American code provision for cracking moment is based on Eq. 2.29, where M_{cr} is the theoretical cracking moment.

$$M_{cr} = f_r \frac{I_g}{y_t} \tag{2.17}$$

where f_r is $0.62\lambda\sqrt{f_c'}$, λ is a factor for depending on the density of the concrete and is equal to 1 for normal density concrete and 0.85 for semi-low-density concrete, I_g is gross moment of inertia of the reinforced concrete section (the steel bars can be ignored), and y_t is the distance from centroid to extreme tension fibre.

2.3.2.3 The European code [EC2-04] provisions

The European code for cracking moment is based on Eq. 2.30, where M_{cr} is the theoretical cracking moment. Unlike CSA A23.3-14 and ACI 318-08T, the gross moment of inertia I_g is calculated using the transformed section in which the steel bars shall be considered.

$$M_{cr} = f_r \frac{I_g}{y_t} \tag{2.18}$$

The modulus of rupture of concrete f_r is calculated based on Eq. 2.19;

$$f_r = max\left[\left(1.6f_{ctm} - \frac{hf_{ctm}}{1000}\right), f_{ctm}\right] \tag{2.19}$$

where

$$f_{ctm} = 0.3\eta_1 f_{ck}^{\frac{2}{3}} \; for\, f_{ck} \le 50MPa$$

$$f_{ctm} = 0.3\eta_1 2.12 \ln\left[1 + \frac{f_{ck} + 8}{10}\right] for\, f_{ck} > 50MPa$$

$$\eta_1 = 0.4 + 0.6\frac{w}{2200}$$

where f_{ctm} is the mean value of axial tensile strength of concrete, f_{ck} is the characteristic compressive cylinder strength, y_t is the distance from centroid to extreme tension fibre, h is the depth of the beam, η_1 is a reduction factor for lightweight concrete, and w is the concrete density.

2.3.2.4 Model Code [CEB-FIP 1990] Provision

In the Model Code CEB-FIP 1990, the theoretical cracking moment M_{cr} for a flexural member is calculated using Eq. 2.20. Similar to The European code EC2-04, the gross moment of inertia I_g is calculated using the transformed section.

$$M_{cr} = f_r \frac{I_g}{y_t} \tag{2.20}$$

The modulus of rupture of concrete f_r is calculated based on Eq.(2.21).

$$f_r = \left[\frac{1+1.5(h/100)^{0.7}}{1.5(h/100)^{0.7}} \right] f_{ctm} \tag{2.21}$$

where

$$f_{ctm} = 0.3\eta_1 f_{ck}^{\frac{2}{3}}$$

$$\eta_1 = 0.4 + 0.6\frac{w}{2200}$$

where f_{ctm} is the mean value of axial tensile strength of concrete, f_{ck} is the characteristic compressive cylinder strength, y_t is the distance from centroid to extreme tension fibre, h is the depth of the beam, η_1 is a reduction factor for lightweight concrete, and w is the concrete density.

2.3.3 Prediction of Crack Spacing

2.3.3.1 The European codes [EC2-91 and EC2-04] Provisions

In the Eurocode EC2-91, the stabilized average crack spacing for reinforced concrete members containing no fibre can be calculated by the following equation:

$$s_{rm} = 50 + 0.25k_1k_2d_b / \rho_{eff} \tag{2.23}$$

where

$$\rho_{eff} = \frac{A_s}{A_{ceff}}$$

where s_{rm} is the average crack spacing, k_1 is a coefficient relying on the bonding between the concrete and the reinforcement; k_1=0.8 for high bond bars and 1.6 for plain bars, k_2 is a coefficient relying on the shape of the strain diagram; k_2=0.5 for a member subjected to pure moment and k_2=1 for a member subjected to axial tension, d_b is the bar diameter, A_s is the area of the reinforcement and A_{ceff} is the effective tension area that is generally taken as 2.5 times the distance between the maximum tension side of the section to the centroid of the reinforcement.

Eurocode EC2-04 gives the following equation for predicting the maximum crack spacing. The components of the equation are similar to the ones incorporated in the Eurocode2-91. However, the clear concrete cover (c) is taken into account in Eurocode EC2-04.

$$s_{rm,max} = 3.4c + 0.425k_1k_2d_b / \rho_{eff} \tag{2.23}$$

2.3.3.2 Model Code [CEB-FIP 1978] Provision

The following equation for predicting the average crack width for members subjected to uniaxial strain was adopted by the early CEB-FIB (1978) provision.

$$s_m = 2\left(c + \frac{s}{10}\right) + k_1 k_2 d_b / \rho_{eff} \tag{2.24}$$

where

$$\rho_{eff} = \frac{A_s}{A_{ceff}}$$

where s_m is the final average crack width, c is the clear concrete cover, s is the maximum spacing between the longitudinal reinforcing bars, k_1 is a coefficient depending on the bonding between the concrete and the reinforcement; k_1=*0.4* for high bond bars and 0.8 for plain bars, k_2 is a coefficient depending on the strain gradient; k_2=0.25 for uniaxial strain condition, d_b is the bar diameter, A_s is the area of the reinforcement and A_{ceff} is the effective tension area.

2.3.3.3 RILEM TC 162-TDF

The technical document RILEM TC-162-TDF 'Test and design methods for steel fibre reinforced concrete' accounts for the existence of steel fibre in calculating the average crack spacing. The inclusion of fibre in Eq. 2.25 is expressed through the aspect ratio l_f / d_f .

$$s_{rm} = \left(50 + 0.25 k_1 k_2 \frac{d_b}{\rho_{eff}}\right)\left(\frac{50}{l_f / d_f}\right) \tag{2.25}$$

$$\rho_{eff} = \frac{A_s}{A_{ceff}}$$

where s_{rm} is the average crack spacing, k_1 is a coefficient relying on the bonding between the concrete and the reinforcement; k_1=0.8 for high bond bars and 1.6 for plain bars, k_2 is a coefficient relying on the shape of the strain diagram; k_2=0.5 for a member subjected to pure moment and k_2=1 for a member subjected to axial tension, d_b is the bar diameter, A_s is the area of the reinforcement and A_{ceff} is the effective tension area that is generally taken as 2.5 times the distance between the maximum tension side of the section to the centroid of the reinforcement.

2.3.4 Prediction of Crack Width

2.3.4.1 Canadian Code [CSA A23.3-14] and American Code [ACI 318-95]

The well-known Gergely-Lutz Eq. 2.26 is adapted by the current Canadian code, CSA A23.3-14 to predict crack widths for non-fibrous reinforced concrete beams and the same equation is also used to predict crack width in ACI 318-95. This equation was developed based on a statistical analysis, which was performed utilizing crack width data collected from different experiments. This equation is meant to estimate the maximum flexural crack width initiated at the tensile fibre of the beams.

$$w = 11x\,10^{-6}\beta f_s \sqrt[3]{d_c A} = 11x\,10^{-6}\beta z \qquad (2.26)$$

where

$$z = \beta f_s \sqrt[3]{d_c A}$$

where w is the maximum crack width in mm, β is the ratio of the distance from the tension face and from steel centroid to the neutral axis, equal to h_2 / h_1 as shown in Figure 2.5, f_s the stress in the longitudinal reinforcement at the assumed service load in MPs, d_c is the distance from the extreme tension fibre to the center of the reinforcing bar in (mm), and A is the area of effective tension surrounding the tension reinforcement with the same centroid as the tension reinforcement in divided by the number of bars, mm^2.

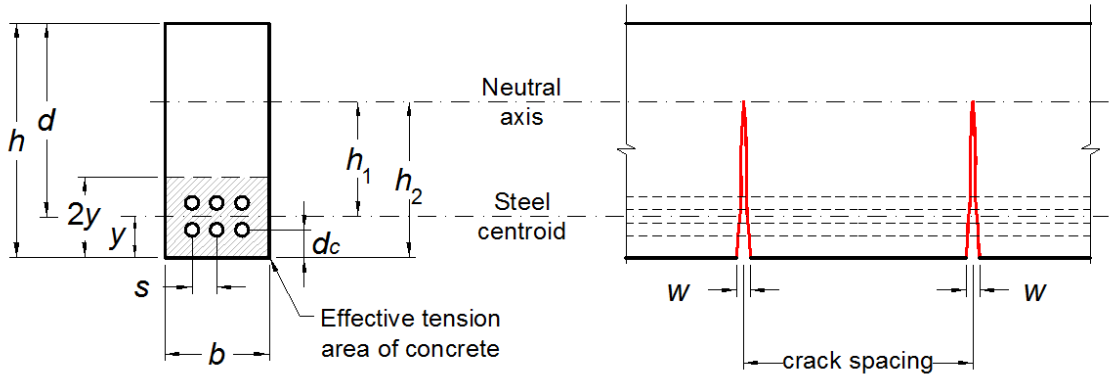

Figure 2.5: Definition for Crack Width Parameters.

2.3.4.2 The American Code [ACI 318-08] Provision

The American code provision for predicting the crack widths of reinforced concrete beams containing no steel fibre is based on Eq. 2.27. This equation was presented by Frosch (1999) on the basis of fundamental crack control concepts developed by Broms (1965).

$$w = 2\frac{f_s}{E_s}\beta + \sqrt{d_c^2 + \left(\frac{s}{2}\right)^2} \qquad (2.27)$$

where w is the maximum crack width in mm, β is the ratio of the distance from the tension face and from steel centroid to the nutria axis, equal to h_2 / h_1, f_s the stress in the longitudinal reinforcement at assumed service load in MPa, E_s is Young's modulus of the longitudinal reinforcement in MPa, d_c is the distance from the extreme tension fibre to the center of the reinforcing bar in (mm), and s is center-to-center spacing between bars in mm. Based on Frosch (2001), the coefficient β can be approximated to be 1.0 $+0.0031 d_c$.

2.3.4.3 The European Code [EC2-91] Provision

The EC2-91 code uses equation 2.28 to predict the crack width. This equation was derived for calculating the average crack width w_m for a member subjected to an axial force, bending moment or both.

$$w_m = s_{rm} \cdot \varepsilon_{sm} \tag{2.28}$$

Where

$$s_{rm} = 50 + 0.25 k_1 k_2 d_b / \rho_{eff}$$

$$\varepsilon_{sm} = \frac{\sigma_s}{E_s}\left(1 - \beta_1 \beta_2 \left(\frac{\sigma_{sr}}{\sigma_s}\right)^2\right)$$

Where w_m is the average crack width, s_{rm} is the average final crack spacing between cracks, ε_{sm} is the mean strain in the tension reinforcement, σ_s is the stress in the tensile reinforcement calculated based on cracked section, σ_{sr} is the stress in tensile

reinforcement under the first crack, E_s is the modulus of elasticity of the longitudinal reinforcement, β_1 is a coefficient taken as 0.8 for high bond bars and β_2 is a coefficient related to the loading duration and taken as 1.0 for single short-term loading.

To calculate the maximum or the design crack width, it is assumed that the maximum crack width is equal to the coefficient β times the average crack width; where β might be taken as 1.7 for beams whose minimum dimension exceeds 800 mm, and β might be taken as 1.3 for beams with minimum dimension less than 300 mm.

2.3.4.4 The European Code [EC2-04] Provision

The EC2-04 code for predicting the crack width of flexural members is based on equation 2.29, where w_k is the maximum or the design crack width.

$$w_k = s_{rm,max}\left(\varepsilon_{sm} - \varepsilon_{cm}\right) \tag{2.29}$$

where

$$s_{rm,max} = 3.4c + 0.425k_1k_2d_b / \rho_{eff}$$

$$\varepsilon_{sm} - \varepsilon_{cm} = \frac{\sigma_s}{E_s} - \frac{k_t f_{ctm}\left(1+n\rho_{eff}\right)}{E_s\rho_{eff}} \geq 0.6\frac{f_s}{E_s}$$

where $s_{rm,max}$ is the maximum crack spacing, ε_{sm} is the mean strain in the reinforcement the relevant combination of loads, including the effect of imposed deformations and taking into account the effects of tensioning, ε_{cm} is the mean strain in concrete between cracks, σ_s is the stress in the tension reinforcement calculated based on a cracked section, E_s is the modulus of elasticity of the longitudinal reinforcement, k_t is a factor

depending on the duration of loading: , k_t =0.6 and 0.4 for short term loading and long term loading respectively, f_{ctm} is the mean value of tensile strength of the concrete.

2.3.4.5 RILEM TC 162-TDF

The technical document RILEM TC-162-TDF for calculating the crack width for steel fibre members is based on Eq. 2.30, where w_k is the maximum crack width.

$$w_m = \beta . s_{rm} \cdot \varepsilon_{sm} \tag{2.30}$$

where

$$s_{rm} = \left(50 + 0.25 k_1 k_2 \frac{d_b}{\rho_{eff}}\right)\left(\frac{50}{l_f / d_f}\right)$$

$$\varepsilon_{sm} = \frac{\sigma_s}{E_s}\left(1 - \beta_1 \beta_2 \left(\frac{\sigma_{sr}}{\sigma_s}\right)^2\right)$$

where β is a coefficient relating the average crack width to the design value and is taken as 1.7, s_{rm} is the average final crack spacing between cracks, ε_{sm} is the mean strain in the tension reinforcement, σ_s is the stress in the tensile reinforcement calculated based on cracked section, σ_{sr} is the stress in tensile reinforcement under the first crack, E_s is the modulus of elasticity of the longitudinal reinforcement, β_1 is a coefficient taken as 1.0 for high bond bars and β_2 is a coefficient related to the loading duration and taken as 1.0 for single short-term loading.

2.3.5 Summary of Code Equations

The current North American Codes do not have design provisions for steel fibre reinforced concrete. The RILEM TC 162 TDF recommendations are the only ones available for steel fibre reinforced concrete. The provisions were primarily developed for normal strength normal weight concrete. Hence, further validation of these code equations and models by experimental results is still needed especially for different types of concrete such as high strength normal and light weight aggregate concrete.

Chapter 3

Material properties

3.1 Introduction

High strength lightweight and normal weight concrete mixes were used in this study. Due to the fact that lightweight aggregate concrete has different characteristics in comparison to normal weight concrete, and to obtain similar targeted compressive strength, a number of trial mixes were carried out. After several mixes and testing for the desired compressive and flexural properties, three different mixtures were chosen for each type of concrete. In this chapter, different materials , additives and mixtures that were used are described in detail. It is important to mention that lightweight concrete is more brittle than normal weight concrete. Hence, the properties of lightweight aggregate are significantly different than normal weight aggregate.

In this current research, the main variable for each type of concrete was the fibre volume ratio. Three levels of steel fibre volume were chosen and used, these levels were 0 %, 0.375 %, and 0.75 %. To evaluate the mechanical properties of hardened concrete, different standard tests were undertaken. Those tests included the compressive strength, the splitting strength, the modulus of rupture, and the modulus of elasticity test.

3.1.1 Concrete and Aggregates Properties

Ordinary Portland cement (GU) was used in addition to silica fume as a supplementary cementations material. For normal weight concrete, the aggregate was crushed sandstone with a maximum size of 10 mm and bulk specific gravity of 2.6. For

LWAC, expanded slate aggregate was used. This type of aggregate is produced by rotary kiln process. The specific gravity for the expanded slate was 1.53 and the absorption was about 6 % measured in accordance to ASTM C127-15. Similar to the normal weight aggregate, the lightweight aggregate had a maximum size of 10 mm. Thus any effects that aggregate size might cause are eliminated. Both types of concrete contained the same fine aggregate with specific gravity of 2.6.

During casting, chemicals were added to the mix water. These chemicals consisted of both superplasticizer and retarder. The aim of using superplasticizer was to reduce the amount of water needed to produce high strength concrete and also improve the workability of the mix, particularly for the mixes that contained steel fibres. The time required to cast each beam was lengthy as a consequence of the time needed to mix, pour, and refill the mixer. Since three batches were required to cast each beam, the use of retarder was essential to delay the initial setting time of concrete.

Even though the measured slump tests were not equal for all mixes due to the existence of different steel fibre volume ratio and different aggregate types, the amount of both superplasticizer and retarder were maintained. Each batch of 120 liters of concrete had 230 mL of superplasticizer and 60 mL of retarder. The concrete mixes used in the fabrication of all beams had slump values that fluctuated from 140 mm to 180 mm. Proportions for both high strength normal weight and lightweight aggregate concrete mixtures used in casting each of test beams are shown in Tables 3.1 and 3.2, respectively. The trial mixtures were evaluated on the basis of workability, set time and targeted strength. The reason of selecting set time as a criterion was due to the use of several

mixtures to pour each beam. Hence, it was necessary to ensure that each batch had sufficient setting time.

Table 3.1: Mixture Proportions For One Cubic Meter of Normal Weight Concrete.

Materials	Mix1	Mix2	Mix3
Cement (kg)	460	460	460
Silica Fume (kg)	40	40	40
Coarse Aggregate (kg)	1046	1041	1035
Fine Aggregate (kg)	698	694	690
Water (L)	165	165	165
Steel Fibre Ratio (%)	0	0.375	0.75
Steel Fibres (kg)	0	29.4	58.9
Beams	NB1 and NB4	NB2 and NB5	NB3 and NB6

Table 3.2: Mixture Proportions For One Cubic Meter of Lightweight Aggregate Concrete.

Material	Mix4	Mix5	Mix6
Cement (kg)	500	500	500
Silica Fume (kg)	40	40	40
Coarse Aggregate (kg)	597	594	590
Fine Aggregate (kg)	676	672	668
Water (L)	173	173	173
Steel Fibre Ratio (%)	0	0.375	0.75
Steel Fibres (kg)	0	29.4	58.9
Beams	LB1 and LB4	LB2 and LB5	LB3 and LB6

3.1.2 Steel Fibres

The steel fibres utilized in this current research had dimensions of 35 mm in length, L, 0.55 mm in diameter, d, an aspect ratio, L/d, of 65 and weight of 8kg per meter cube. Tensile strength and the modulus of elasticity were 1345 MPa and 210,000 MPa, respectively. This type of steel fibres come in a form of small hocked pieces glued to each other as shown in Figure 3.1.

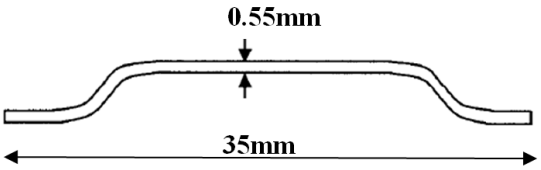

Figure 3.1: Steel Fibres.

3.1.3 Longitudinal Reinforcements

Grade 400 cold-worked ribbed bars with two different diameters were used in the tests. Both 15M and 20M bars with actual bar diameters of 16 mm and 19.5 mm were selected to reinforce the test beams. Two samples with a length of 800 mm were tested for each bar diameter and the average of the results was used. The average yielding stress was 430 MPa and 470 MPa for the 15M and 20M bars respectively, and the ultimate strength was measured and found to be 575 MPa for both used bars. The stirrups used to enhance the shear capacity were constructed using 10M bars that has an actual diameter of 11.3 mm and tensile strength of 470 MPa.

3.2 Properties of Hardened Concrete

3.2.1 Compressive Strength

The compressive strength test of concrete was conducted in accordance with ASTM C39-17 standards with a load rate 0.25 MPa per second. The machine used to perform the compressive strength is shown in Figure 3.2. Three cylinders with dimensions of 100 mm × 200 mm were cast from each batch of concrete. The cylinders were stored and cured with their corresponding beam under the same conditions. At the same day when the beam was tested, the compressive strength test was also performed. It was observed that normal and lightweight concrete mixes that contained steel fibres had a compressive strength higher than the non-fibred ones. The measured compressive strength for all beams are shown in Table 3.3. The maximum compressive strength recorded for normal weight concrete and lightweight aggregate concrete were 90 MPa and 86 MPa, respectively. Furthermore, during the compressive strength test and

regardless of the type of concrete when the non-fibrous cylinders reached their maximum compressive strength, a loud bang accompanied by sudden fragmentation occurred as shown in Figure 3.3. the cylinders that contained steel fibres did not shatter when the ultimate strength was reached.

Figure 3.2: The Concrete Compression Testing Machine.

Figure 3.3: Plain LWAC Concrete Cylinder at Failure.

3.2.2 Splitting Tensile Strength

The splitting tensile strength test was performed in accordance with ASTM C496-17. For each beam , three 100 mm × 200 mm cylinders were used to conduct the test in accordance with ASTM C31. Before applying the load to the tested cylinder, diametral line splitting the specimen into two symmetrical planes had to be drawn to ensure that the applied load would be centric. A diametric compressive load at a constant rate of 533 N/s was applied to the specimen along the marked line until failure occurred, as shown in the Figure 3.4 . The maximum applied load indicated by the compression machine was recorded and the splitting tensile strength was calculated afterwards. The measured values of the splitting tensile strength of all mixes are presented in Table 3.3. In general, when comparing normal weight concrete to lightweight aggregate concrete it can be seen that the splitting tensile strength for normal weight concrete is higher than lightweight concrete regardless of the presence of the steel fibres.

The action of fibres in resisting the opening of the crack was clear and reflected a noticeable increase in splitting tensile strength when compared to plain concrete for both high strength normal weight concrete and lightweight aggregate concrete. Moreover, an increase in the splitting strength was also found when the steel fibre volume ratio was increased from 0.375 % to 0.75 % for both types of concrete. Also, for both type of concrete, the splitting tensile strength appeared to be influenced by the slight difference in the compressive strength between mixes. The increase in the compressive strength corresponded to an increase in the splitting tensile strength for both type of concrete.

Figure 3.4: Splitting Tensile Test Setup.

3.2.3 Modulus of Elasticity

The modulus of elasticity tests were performed in accordance with ASTM C469-14. The test was carried out using 100 mm × 200 mm cylindrical samples. Two compressometers equipped with a Linear Variable Differential Transducer (LVDT) were attached to the cylinders and then connected to a data acquisition system as shown in Figures 3.5 and 3.6. A stress of 40 % of the maximum stress was used to calculate the modulus of elasticity. The calculated values of the modulus elasticity are presented in Table 3.3. The results show that normal weight concrete had a higher modulus of elasticity than lightweight aggregate concrete regardless of the presence of steel fibres. Also, for both types of concrete, the addition of steel fibres appeared to increase the modulus of elasticity. A significant increase in the modulus of elasticity was found when the steel fibre volume ratio was increased from 0.375 % to 0.75 % for both high strength normal weight and lightweight concrete as shown in Figures 3.7 and 38.

Figure 3.5: Modulus of Elasticity Test.

Figure 3.6: A Photograph of Cylinder During the Modulus of Elasticity Test.

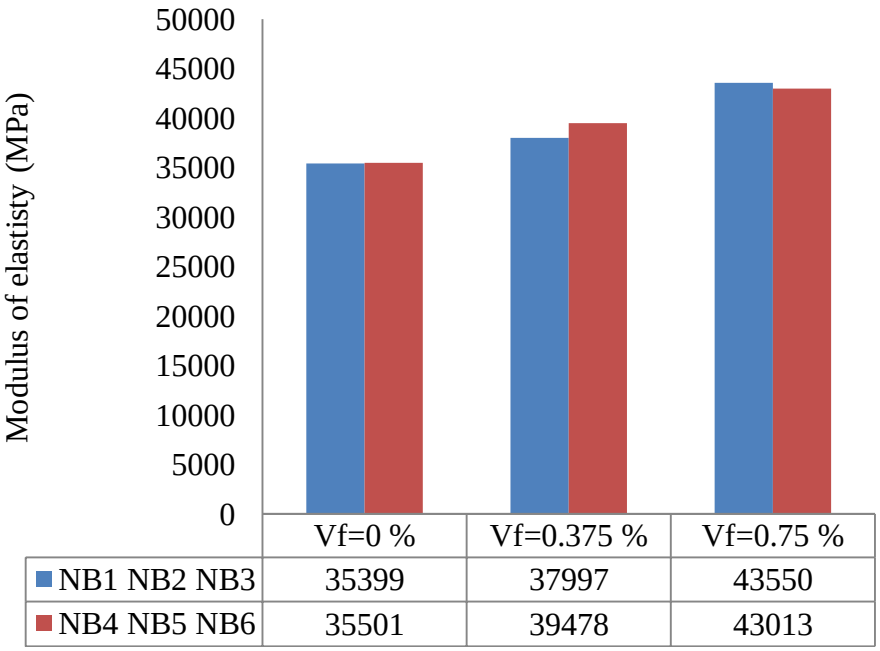

	Vf=0 %	Vf=0.375 %	Vf=0.75 %
NB1 NB2 NB3	35399	37997	43550
NB4 NB5 NB6	35501	39478	43013

Figure 3.7: Effect of Steel Fibre Volume Ratio on the Modulus of Elasticity (MPa) of NWC.

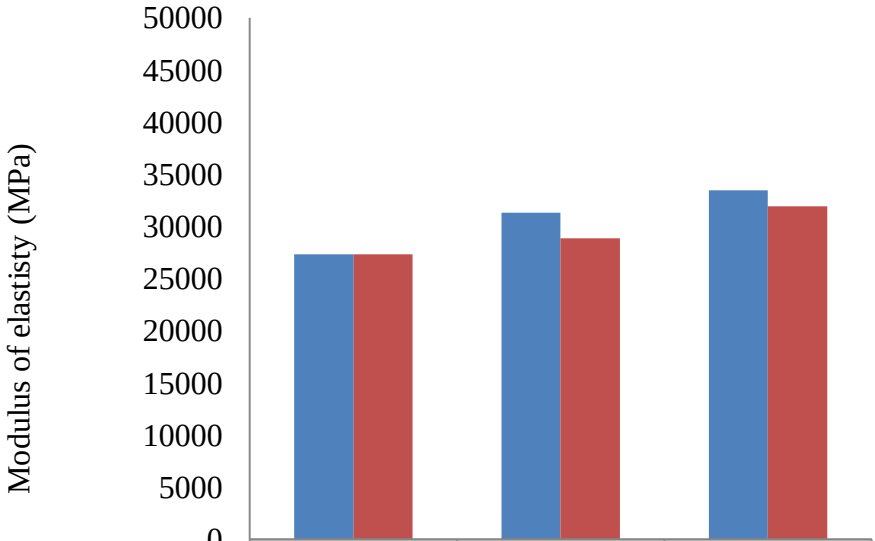

	Vf=0 %	Vf=0.375 %	Vf=0.75 %
LB1 LB2 LB3	27310	31349	33451
LB4 LB5 LB6	27360	28851	31920

Figure 3.8: Effect of Steel Fibre Volume Ratio on the Modulus of Elasticity (MPa) of LWAC.

3.2.4 Modulus of Rupture

The modulus of rupture for each mixture is measured in accordance with ASTM C78-16, using a simple beam with four-point loading as shown in Figure 3.9. At least two concrete prisms with dimensions of 100 mm × 100 mm × 400 mm were cast for each beam at the same time as casting the beam. All prisms were kept at the same location of beams under same conditions. The displacement control approach was used to perform the test. The loading rate was 0.15 mm per minute.

Table 3.3 shows the values of the modulus of rupture for all mixes. These value were obtained based on the following equation:

$$f_r = \frac{PL}{bd^2} \tag{3.1}$$

where, f_r is modulus of rupture (MPa), P is the first peak load or the first crack load (N), L is the span length, b is specimen's average width, and d is specimen's average depth.

It can be seen that in comparison to plain concrete, the addition of steel fibres increased the modulus of rupture for both high strength lightweight and normal weight concrete. Also increasing the fibre volume ratio from 0.375 % to 0.75 % increased the modulus of rupture for both types of concrete.

It was also found that the modulus of rupture for normal weight concrete prisms containing no steel fibres are higher than their corresponding lightweight concrete prisms Furthermore, a similar results was observed when comparing fibrous normal weight concrete prisms to lightweight concrete prisms.

Figure 3.9: Modulus of Rupture Test Machine.

Table 3.3: Mechanical Properties of the Test Beams.

Concrete Type	Beam	Mixture Number	Fibre Volume Ratio V_f %	Comp. Strength f_c' MPa	Splitting Tensile Strength f_{sp} MPa	Modulus of Rupture f_r MPa	Modulus of Elasticity E_c MPa
NWC	NB1	Mix1	0	80	3.3	8.5	35399
	NB2	Mix2	0.375	88	5.4	9.5	37997
	NB3	Mix3	0.75	90	7.6	10.9	43550
	NB4	Mix1	0	81	2.7	7.9	35501
	NB5	Mix2	0.375	90	6.2	9.2	39478
	NB6	Mix3	0.75	87	7.6	9.8	43013
LWAC	LB1	Mix4	0	81	2.4	5.9	27310
	LB2	Mix5	0.375	85	5.3	5.9	31349
	LB3	Mix6	0.75	86	6.5	7.7	33451
	LB4	Mix4	0	80	2.3	5.0	27360
	LB5	Mix5	0.375	80	5.0	5.7	28851
	LB6	Mix6	0.75	82	6.1	6.3	31920

3.2.5 Flexural Load Deflection Curve for Prisms.

Figure 3.11 and 3.12 represent the load deflection curves for both normal weight and lightweight concrete prisms with and without steel fibres. The load-deflection curves for high strength lightweight aggregate concrete are quite similar to the load-deflection curves for high strength normal weight concrete. It was also observed that plain lightweight and normal weight concrete prisms failed suddenly in two pieces once the prisms reached the maximum load and could not carry more load nor undergo any more deformation. However, fibrous lightweight and normal weight concrete prisms behaved in different way as they did not break in two pieces when the maximum load reached and they instead tended to carry some load creating a descending branch in the load-deflection curve. Figures 3.10 and 3.11 shows plain and fibrous prisms failure.

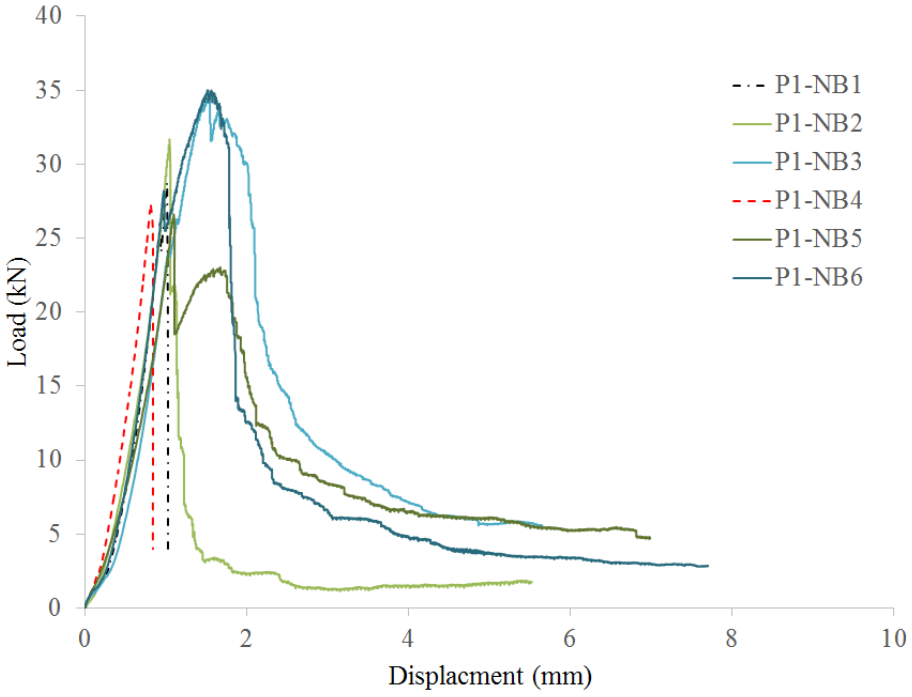

Figure 3.10: Load vs Deflection Curves for NWC Prisms Specified for Each Beam.

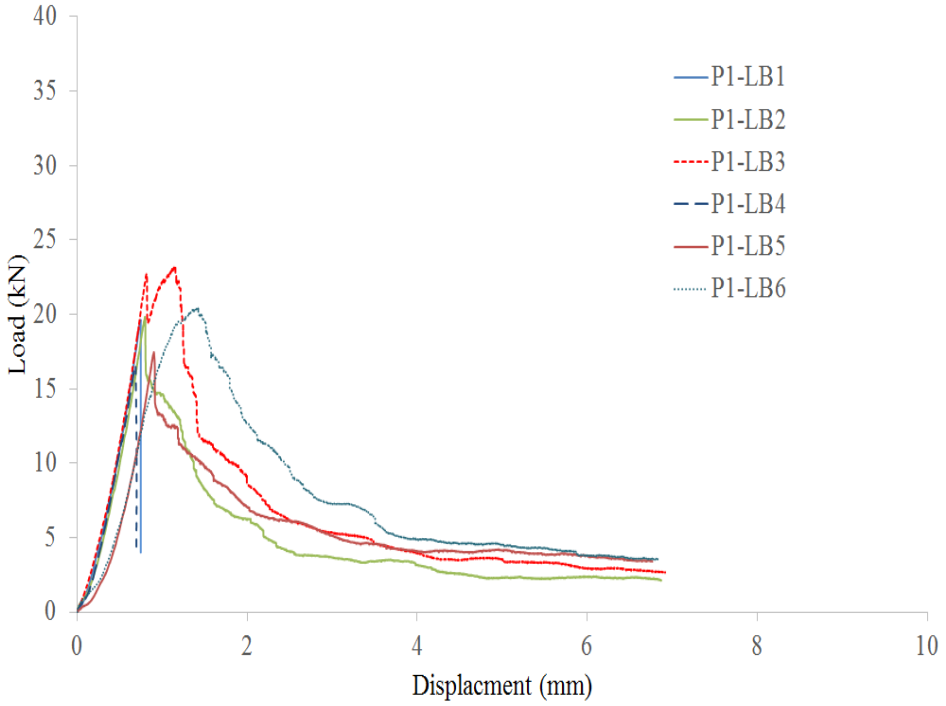

Figure 3.11: Load vs Deflection Curves for LAWC Prisms Specified for Each Beam.

Tables 3.6 and 3.7 show the maximum load and deflection at the maximum load for all tested prisms. In general, fibrous and non-fibrous lightweight aggregate concrete prisms had less capacity compared to their counterpart normal weight concrete prisms. In addition, it was noted that the addition of fibres increased the maximum load for both types of concrete. For both types of concrete, the deflection corresponding to the maximum load increased with the increase of the fibre volume ratio.

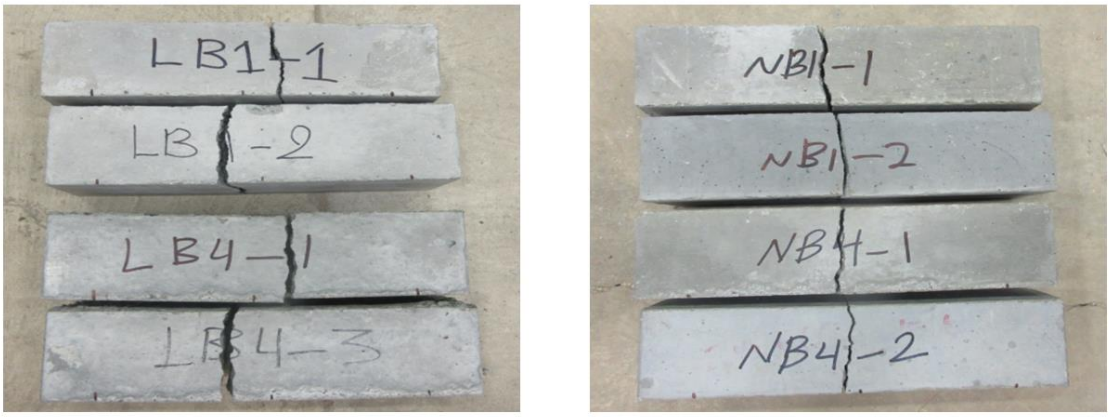

(a) Plain LWAC Prisms Failure (b) Plain NWC Prisms Failure

Figure 3.12: Plain LWAC and NWC Prisms Failure.

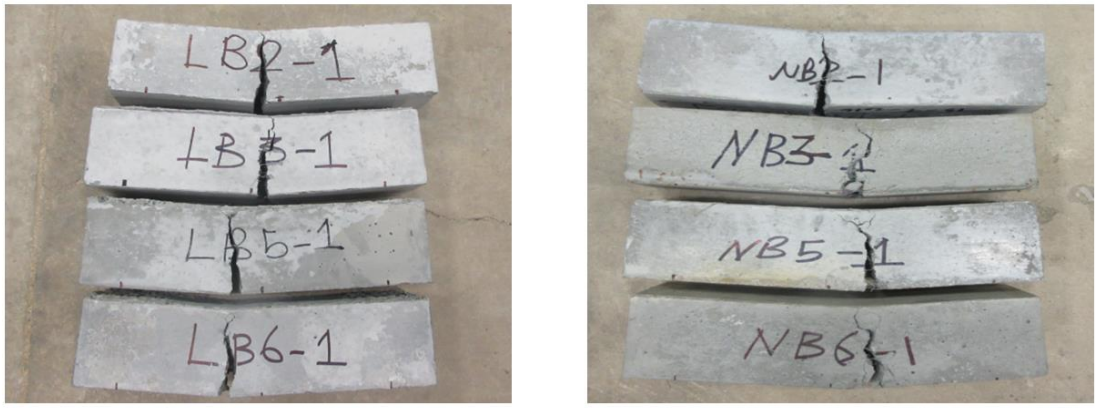

(a) Fibrous LWAC Prisms Failure (b) Fibrous NWC Prisms Failure

Figure 3.13: Fibrous LWAC and NWC Prisms Failure.

3.2.6 Flexural Toughness

Toughness can be defined as the energy absorption capacity. In accordance to ACI 544.1R , the flexural toughness can be defined as the area under the load deflection curve in flexure which is the total energy absorbed prior to complete separation of the specimen.

The energy absorption capacity for all tested prisms specified for each beam is presented in Table 3.6 and 3.7. It can be noted that regardless of the existence of steel fibres, the energy absorption capacity for the high strength normal weight concrete prisms was higher than the energy absorption capacity for high strength lightweight concrete prisms.

The addition of steel fibres was found to enhance the energy absorption capacity for both type of concrete. the energy absorption capacity increased when steel fibres were added to both types of concrete. Also, increasing the steel fibre volume ratio from 0.375 % to 0.75 % resulted in a significant improvement in the energy absorption capacity for both high strength lightweight and normal weight concrete.

Table 3.4: Observed Maximum Load, Displacement at the Maximum Load and Energy Absorption Capacity for NWC Prisms.

Prism	Mixture	Fibre Vol. Ratio V_f %	Maximum Load P kN	Disp. at the Max. Load Δ mm	Energy Absorption N.mm
P1-NB1	Mix1	0.00%	28.76	1.02	10759
P2-NB1	Mix1	0.00%	27.82	0.90	8480
P1-NB2	Mix2	0.375%	31.69	1.05	23807
P1-NB2	Mix2	0.375%	30.79	1.32	59142
P1-NB3	Mix3	0.75%	34.57	1.54	72695
P2-NB3	Mix3	0.75%	38.05	1.65	86440
P1-NB4	Mix1	0.00%	27.20	0.81	8656
P2-NB4	Mix1	0.00%	25.58	1.11	11362
P1-NB5	Mix2	0.375%	26.61	1.10	65111
P2-NB5	Mix2	0.375%	29.18	1.51	40162
P1-NB6	Mix3	0.75%	34.99	1.51	65904
P2-NB6	Mix3	0.75%	30.95	1.21	65357

Table 3.5: Observed Maximum load, Displacement at the Maximum Load and Energy Absorption Capacity for LWAC Prisms.

Prism	Mixture	Fibre Vol. Ratio V_f %	Maximum Load P kN	Disp. at the Max. Load Δ mm	Energy Absorption N.mm
P1-LB1	Mix4	0.00%	19.61	0.75	6053
P2-LB1	Mix4	0.00%	19.69	0.84	7175
P1-LB1	Mix5	0.375%	19.82	0.80	33546
P1-LB2	Mix5	0.375%	20.02	0.84	40221
P1-LB3	Mix6	0.75%	23.24	1.15	46526
P2-LB3	Mix6	0.75%	28.09	1.10	42895
P1-LB4	Mix4	0.00%	16.57	0.68	4718
P2-LB4	Mix4	0.00%	17.90	0.74	5326
P1-LB5	Mix5	0.375%	17.45	0.90	37944
P2-LB5	Mix5	0.375%	20.82	0.85	49249
P1-LB6	Mix6	0.75%	20.41	1.40	52370
P2-LB6	Mix6	0.75%	21.69	1.30	60755

Chapter 4

Experimental program

4.1 Introduction

This chapter provides the details of the experimental program which was carried out to investigate both high strength normal weight and lightweight steel fibre reinforced concrete. The experimental program was comprised of two main stages. The first stage was to develop high strength normal weight and lightweight aggregate concrete with and without steel fibre. The second stage was to cast, test and evaluate the structural behaviour of twelve large scale beams using the developed concrete mixtures. The Instrumentation that was used to measure the load, deformation and strains are presented in this chapter, as well as the details of the preparation procedure.

4.2 Test specimens

Two main groups were used to categorize the test beams, lightweight aggregate concrete LWAC beams and normal weight concrete NWC beams. Each of these groups was divided into two subgroups based on the reinforcement ratio, ρ, each subgroup has different levels of steel fibre volume ratios , V_f %, equal to 0 %, 0.375 %, 0.75 %, with constant shear ratio a/d, dimensions, and stirrups spacing, three main variables. The three variables are aggregate type, reinforcement ratio and fibre volume ratio. Details of the test beams are given in Table 4.1.

All beams had the same dimensions of 200 mm × 400 mm × 3200 mm. Within the same group, the beams had different steel ratios and different steel fibre volume ratios of 0 %,

0.375 %, and 0.75 %. Based on the flexural reinforcement ratio, ρ , of 0.85 % and 1.50 %, subgroups were introduced in each of these main groups based on steel fibre volume ratio. All beams were tested with constant shear span to depth ratio, a/d ,equal to 2.9. The concrete clear cover in all sides was equal to 30 mm . Due to the fact that flexural behaviour was under the consideration of this study, it was a necessity to enhance the shear resistance of beams and to avoid any shear failure. Hence, steel stirrups were added with center to center spacing equal to 200 mm throughout the length of the beams based on Canadian Code CSA A23.3-14.

All beams were under-reinforced. The two reinforcement ratios were selected to satisfy the minimum reinforcement area recommended by the Canadian Code CSA A23.3-14. Consequently, the selected flexural reinforcement area, A_s , had to be greater or equal to the minimum reinforcement area, $A_{s,min}$. The minimum reinforcement ratio can be calculated by applying the following formula:

$$A_{s,min} = \frac{0.2\sqrt{f_c^{'}}}{f_y} b_t h \tag{4.1}$$

where $f_c^{'}$ is the compressive strength of the concrete (MPa), f_y is the tensile yield strength of reinforcement (MPa), b_t is the width of the tension zone of the section (mm), and h is the height of the section (mm).

Table 4.1: Details of Test Beams.

Concrete Type	Beam	b mm	h mm	Cover mm	V_f %	ρ_s' %	ρ %
NWC	NB1	200	400	30	0	0.85	0.85
	NB2	200	400		0.375	0.85	0.85
	NB3	200	400		0.75	0.85	0.85
	NB4	200	400	30	0	0.85	1.50
	NB5	200	400		0.375	0.85	1.50
	NB6	200	400		0.75	0.85	1.50
LWAC	LB1	200	400	30	0	0.85	0.85
	LB2	200	400		0.375	0.85	0.85
	LB3	200	400		0.75	0.85	0.85
	LB4	200	400	30	0	0.85	1.50
	LB5	200	400		0.375	0.85	1.50
	LB6	200	400		0.75	0.85	1.50

4.3 Casting and curing of the Beams

Beams were cast in formwork that was designed and assembled using 25mm thick wood sheets. The reinforcement cage was prepared and placed in the formworks on concrete chairs that were located at the edge and middle of the beam, and thus uniform clear cover was achieved throughout the length of the specimens. A sample of the used formwork and reinforcement cage are shown in Figure 4.1.

Figure 4.1: The Used Wood Formwork and the Steel Frame with ρ =0.85%.

The concrete mixing was done by using drum mixer with total capacity of 150 liters. The sequence of casting was similar for all beams. All dry materials except cement were placed in the mixer and then were mixed together. After the mix became homogeneous and steel fibres dispersed well in the mix, the cement and water with additives were gradually added. All materials were afterwards mixed between 8 to 10 minutes before placing the concrete in the formwork.

Each beam required three batches and the volume of each batch was 110 litters. To ensure that the concrete would cover the steel bars well, an extreme attention was paid especially to coMPacting and vibrating the first layer that extended just above steel bars. Twelve cylinders and at least two prisms were taken during the casting to evaluate the compressive strength, splitting tensile strength and the modules of rupture of the each beam. Figure 4.2 shows a beam during the casting process.

Once the beams were cast, they were covered with plastic sheets in order to prevent the evaporation of water from the surface of beams. The cast beams were then sprayed by water one to two times a day for approximately eight successive days.

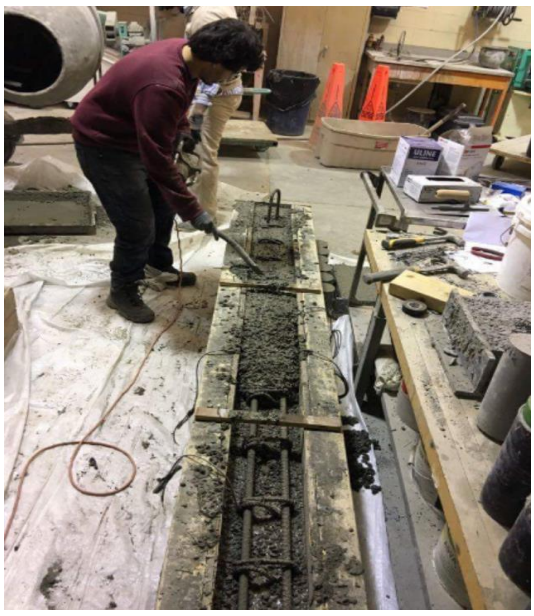

Figure 4.2: A Photograph During the Casting Process.

4.4 Experimental Setup and Instrumentations

Figure 4.3 shows a photograph of the test frame. The frame was fastened to a 1 m thick reinforced concrete floor using 38 mm anchor bolts. The hydraulic actuator used in the tests had a capacity of 450 kN. Different types of strain gauges were used in this study. To measure the strain in the reinforcement, 10 mm electric strain gauges were used. In total, four strain gauges were glued to the reinforcement. Figure 4.4 shows a sample of steel strain gauges installation. Care was taken to prevent any damage that water might cause to the gauges during the pouring process.

Figure 4.3 : The test Frame.

The steel strain gauges were coated with silicon and covered by duct tape. Nevertheless, some of these strain gauges were damaged during the casting. The locations of strain gauges were selected to measure the strain in the maximum flexural zone. Two of the strain gauges were placed in the middle of the beam and the other two were placed at the ends of the constant moment region as shown in Figure 4.5. Furthermore, Three electrical stain gauges with a length of 60 mm were used for concrete, the surface of concrete had been smoothened and covered by a very thin layer of epoxy, and then the strain gauge was glued to the beam. This strain gauge was located in the middle of the beam in the compressed concrete side as shown in Figure 4.6.

Figure 4.4: Strain Gauge Installation on the Steel Bars.

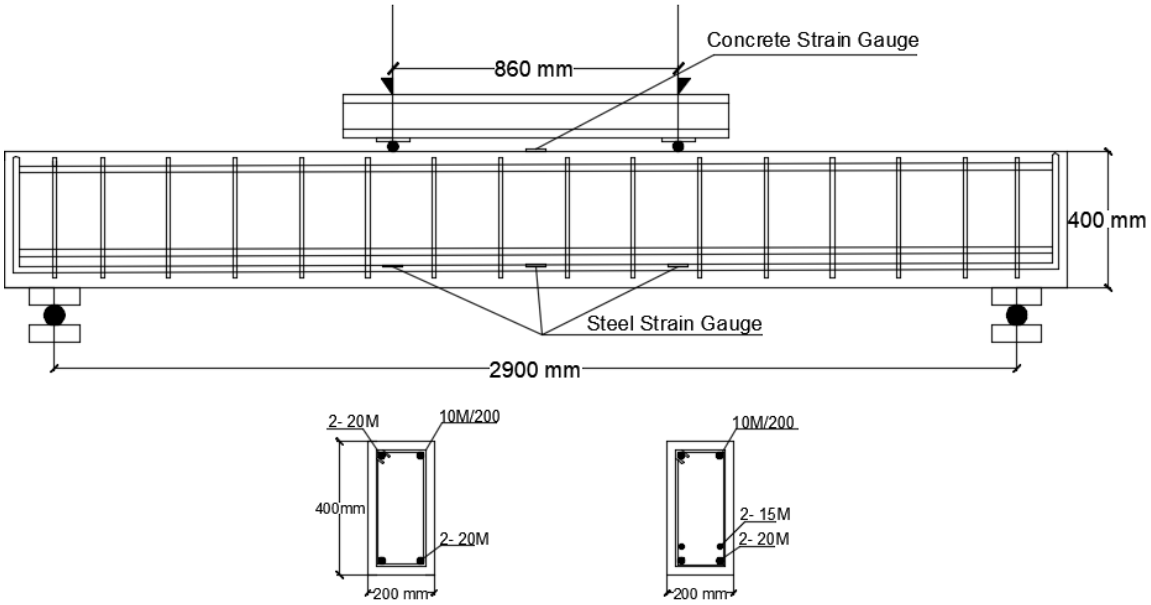

Figure 4.5: Specimens Details and Strain Gauges Locations.

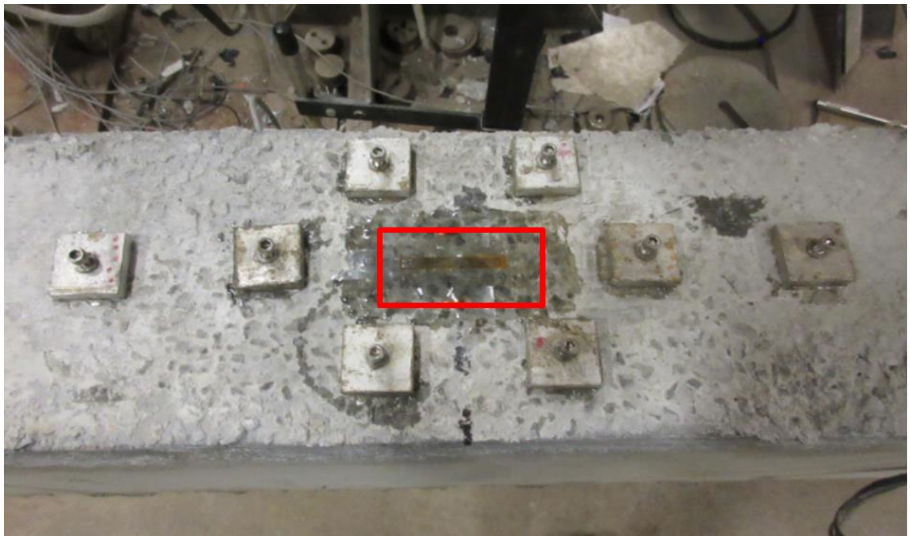

Figure 4.6: Strain Gauge Installation on the Beam Compression Side.

In order to measure the deflection occurring to beams, three Linear Variable Differential Transformers (LVDTs) were used. One of these (LVDTs) was placed in the middle of the bottom side of the beam, and the other two were located underneath loading points. The locations of LVDTs are shown in Figure 4.7.

All gauges, (LVDTs) and load cell were connected to the computer through data acquisition system. The data acquisition system was controlled by LABVIEW software. The readings were recorded every 1 seconds.

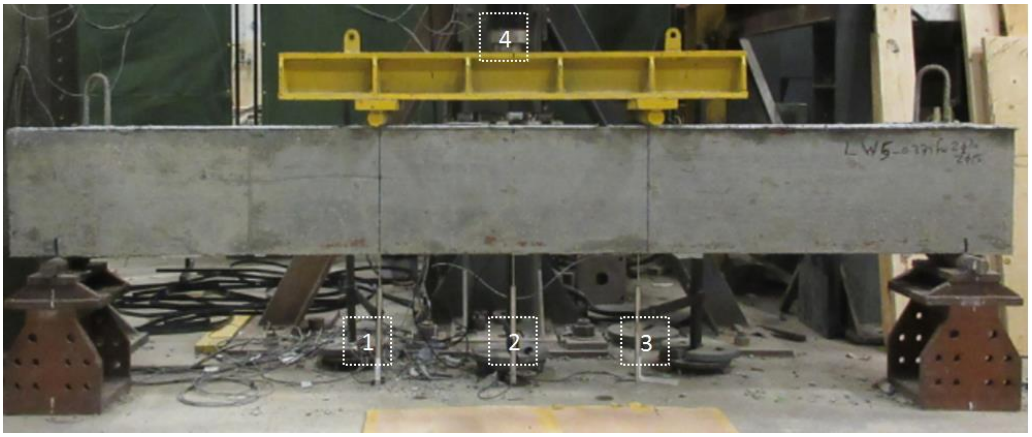

Figure 4.7: Locations of the LVDTs.

4.5 Test Procedure

The beams were tested using four point loading with a simply supported span of 2900 mm. They were loaded through servo-hydraulic MTS actuator in displacement control with a full capacity of 670 kN. The one load point that actuator provided was transferred to the test beams through two load points using a stiff steel spreader beam. Since the serviceability limit state was investigated in this study, small load increments were applied until about 75 % of the ultimate load capacity of the beam and then the load increment was increased.

Three stages of loading were carried out for all beams, the first stage had an increment of roughly 5 kN, thus the cracking load would be observed. Increments of approximately 18 kN to 26 kN are used in the second stage, and this stage was maintained until it was ensured that the possible highest service load was applied. Ultimately the beams were tested with an increment of 30 kN up to failure. During all loading stages, cracks were marked and measured using an optical crack- measurement scope. Figure 4.8 shows a photograph during Testing and Crack Marking. The load, deflection and strains were collected and recorded through LABVIEW program.

Figure 4.8: A Photograph during Testing and Crack Marking.

Chapter 5

Results and Discussion

5.1 Introduction

The results and observations recorded from testing twelve full size beams are presented in this chapter. Three different parameters were investigated to examine their effects on the behaviour of normal weight (NWC) and lightweight aggregate (LWAC) high strength concrete with and without steel fibres. These parameters were the concrete type, steel fibre volume ratio, and the longitudinal reinforcement ratio. The test beams were divided into two main groups based on the concrete type NWC and LWAC. Each group had six beams divided to two subgroups based on the reinforcement ratio. Each subgroup had three beams with different steel fibre volume ratios. Details of the test beams are shown in Table 4.1.

The structural behaviour of the test beams is presented in this chapter in terms of load deflection characteristics, concrete and reinforcement strains, ductility, crack patterns, first crack initiation, cracking moment, crack spacing, crack width, crack widening and strain localization. The results obtained were also compared to those calculated with different codes and models (CSA A23.3-14, ACI318-14, and ACI318-08, EC2-04, EC2-91, CEB-FIP1978, CEB-FIP1990, and RILEM TC 162-TDF). The prediction of the ultimate strength for the fibrous beams was also calculated using different models in the literature (ACI544, Oh Model, and Imam Model).

5.2 Load Deflection Characteristic

As mentioned earlier in section 4, three Liner Variable Differential Transformers (LVDTs) were utilized in order to obtain the deflection of beams at the middle and at the two ends of the constant moment zone on the tension side. Throughout the testing process, the applied load was paused at the end of each load step to allow the measurement of the crack width and map the propagation of the cracks. Stopping the system at different intervals caused a slight release in the applied load since beams were loaded in displacement control. Therefore, the load deflection curves had some negligible drops in the load which had no effects on the behaviour and the capacity of the beams.

The shape of load-deflection curve of beams at midspan was approximately similar to those at the two ends of the constant moment zone. As expected, the deflection measured at midspan was higher than that at the two ends of the constant moment zone. The readings of the two LVDTs placed at the ends of constant moment zone were to some extent identical. Consequently, it can be concluded that test beams were loaded symmetrically throughout test duration. All load deflection curves obtained via LVDTs are presented in Appendix A.

In this section, only load versus mid span deflection curves will be presented and discussed. Generally, NWC beams displayed similar load deflection curve to the LWAC ones regardless of the presence of steel fibres. Figures 5.1 and 5.2 show an idealization of the load deflection behaviour for non-fibrous and fibrous NWC and LWAC beams respectively. Four distinct stages can be used to define load deflection curves for all beams; pre-cracking stage that starts from zero load up to the initiation of the first crack, post-cracking stage that starts from the initiation of multiple hairline cracks up to the

yielding of reinforcement, third stage that starts from the yielding of reinforcement up to the ultimate load (peak load), fourth stage that starts at the peak load up to the failure of beams.

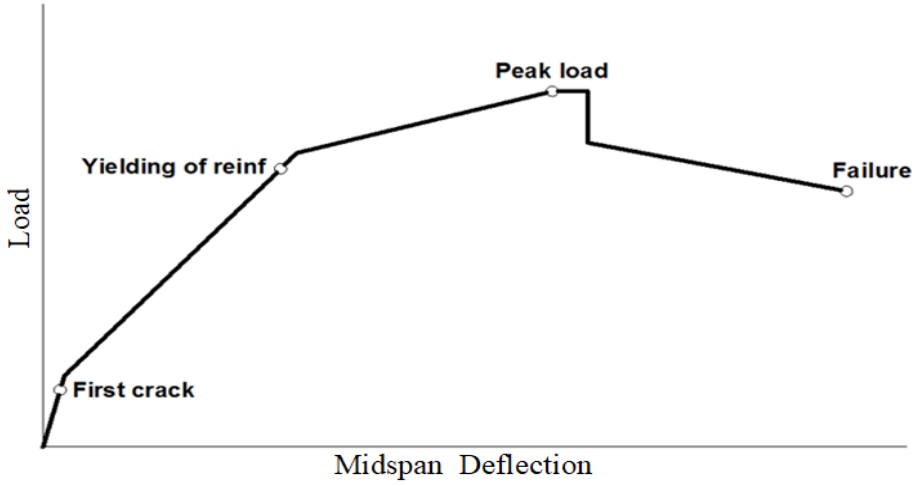

Figure 5.1: Load Deflection Curve idealization for non-Fibrous Beams.

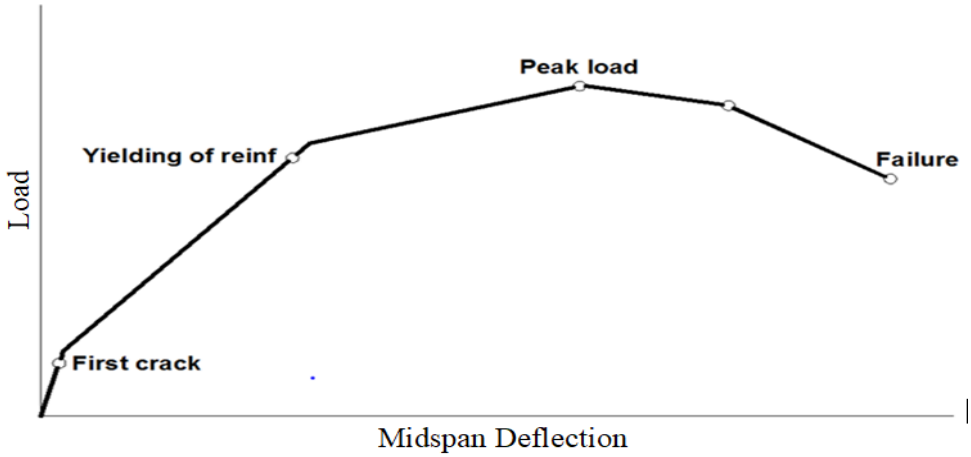

Figure 5.2: Load Deflection Curve Idealization for fibrous Beams.

Figures 5.3 and 5.4 show the load deflection curves for all NWC and LWAC beams, which will be referred to as NB and LB throughout the discussion.

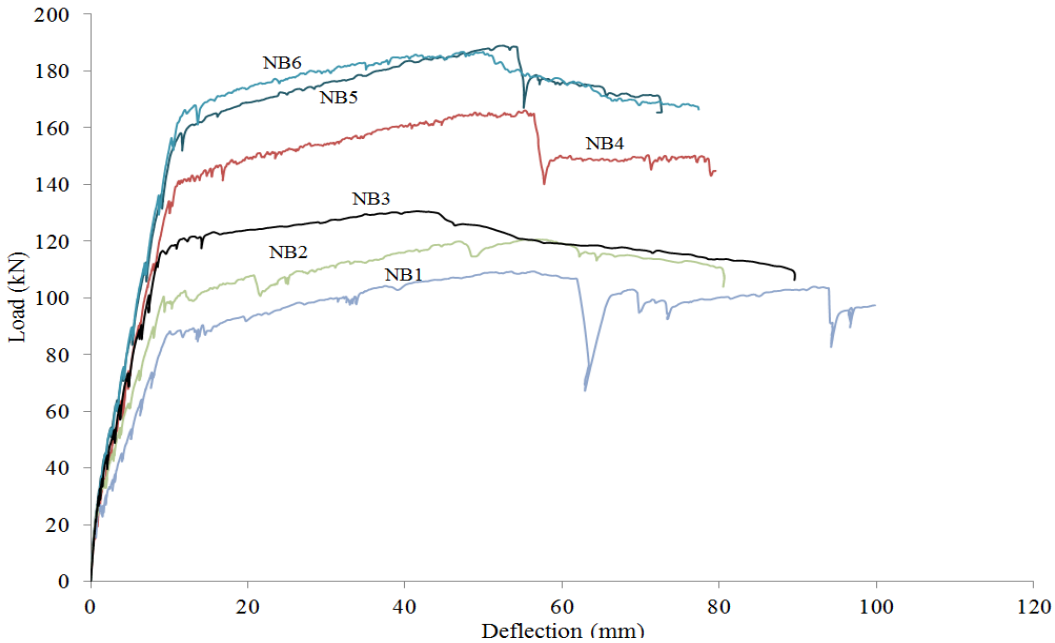

Figure 5.3: Load vs. Central Deflection for NWC Beams.

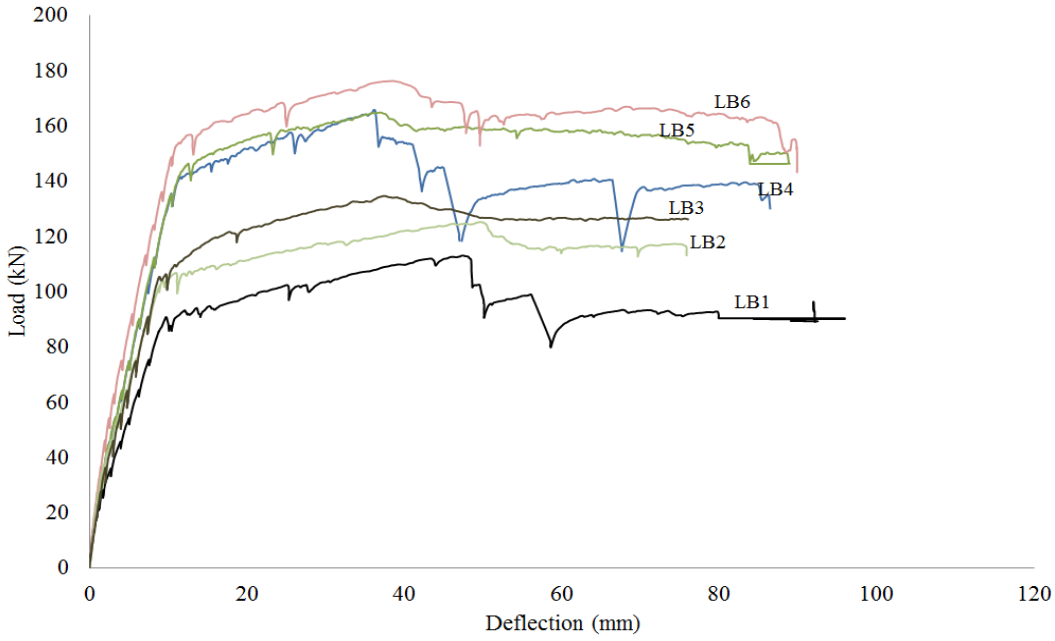

Figure 5.4: Load vs. Central Deflection for LWAC Beams.

For all beams, the first stage had a steeper slope in comparison with the second stage; this can be attributed to the stiffness of un-cracked beams which is higher than the stiffness after cracking occurs. When the applied load was increased up to a certain level, flexural cracks formed in the tension side of the beams leading to a gradual reduction in the stiffness. The transition between the two lines was smooth, which indicated that beams did not suddenly lose their un-cracked stiffness when the cracks occurred. The slope of the post-cracking stage continued to be approximately consistent with the increase of load up to the yielding of the tensile steel.

In the fourth stage, after the peak load is reached, the spalling of concrete cover occurred, and the beams started to gradually lose their load carrying-capacity. The loss of load carrying capacity when the compressed concrete zone crushed appears to be interrelated to the existence of steel fibres. A sudden drop in the load carrying capacity occurred in the beams that contained no steel fibres as shown in Figure 5.1. This could be attributed to the abrupt crushing of compression concrete zone. This was accoMPanied with the spalling of the concrete cover that was caused by the buckling of the compression reinforcing bars. In addition, when steel fibres were added, the drop in the load carrying capacity was not sudden. Instead, the beams began to lose their load carrying capacity gradually due to the less brittle crushing of the compression zone as shown in Figure 5.2. Accordingly, steel fibres seemed to prevent the buckling of compression reinforcement bars, cause a gradual compression failure in the concrete, and hold the concrete cover to the core of beams.

From Table 5.1, it is apparent that the first-crack load for LWAC beams was less than that for NWC beams. It was also noted that the deflection of the LWAC beams at the

first-crack load was higher than the NWC beams. The only anomaly found was for beam LB6 which underwent less deflection compared to its identical NWC beam NB6. The stiffness of LWAC and NWC beams in the pre-cracking and post-cracking stages, load and deflection values at the first crack are represented in Table 5.1.

The stiffness of a beam is defined as a load that causes one unit displacement at the center of a beam. The pre-cracking stiffness, K_t, is the tangential value of the slope of the load deflection curve at un-cracked stage. Whereas, the post-cracking stiffness, K_{cr}, is the tangential value of the slope of the load-deflection curve after the transition stage had ended. When keeping all parameters except concrete type to be similar, the pre-cracking of LWAC beams appeared to be less than their corresponding NWC beams. This can be attributed to the lower modulus of elasticity, E_c, of the LWAC beams. For example, beam LB1 had of 29 % lesser pre-cracking stiffness compared to its identical NB1 beams with no steel fibres and 0.85 % reinforcement ratio. Also, the post-cracking stiffness of the LWAC beams was slightly less than the NWC beams with the exception of LB1 and LB6 beams as shown in Table 5.1. Beam LB6 showed 8 % higher post-cracking stiffness compared to its corresponding NB6 with 0.75 % steel fibre volume ratio and 1.50 % reinforcement ratio.

While keeping concrete type and longitudinal reinforcement ratio the same, the effect of steel fibres was observed. Like all NWC beams, LWAC beams seemed to have a stiffer pre-cracking and post cracking response when the steel fibres were added except for beams LB3 and LB5. These two beams showed smaller un-cracked stiffness compared to their identical LB1 and LB4 containing no steel fibres. Also, the cracked

stiffness for the all the NWC and LWAC beams increased with increasing steel fibre volume ratio. However, there was no consistent un-cracked stiffness trend that could be seen as a result of increasing the fibre volume ratio from 0.375 % to 0.75 %.

Table 5.1: Deflection at the First Crack Load, Cracked and Un-Cracked Stiffness Values.

Conc. type	Beam	Comp Streng f_c' MPa	Rein. Ratio ρ %	Fibre Vol. Ratio V_f %	First Crack Load P_{cr} kN	Def. at First Crack mm	Un-Cracked Stiff. K_t kN/mm	Cracked Stiff. K_{cr} kN/mm
NWC	NB1	80	0.85	0	22.20	0.84	30.39	10.35
	NB2	88	0.85	0.375	26.70	0.84	38.00	13.65
	NB3	90	0.85	0.75	31.10	1.13	32.02	15.90
	NB4	81	1.50	0	22.20	0.80	32.90	15.52
	NB5	90	1.50	0.375	26.70	0.80	40.33	17.98
	NB6	87	1.50	0.75	31.10	1.08	41.34	18.05
LWAC	LB1	81	0.85	0	18.30	0.89	23.53	10.69
	LB2	85	0.85	0.375	22.30	0.86	24.54	13.56
	LB3	86	0.85	0.75	26.70	1.17	21.10	12.90
	LB4	80	1.50	0	20.00	0.84	26.64	15.19
	LB5	80	1.50	0.375	21.60	0.98	21.94	15.44
	LB6	82	1.50	0.75	26.50	0.90	30.22	19.50

As evident from the results tabulated in Table 5.2, increasing the longitudinal reinforcement ratio increased both the un-cracked and cracked stiffness for both types of concrete. For instance, beam NB3 that contained 0.85 % reinforcement ratio had 16.0 % lower un-cracked stiffness and had 29.1 % lower cracked stiffness compared to its identical NB6 with 1.50 % steel ratio. Unlike other beams, the LB5 beam with 1.50 % reinforcement ratio possessed a lower cracked stiffness compared to its identical LWAC beam LB2 with 0.85 % reinforcement ratio.

The load and defection at yielding of the flexural reinforcement, and the ultimate load, and the corresponding deflection are presented in Table 5.2. It can be seen that with the exception of beam LW6, the yielding load for NWC and LWAC beams increased with the addition of steel fibres. For example, non-fibrous beam LB1 had a yielding load of 74.34 kN compared to 85.7 kN for LB2 with 0.375 % fibre volume ratio and same longitudinal reinforcement ratio. The deflection at the yielding load was also influenced by the addition of steel fibres. In general, the addition of steel fibres seemed to decrease the deflection at the yielding load for both types of concrete.

It can be also observed that the change in steel fibre volume ratio increased the load at which the longitudinal reinforcement yielded for both types of concrete. In addition, it was found that the concrete type had no significant effect on the yielding load since there were no trends that can be noted. From Table 5.2, it is evident that the increase of reinforcement ratio increased the yielding load for both LWAC and NWC beams.

The load-deflection curves for the LWAC beams and their identical NWC beams are shown in Figures 5.3 to 5.6. It can be seen that the LWAC beams were to some extent close to the NWC beams in terms of the ultimate load. As shown in the Table 5.2, the slight differences in the ultimate load between the LWAC and NWC beams can be attributed to the different compressive strength of each beam. Similar to yielding load, the addition of steel fibres resulted in an increase the ultimate load for both LWAC and NWC beams. However, LB5 beam with 0.375 % fibre volume ratio and 1.50 % longitudinal reinforcement ratio showed no increase in the ultimate load. In general, adding 0.75 % fibre volume ratio to either LWAC or NWC beams resulted in an increase in the ultimate load by 14 %. It was also noted that when keeping all other parameters other than

concrete type to be the same, LWAC beams showed less deflection values at the ultimate load compared to their corresponding NWC beams. For both types of concrete, the increase in steel fibre volume ratio increased the ultimate load. For example, an increase of 8 % in the ultimate load was observed for beam LW3 with 0.75 % fibre volume ratio compared to LB2 with 0.375 % fibre volume ratio and same longitudinal reinforcement. However, an anomaly was noticed in beams NW6 in compression to its identical NB5 beam with same steel ratio and different fibre volume ratio.

The load-deflection curves for LWAC and NWC beams that have different reinforcement ratios are shown in Figures 5.5 to 5.10. It could be noticed that increasing the longitudinal reinforcement ratio increased the ultimate load and yield load at the same time. Also, increasing the longitudinal reinforcement ratio appeared on average to decrease the deflection of the ultimate load for both the LWAC and NWC beams.

Table 5.2: Central Deflection Values of The Yielding Load and Ultimate load.

Conc. Type	Beam	Comp. Streng f_c' MPa	Rein. Ratio ρ %	Fibre volume Ratio V_f %	Yield Load P_y kN	Yield Load Def. Δ_y mm	Ult. Load P_u kN	Ult. Load Def. Δ_u mm
NWC	NB1	80	0.85	0	77	8.32	109	56.26
	NB2	88	0.85	0.375	82	7.17	121	56.91
	NB3	90	0.85	0.75	87	5.98	131	41.71
	NB4	81	1.50	0	118	8.57	166	55.21
	NB5	90	1.50	0.375	123	7.95	189	52.62
	NB6	87	1.50	0.75	125	7.81	187	47.39
LWAC	LB1	81	0.85	0	74	7.70	113	47.38
	LB2	85	0.85	0.375	86	6.96	125	49.63
	LB3	86	0.85	0.75	95	7.92	135	37.55
	LB4	80	1.50	0	109	8.10	165	36.11
	LB5	80	1.50	0.375	111	8.15	165	36.98
	LB6	82	1.50	0.75	107	6.60	176	38.39

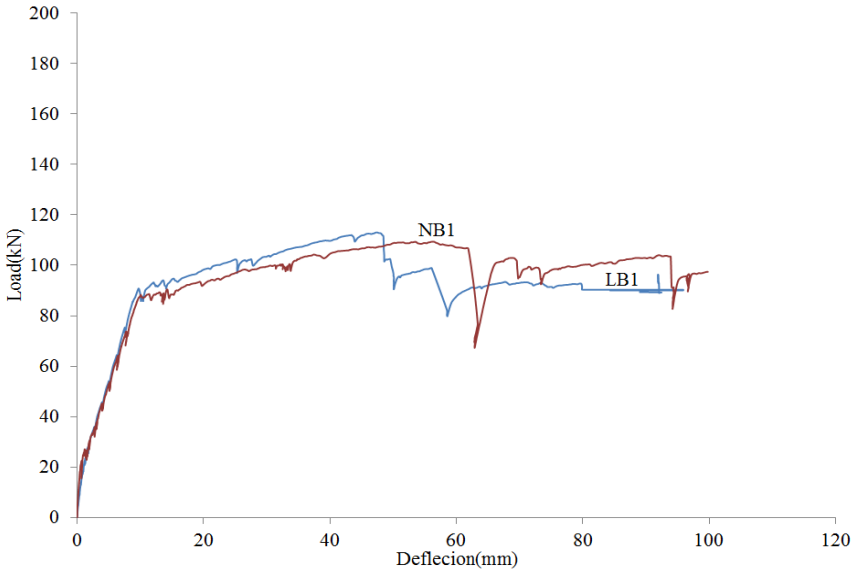

Figure 5.5: Load vs. Central Deflection for NWC and LWAC Beams with V_f= 0% and ρ = 0.85%.

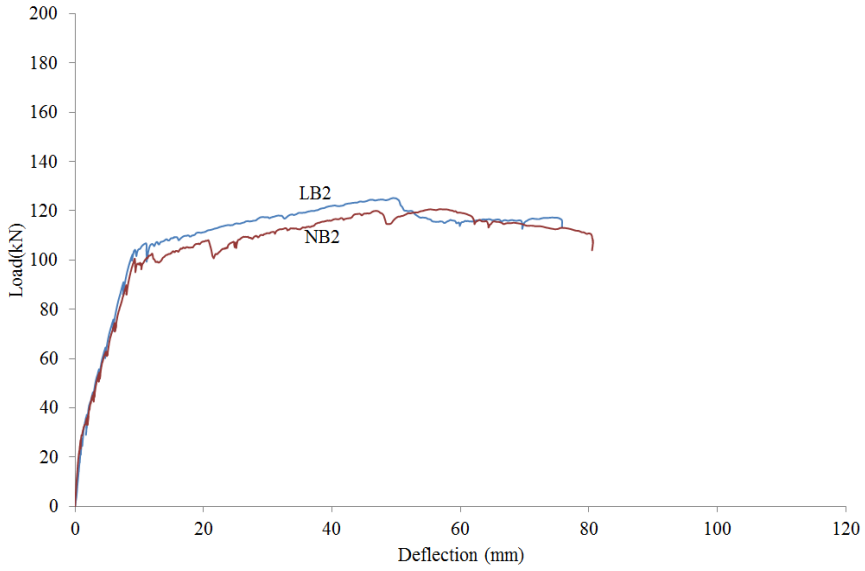

Figure 5.6: Load vs. Central Deflection for NWC and LWAC Beams with V_f = 0.375% and ρ = 0.85%.

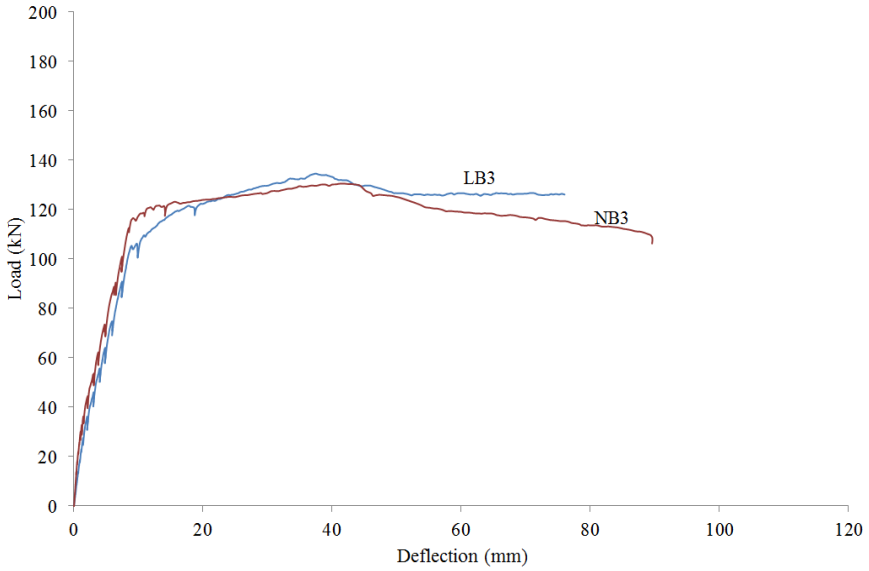

Figure 5.7: Load vs. Central Deflection for NWC and LWAC Beams with V_f = 0.75% and ρ = 0.85%.

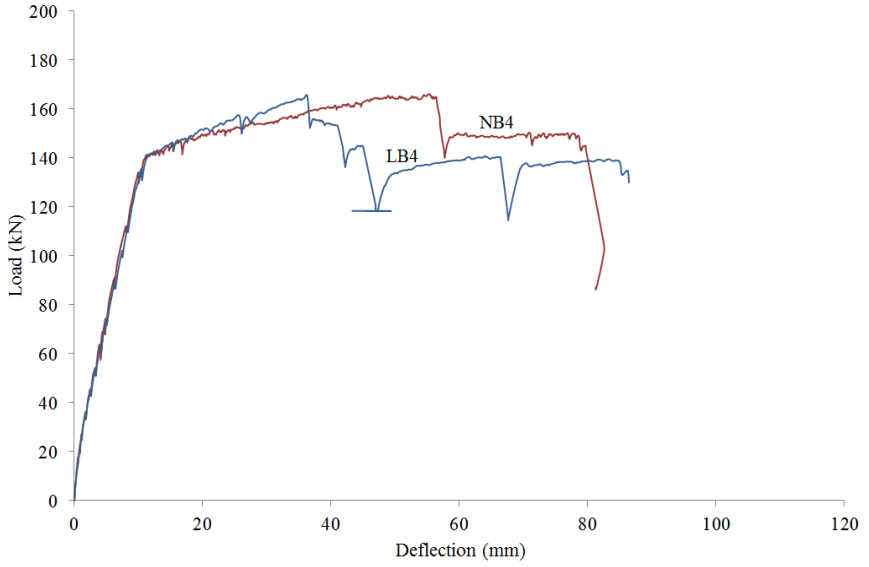

Figure 5.8: Load vs. Central Deflection for NWC and LWAC Beams with V_f = 0% and ρ = 1.50%.

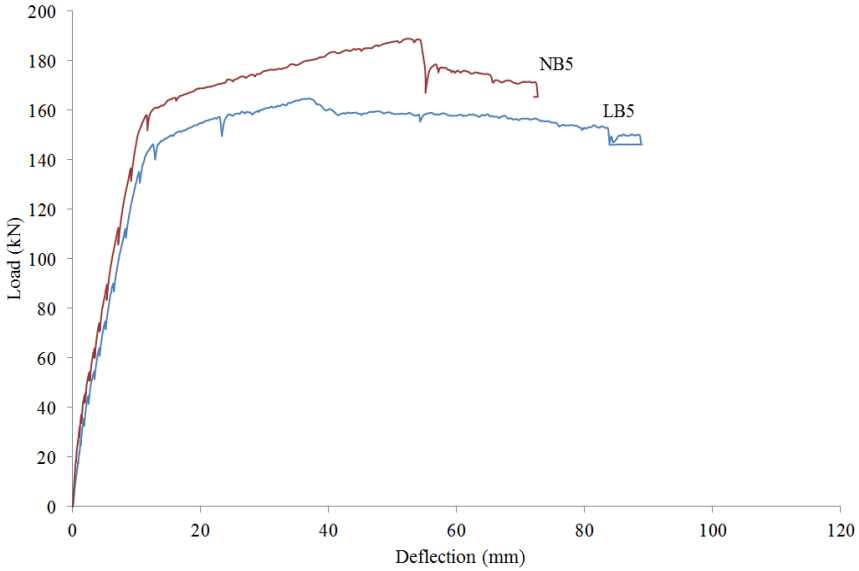

Figure 5.9: Load vs. Central Deflection for NWC and LWAC Beams with V_f = 0.375% and ρ = 1.50%.

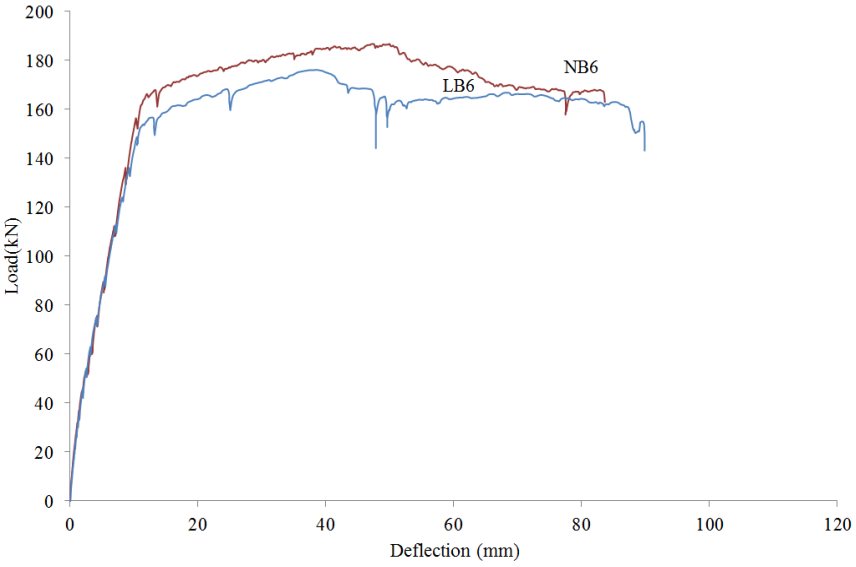

Figure 5.10: Load vs. Central Deflection for NWC and LWAC Beams with V_f = 0.75% and ρ = 1.50%.

5.3 Ductility

Ductility can be defined as the ability of the beam to perform inelastic behaviour and absorb energy. In other words, it is the measure of the capacity of the beam to undergo a deformation at or close to the failure without losing a significant amount of flexural strength. Three different indexes can be used to evaluate the ductility. These indexes include displacement ductility index, curvature ductility indexes and rotation ductility index. Herein, the displacement ductility index is considered and discussed. Efforts were made to continuously monitor the curvature within the constant moment zone. However, information needed on curvature was insufficient because steel strain gauges stopped reading before the beams reached their ultimate load capacity.

The displacement ductility index, $\mu_{\Delta u}$, is quantified as the ratio between the deflection measured at the ultimate load, Δ_u, to the deflection at yielding of the longitudinal steel, Δ_y. An additional definition of the displacement ductility index was also considered and calculated. The displacement ductility index $\mu_{\Delta f}$ was also defined as the ratio between the deflection at the failure load Δ_f to the deflection at the yielding load Δ_y. The Failure load was defined as roughly 85 % of the ultimate load in the descending branch of the load-deflection curve. Hence, the ductility indexes are defined as:

$$\mu_{\Delta u} = \frac{\Delta_u}{\Delta_y} \quad \text{or, and} \quad \mu_{\Delta f} = \frac{\Delta_f}{\Delta_y} \tag{5.1}$$

Table 5.3 shows the displacement ductility indexes calculated according to the two presented definitions. Figure 5.11 and 5.12 show the ductility indexes for the NWC and LWAC beam, respectively. It can be seen that that $\mu_{\Delta u}$ of LWAC beams varied from 6.07 to 7.94 and from 4.46 to 7.13 for the NWC beams. This indicates that the $\mu_{\Delta u}$ of NWC beams was higher than the LWAC beams.

Also, the results indicate that the addition of steel fibres enhanced the ductility of the LWAC beams. In coMParison to beam LB1 with no steel fibres and 0.85 % steel ratio, $\mu_{\Delta f}$ increased by 67.5 % for beam LB2 that contained steel fibre volume ratio of 0.375 %, and increased by 72.6 % for beam LB3 with 0.75 % steel fibre volume ratio. An increase in the ductility of LWAC beams was also found based on the displacement ductility index, $\mu_{\Delta u}$, except for beam LB3 where a reduction of 22.9 % in ductility occurred.

The ductility of the NWC beams based on the two definitions increased in the presence of steel fibres. For example, an improvement of 92.7 % in $\mu_{\Delta f}$ was gained in beam NB5 with 0.375 % fibre volume ratio compared to its identical beam NB4 with no steel fibres. However, for the same beam NB5, an improvement of only 1.8 % in the ductility $\mu_{\Delta u}$ was obtained. It was also noted that when keeping all other parameters the same, increasing steel fibre volume form 0.375 % to 0.75 % resulted in an increase in the displacement ductility index, $\mu_{\Delta f}$, of both the LWAC and NWC beams. Beams LB6 and NB6 beams with 0.75 % steel fibre volume ratio improved by 24 % and 10.9 %,

respectively, compared to their corresponding beams with 0.375 % steel fibre volume ratio. However, the calculations of displacement ductility index in accordance to the deformation at the ultimate load, Δ_u , showed a decrease in the ductility as a result of increasing the steel fibre volume ratio form 0.375 % to 0.75 % for both NWC and LWAC beams, with the exception of beam LB6.

Table 5.3: Ductility Measurement at Ultimate and Failure Load.

Beam	Reinf. Ratio	Fibre Vol. Ratio	Def. at Yielding	At Ultimate Load		At Failure Load	
	ρ %	V_f %	Δ_y mm	Δ_u mm	$\mu_{\Delta u}$	Δ_u mm	$\mu_{\Delta f}$
NB1	0.85	0	8.32	56.26	6.76	61.89	7.44
NB2	0.85	0.375	7.17	56.91	7.94	80.48	11.22
NB3	0.85	0.75	5.98	41.71	6.97	87.92	14.70
NB4	1.50	0	8.57	55.21	6.44	57.67	6.73
NB5	1.50	0.375	7.95	52.62	6.62	103.14	12.97
NB6	1.50	0.75	7.81	47.39	6.07	112.37	14.39
LB1	0.85	0	7.70	47.38	6.15	50.06	6.50
LB2	0.85	0.375	6.96	49.63	7.13	75.82	10.89
LB3	0.85	0.75	7.92	37.55	4.74	88.85	11.22
LB4	1.50	0	8.10	36.11	4.46	42.01	5.19
LB5	1.50	0.375	8.15	36.98	4.54	88.93	10.91
LB6	1.50	0.75	6.60	38.39	5.82	89.84	13.61

The spacing of the lateral ties was 200 mm. Using steel fibres seemed to reduce the possibility of buckling of the compression bars which causes the spalling of the concrete cover and lead to the disintegration of the confined concrete core. Therefore, the presence of fibres prevented the sudden loss of the ultimate capacity which was positively reflected on the displacement ductility index, $\mu_{\Delta f}$. Figures 5.13 and 5.14 show a crushed

cover concrete and buckled compression bars in beam LB4 with no steel fibres, and reinforcement ratio of 1.50 % and nominal ties at a spacing of 200 mm. This bucking can be attributed to unsupported length of the compression bars which was the ties spacing of 200mm.

For non-fibrous LWAC and NWC beams, increasing the reinforcement ratio caused both displacement ductility indexes to decrease. It is important to mention that, the addition of steel fibres improved the displacement ductility index , $\mu_{\Delta f}$, of beams containing higher reinforcement ratio and made them sometimes as ductile as their corresponding beams with lesser reinforcement ratio. For example, for the same amount of steel fibres, beam LB2 with steel ratio of 0.85 % possessed 0.18 % lesser $\mu_{\Delta f}$ compared to its identical beam LB5 with reinforcement ratio of 1.50 %.

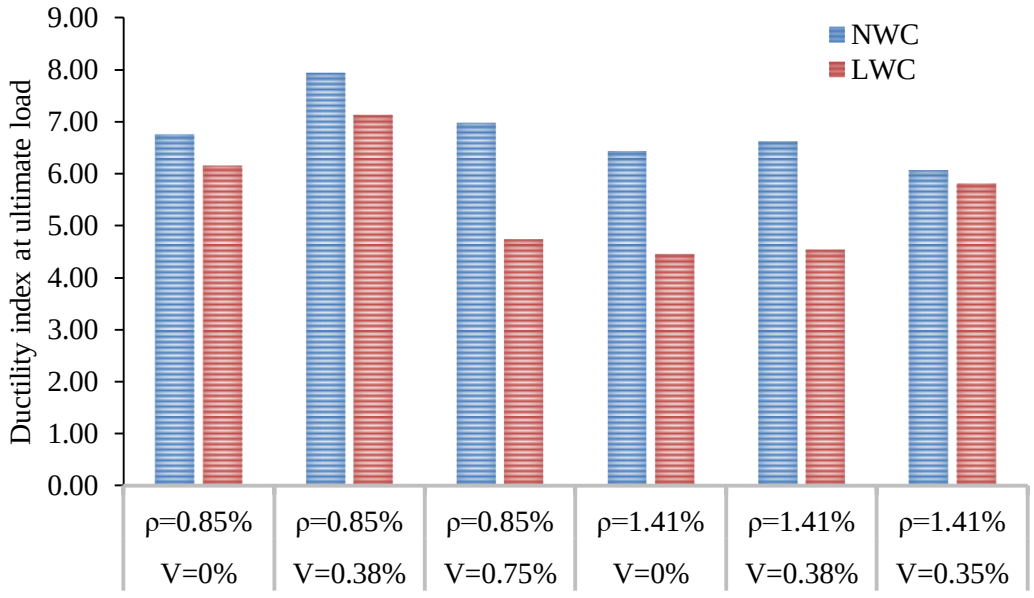

Figure 5.11: Effect of Fibres and the Steel Ratio on the Ductility Measured at the Ultimate Load.

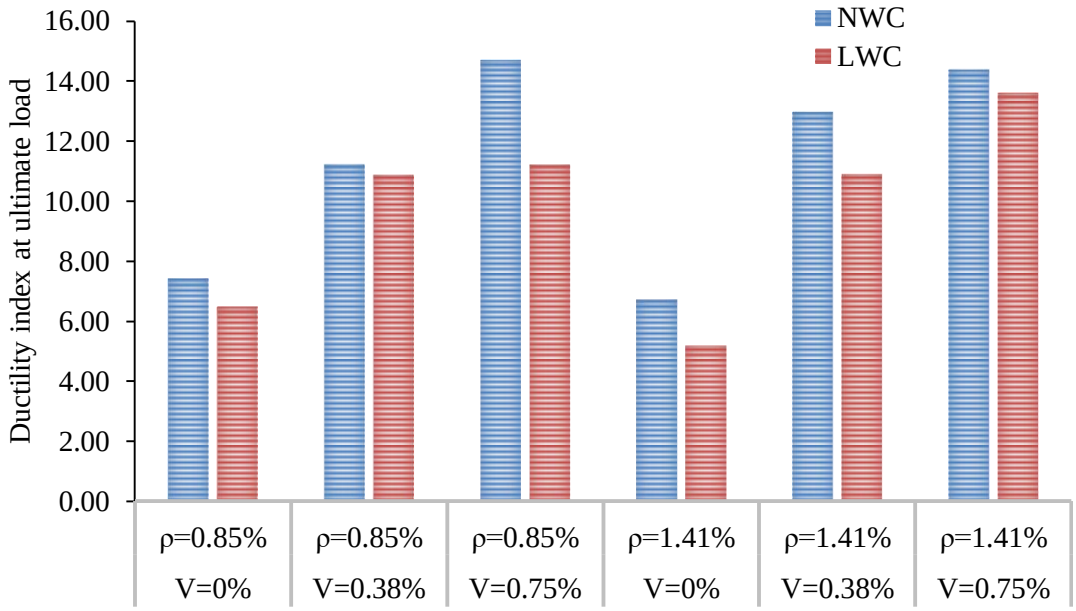

Figure 5.12: Effect of Fibre and The Steel ratio on The Ductility Measured at The Failure Load.

Figure 5.13: Crushing of the Concrete Cover in Beam LB4.

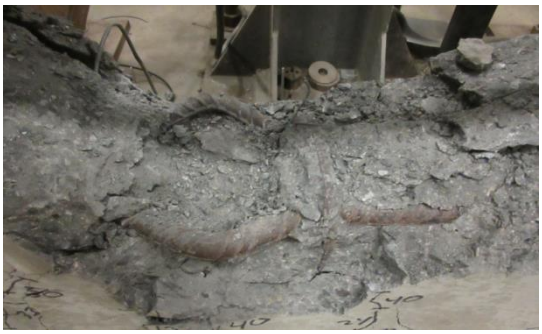

Figure 5.14: Buckled Compression Reinforcement in Beam LB4.

5.4 Prediction of the Deflection at Service Load

In this section, the midspan deflection measurements at service load are compared with those predicated using the elastic bending theory. Two different approaches were used to calculate the flexure rigidity of the beams (Branson method 1965, and the mean moment-curvature method).

The instantaneous deflection of a reinforced concrete members can be determined when the tension stiffening behaviour is considered. When using the elastic bending theory expressed by Eq. 5.1, the tension stiffening effect is considered through the use of an average effective second moment of area, I_e. Different empirical methods are suggested to calculate the average effective second moment of area. The well-known equation developed by Branson (1965) is considered. This equation was developed for normal reinforced concrete beam and is adopted by ACI318-14 and CSA-A23.3-14 codes. The average effective second moment of area, I_e, is established by empirically interpolating between the cracked moment of inertia, I_{cr} at a given load level, and un-cracked moment of inertia, I_g.

$$\delta_s = \frac{M_a}{24E_cI_e}\left(3L^2 - 4a^2\right) \tag{5.1}$$

where

$$I_e = I_{cr} + \left(I_g - I_{cr}\right)\left(\frac{M_{cr}}{M_a}\right)^3 \le I_g$$

Where δ_s is the deflection at assumed service load, M_{cr} is the cracking moment, M_a is applied moment, L is the span, a is the shear span, E_c is the modulus of elasticity of concrete.

The deflection of the beam can be also calculated using conjugate beam method. In this method, the tension stiffening effect is considered in using the mean moment-curvature relationship. For normal reinforced concrete beam, the EC2-91 code adopts Eq. 5.2 to determine the mean moment-curvature relationship. This equation derived by the interpolation between the cracked and un-cracked curvatures by employing the coefficient (ζ).

$$\varphi_m = (1-\zeta)\varphi_1 + \zeta\varphi_2 \tag{5.2}$$

where

$$\varphi_1 = \frac{M_a}{E_cI_g}$$

$$\varphi_2 = \frac{M_a}{E_cI_{cr}}$$

$$\zeta = 1 - \beta_1 \beta_2 \left(\frac{M_r}{M_a} \right)^2 = 1 - (0.5)(0.8) \left(\frac{M_r}{M_a} \right)^2$$

where φ_m is the mean moment-curvature, φ_1 is the un-cracked curvature, φ_2 is the cracked curvature , M_{cr} is the cracking moment, M_a is the applied moment. Thus, The cracked member has a mean flexural rigidity expressed as :

$$(EI)_m = \frac{M_a}{\varphi_m} \tag{5.3}$$

After determining the mean flexural rigidity, $(EI)_m$, the conjugate beam method is used to calculate the deflection using the $M_a / (EI)_m$ diagram. The deflection of any location in the real beam is numerically equal to the moment at the corresponding point in the conjugate beam. A comparison between the test results and the predicated response are shown in Figures 5.15 to 5.26.

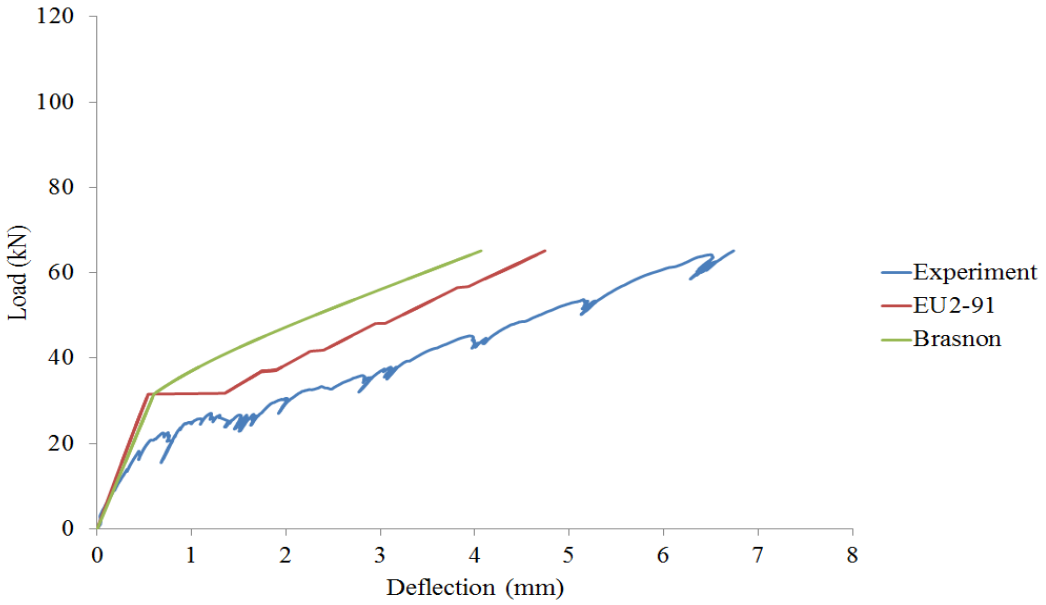

Figure 5.15: Load vs Midspan Deflection for Beam NB1.

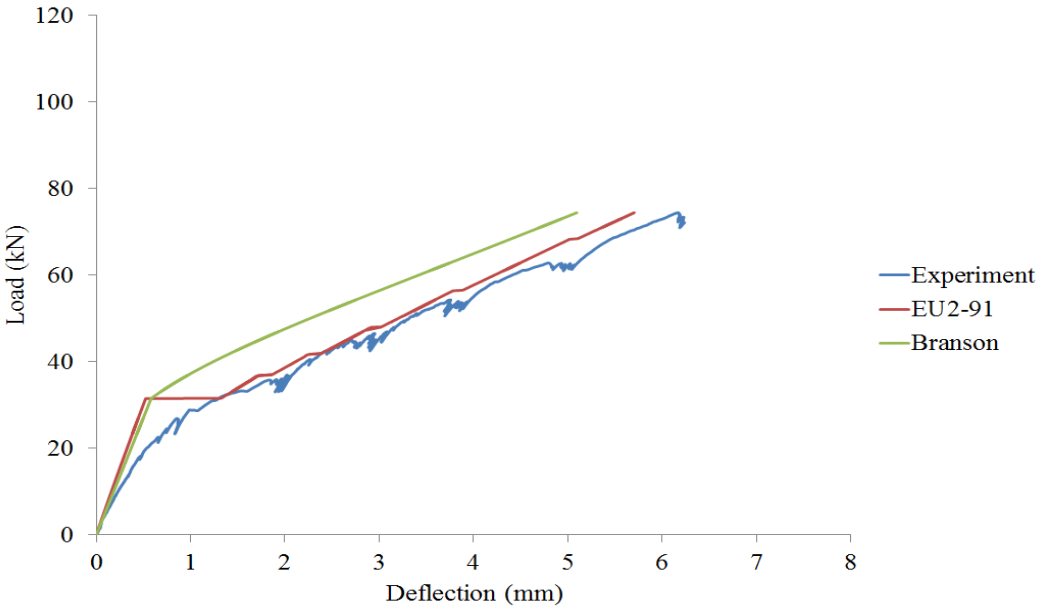

Figure 5.16: Load vs Midspan Deflection for Beam NB2.

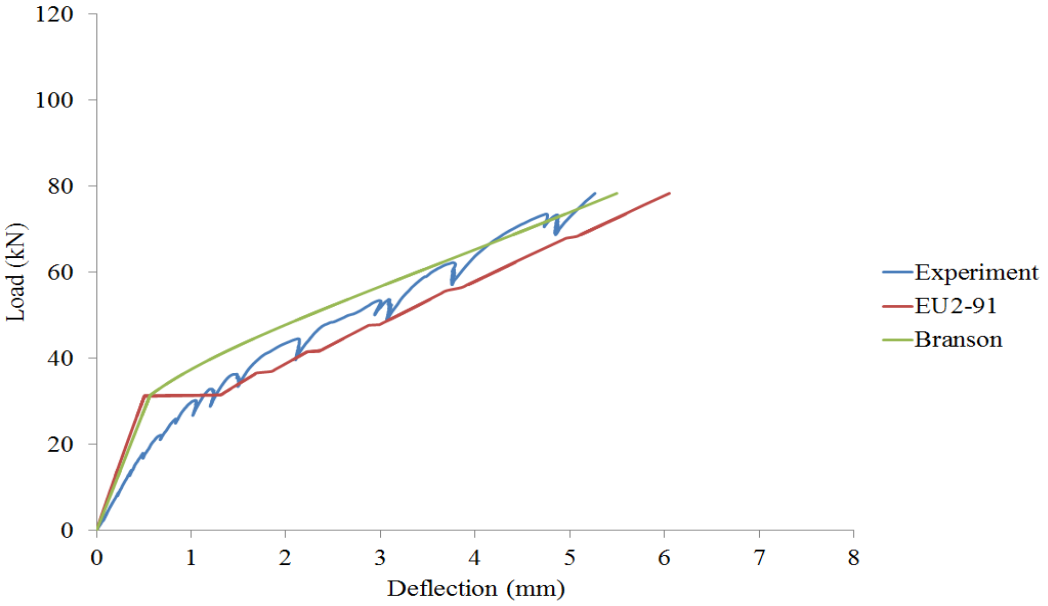

Figure 5.17: Load vs Midspan Deflection for Beam NB3.

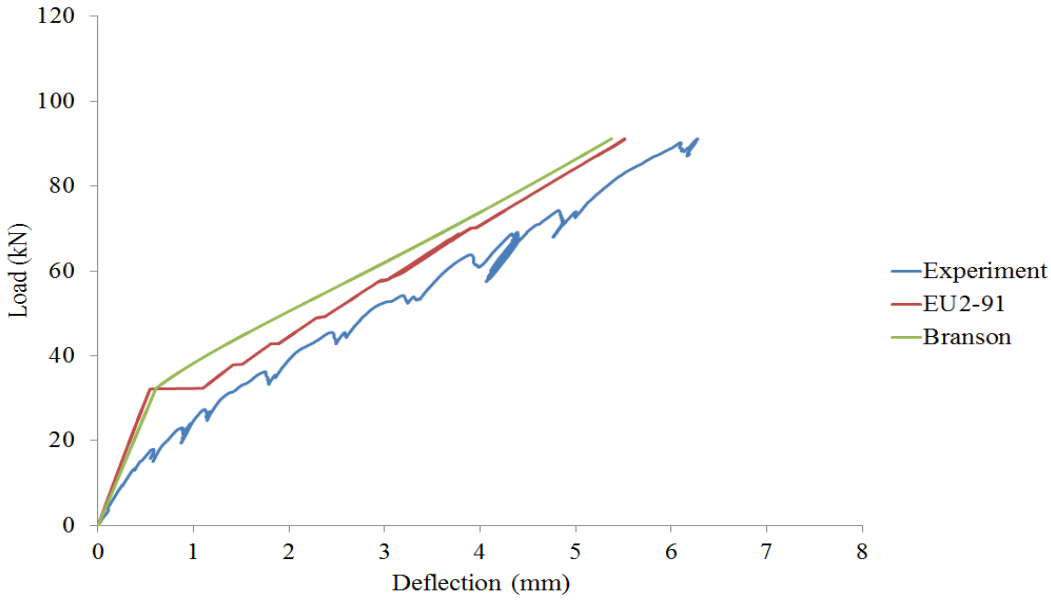

Figure 5.18: Load vs Midspan Deflection for Beam NB4.

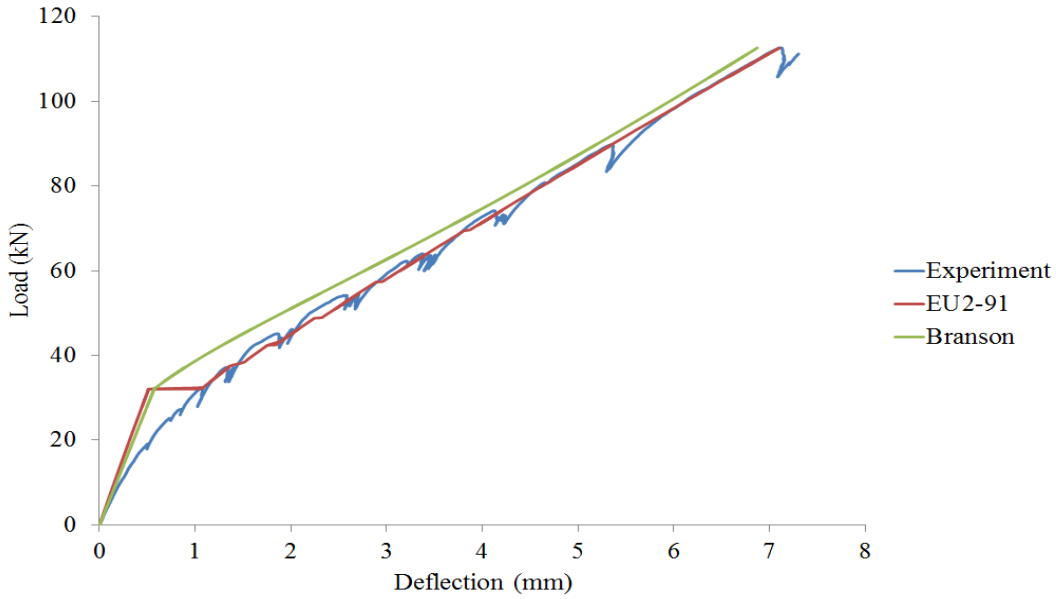

Figure 5.19: Load vs Midspan Deflection for Beam NB5.

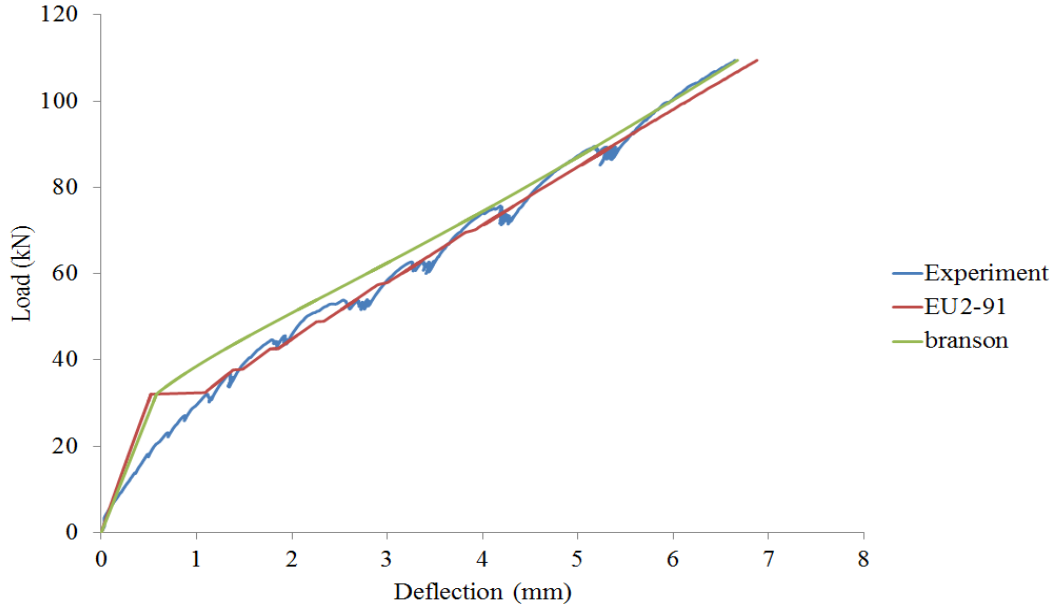

Figure 5.20: Load vs Midspan Deflection for Beam NB6.

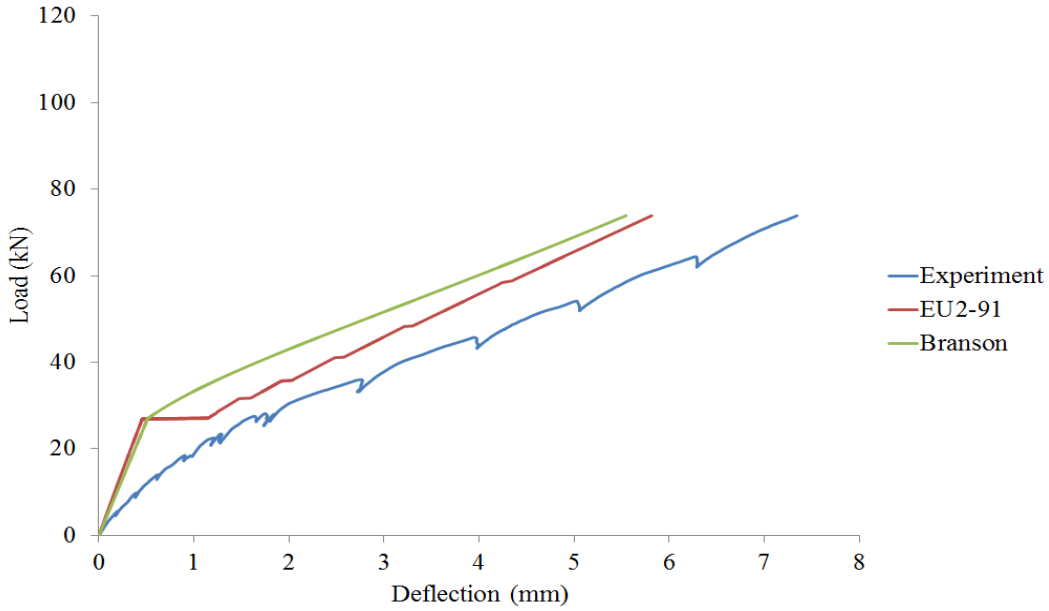

Figure 5.21: Load vs Midspan Deflection for Beam LB1.

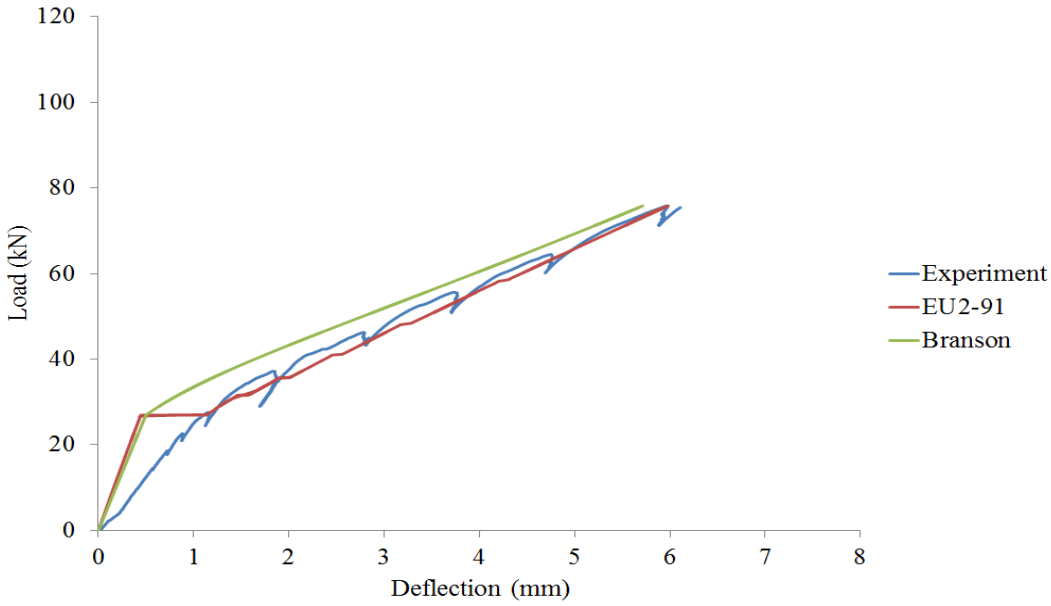

Figure 5.22: Load vs Midspan Deflection for Beam LB2.

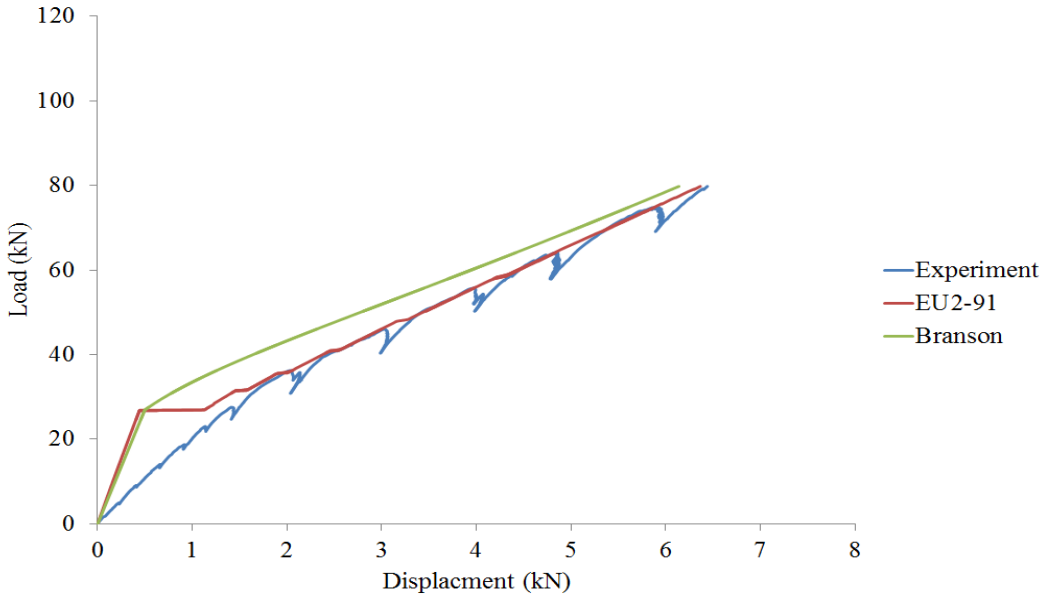

Figure 5.23: Load vs Midspan Deflection for Beam LB3.

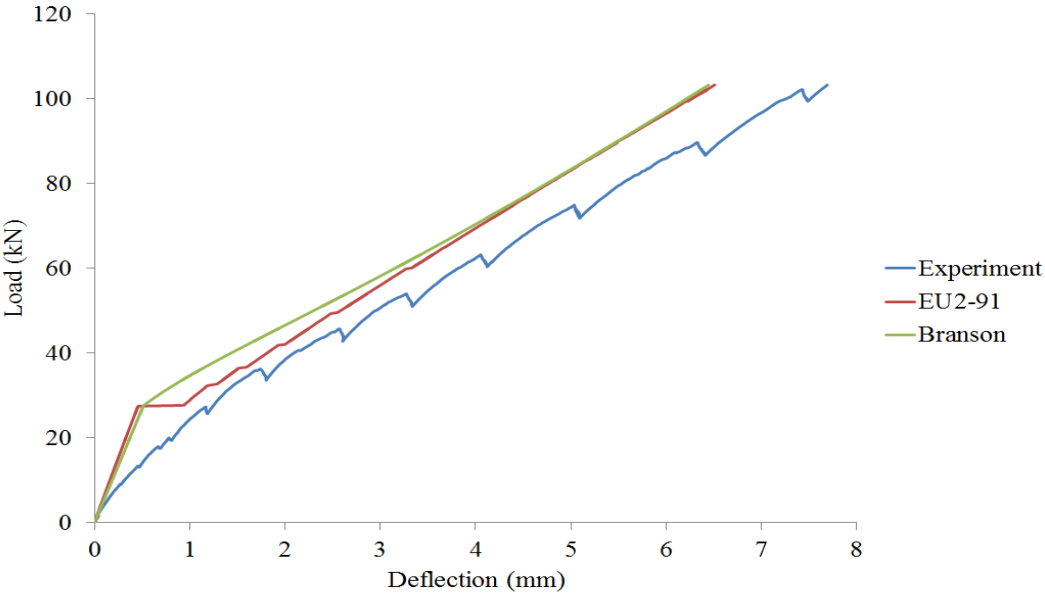

Figure 5.24: Load vs Midspan Deflection for Beam LB4.

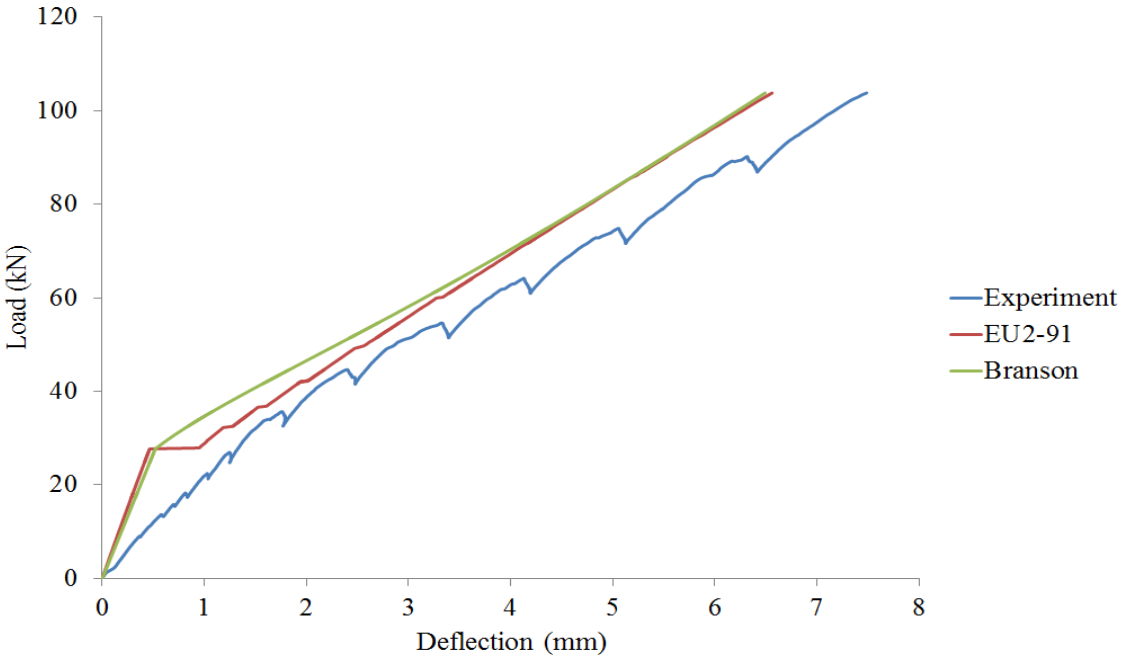

Figure 5.25: Load vs Midspan Deflection for Beam LB5.

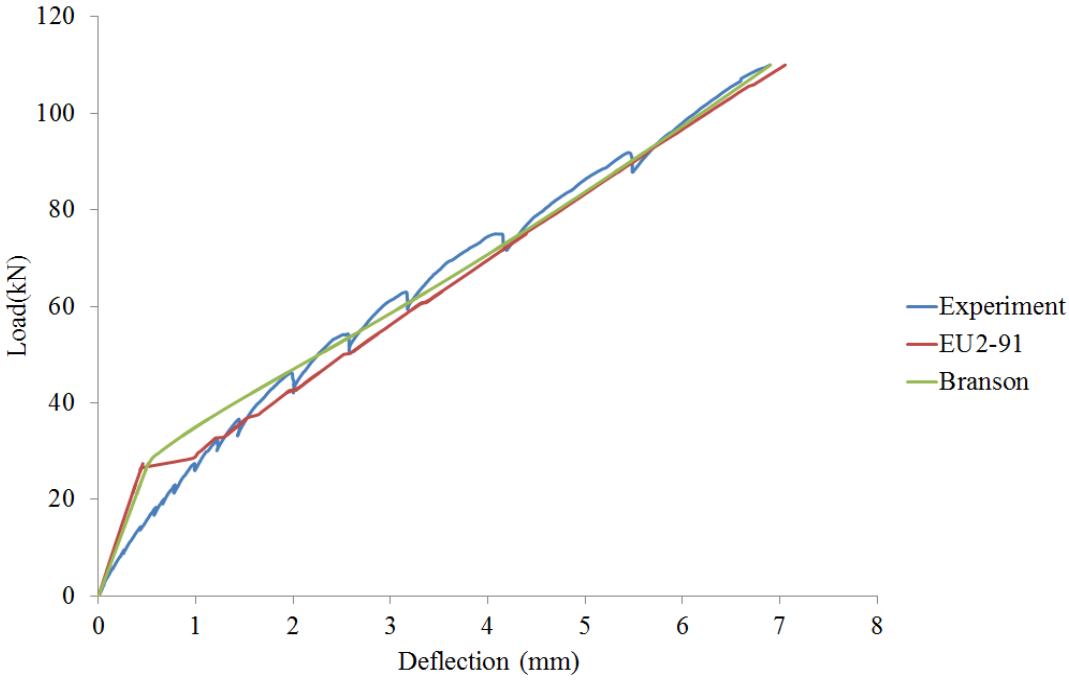

Figure 5.26: Load vs Midspan Deflection for Beam LB6.

Table 5.4 shows the comparison between the calculated and the experimental deflections at an assumed service load equal 0.45 times the ultimate load. The results indicate that both applied methods seem to be conservative when predicating the deflection at the assumed service load for both non-fibrous high strength normal and lightweight concrete beams (NB1, NB4, LB1 and LB4) . Similar observations were also reported by Rashid and Mansur (2005). This can be attributed to the reduction in the modulus of elasticity and the cracking moment due to the shrinkage and the creep effects. Thus, the modulus of elasticity and the theoretical cracking moment should be modified to account for the shrinkage and creep effect. The cracking moment for the beams are discussed in section 5.6.3 of this chapter.

It is important to mention that the tension stiffening behaviour of steel fibre reinforced concrete is different from reinforced concrete. In steel fibre reinforced concrete elements, the steel fibre carry a portion of tensile stress between and across cracks not like reinforced concrete element where all tensile stress between cracks are carried by the reinforcement . Therefore, those two models have to be modified to account for the presence of steel fibres. Nevertheless, the calculated results for fibrous NWC and LWAC beams (NB2, NB3, NB5, NB6, LB2, LB3, LB5, and LB6) appeared to be acceptable. This can be attributed to the reduced shrinkage effect due to the existence of the steel fibre.

Table 5.4: Comparison between the Calculated and Experimental Deflections at Assumed Service Load equal to 0.45 times the ultimate load.

Con. Type	Beam	Service Load	Exp. Deflection	Theoretical Deflection		Ratio of Exp. to Theoretical calculation	
		kN	mm	EC02-91	Branson	EC02-91	Branson
NWC	NB1	49	4.58	3.14	2.20	1.46	2.09
	NB2	54	3.73	3.58	2.73	1.04	1.36
	NB3	59	3.49	4.12	3.28	0.85	1.06
	NB4	75	5.09	4.32	4.11	1.18	1.24
	NB5	85	4.98	5.00	4.82	1.00	1.03
	NB6	84	4.78	4.95	4.77	0.97	1.00
LWAC	LB1	51	4.59	3.55	2.92	1.29	1.57
	LB2	56	3.96	4.02	3.51	0.98	1.13
	LB3	61	4.52	4.54	4.07	0.99	1.11
	LB4	74	4.98	4.35	4.30	1.15	1.16
	LB5	74	5.00	4.35	4.31	1.15	1.16
	LB6	79	4.52	4.69	4.65	0.96	0.97

5.5 Concrete and Reinforcement Strains

This section presents the strain development in the compressive zone of the concrete and tensile strain in flexural reinforcement for the beams. The concrete strains for both LWAC and NWC beams were measured at the centre of the beam on the compression side by means of strain gauges as mentioned earlier in Chapter 4. The loads versus concrete strains for all test beams are shown form Figures 5.27 to 5.30. The maximum compressive strain recorded at ultimate load fluctuated from 0.0033 to 0.0042 for the LWAC beams and from 0.0033 to 0.0043 for the NWC beams. Table 5.4 shows the maximum concrete strain value for each beam. It can be observed that few of the LWAC and NWC beams underwent maximum strain values that is slightly less than the limiting value of 0.0035 which is specified by the Canadian code CSA A23.3-14. On the

other hand, the limiting value adopted by the ACI318-14 code which is equal to 0.003 seemed to be conservative. Therefore, the ACI318-14 value of 0.003 appeared to be an acceptable lower bound for high strength LWAC and NWC beams with or without steel fibres. Considering all parameters employed in this study, no noticeable trend in the maximum strain values measured at ultimate loads can be identified. This can be attributed to the fact that the compression zone of all beams reached crushing.

At an assumed service load of 0.45 the ultimate load, the LWAC beams underwent higher compressive strain values compared to their identical NWC beams. For example, LB1 that contained no steel fibres and steel ratio of 0.85 % had a compressive strain value of 0.00045, whereas its identical NWC beam NB1 reached a value of 0.00040. The compressive strain value measured at the assumed service load for each beam is presented in Table 5.4.

The addition of steel fibres was observed to slightly increase the compressive strain value at assumed service load for both LWAC and NWC beams. For instance, according to control beam LB1 with 0 % steel fibre volume ratio, an increase of almost 16 % in the compressive strain value was noted for beam LB3 with 0.75 % fibre volume ratio. It should be noticed that beams with steel fibres had higher service loads. Also, the increase in fibre volume led to an increase in the service load of the beam.

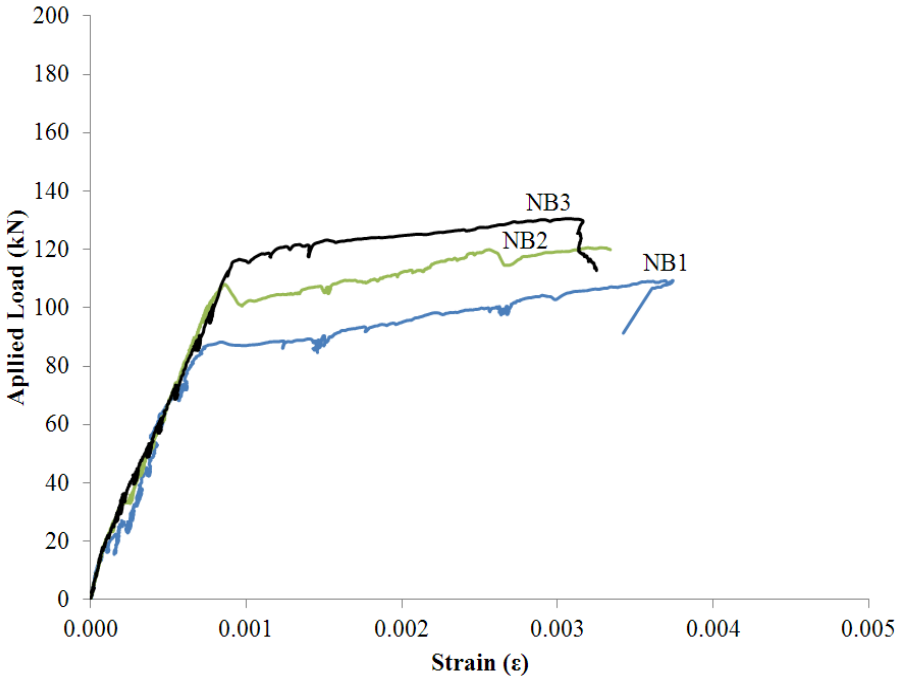

Figure 5.27: Load VS. Concrete Strain for NWC Beams with ρ = 0.85%.

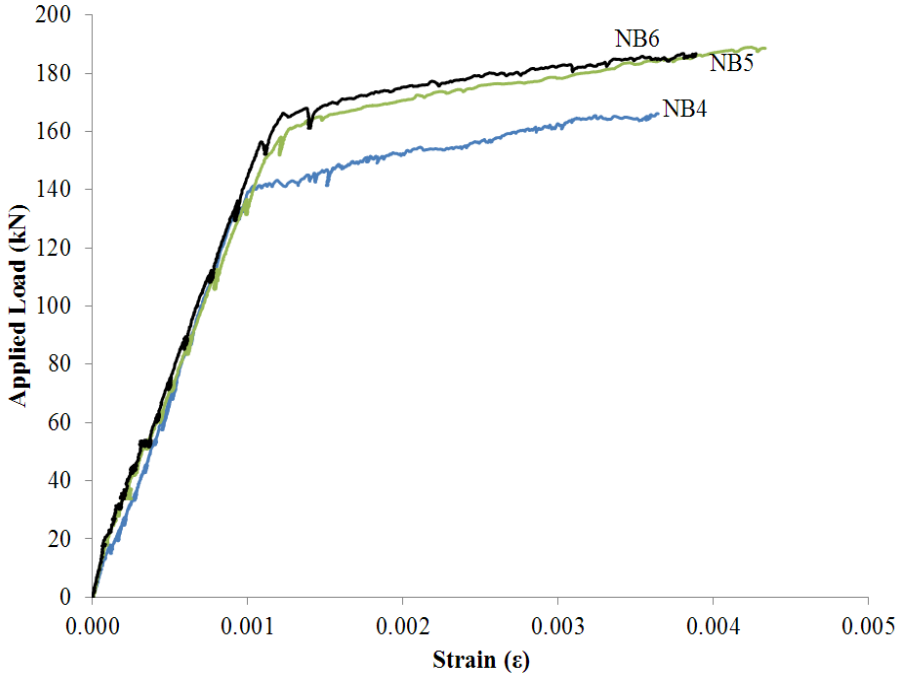

Figure 5.28: Load VS. Concrete Strain for NWC Beams with ρ = 1.50%.

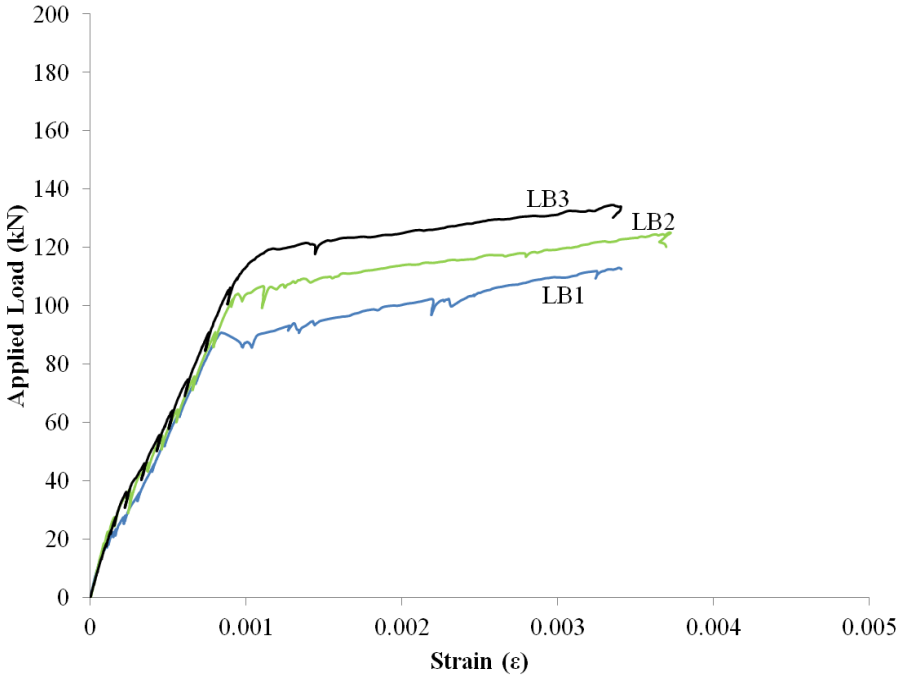

Figure 5.29: Load VS. Concrete Strain for LWAC Beams with ρ = 0.85%.

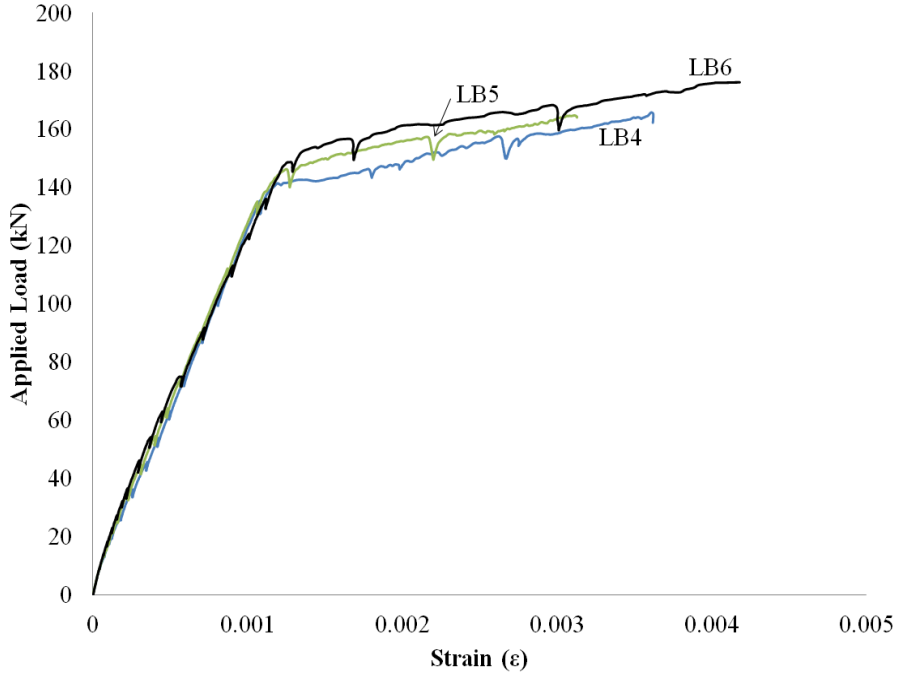

Figure 5.30 : Load VS. Concrete Strain for LWAC Beams with ρ = 1.50%.

Table 5.5: Strain in Concrete at Service and Ultimate load.

Concrete Type	Beam	Reinf. Ratio	Comp. Reinf. Ratio	Fibre Volume Ratio	Comp. Streng.	Concrete Strain at Service Load	Concrete Strain at Ultimate Load
`		ρ	$\rho_s^{'}$	V_f	$f_c^{'}$	ε_s	ε_u
		%	%	%	MPa	mm/mm	mm/mm
NWC	NB1	0.85	0.85	0	80	0.00040	0.0037
	NB2	0.85	0.85	0.375	88	0.00041	0.0033
	NB3	0.85	0.85	0.75	90	0.00043	0.0033
	NB4	1.50	0.85	0	81	0.00054	0.0036
	NB5	1.50	0.85	0.375	90	0.00060	0.0043
	NB6	1.50	0.85	0.75	87	0.00057	0.0039
LWAC	LB1	0.85	0.85	0	81	0.00045	0.0034
	LB2	0.85	0.85	0.375	85	0.00049	0.0037
	LB3	0.85	0.85	0.75	86	0.00052	0.0034
	LB4	1.50	0.85	0	80	0.00060	0.0036
	LB5	1.50	0.85	0.375	80	0.00057	0.0033
	LB6	1.50	0.85	0.75	82	0.00061	0.0042

The strain values listed in Table 5.5 indicate that, in general, there was an increasing trend in the compressive strain value measured at assumed service load with increasing the steel fibre volume ratio from 0.375 % to 0.75 % for both LWAC and NWC beams. Also, similar to NWC beam, the general trend of strain values at assumed service load of LWAC beams reveal that increasing the flexural reinforcement steel ratio was found to increase the concrete strain. For example, concrete strain values for LWAC beams containing 0.85 % reinforcement ratio rated from 0.00045 to 0.00052 and from 0.00057 to 0.00061 for LWAC beams with 1.50 % steel ratio.

As mentioned in section 3.1.3 the average yielding stress was 430 MPa and 470 MPa for the 15M and 20M bars respectively. The reinforcement strains were also measured at different locations by means of four strain gauges glued to the longitudinal

reinforcement as mention in section 4.4. The stain gauge locations were chosen at the center of the beam and at the two ends of the constant moment zone. Some of the strain gauges were damaged during the casting of the beams. Most of the gauges stopped reading at an approximation level of 0.003-0.0035 and before beams reached their ultimate capacity. This made it difficult to measure the maximum strain value of the reinforcement. Figures 5.29 to 5.30 show the load versus strain in the flexural reinforcement at the center of each beam. The figures show that the shape of the load versus steel strain for the LWAC beams is similar to those of the NWC beams. Before the yielding of the steel reinforcement, the load-strain shape for both LWAC and NWC beams can be presented as bilinear shape. The slope of the load-strain curve started to change at approximately the first crack load. The slope of the first line is steeper than the second line. The transition between the two lines is smooth as multiple hairline cracks developed and stresses were transferred to the steel reinforcement. Generally, the addition of steel fibre increased the yield load for both NWC and LWAC beams. Also, increasing the steel fibre volume ratio from 0.375 % to 0.75 % increased the yield load for NWC and LWAC beams.

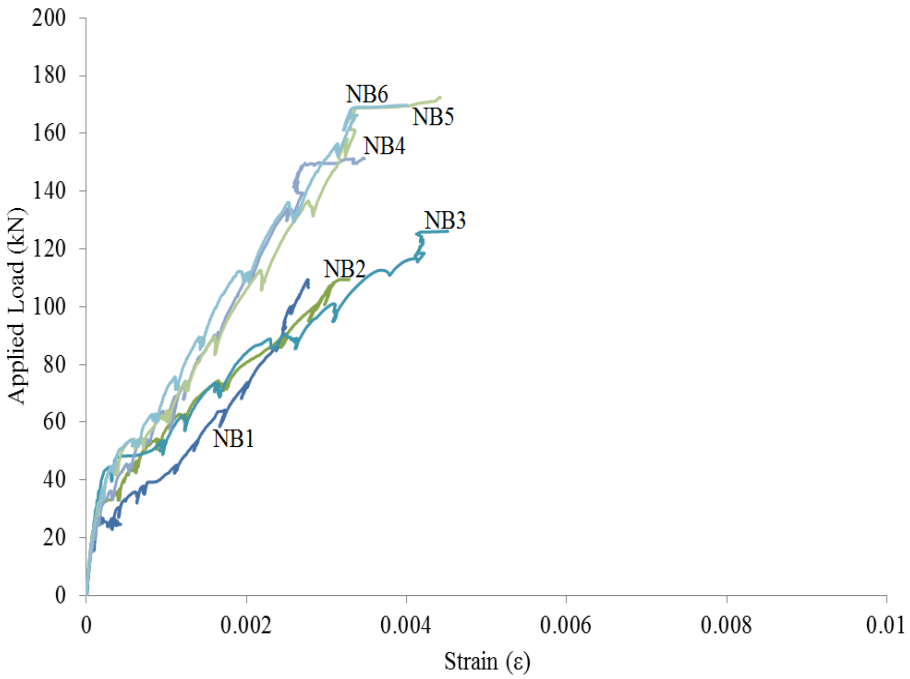

Figure 5.31: Load vs. Steel Strain for NWC Beams.

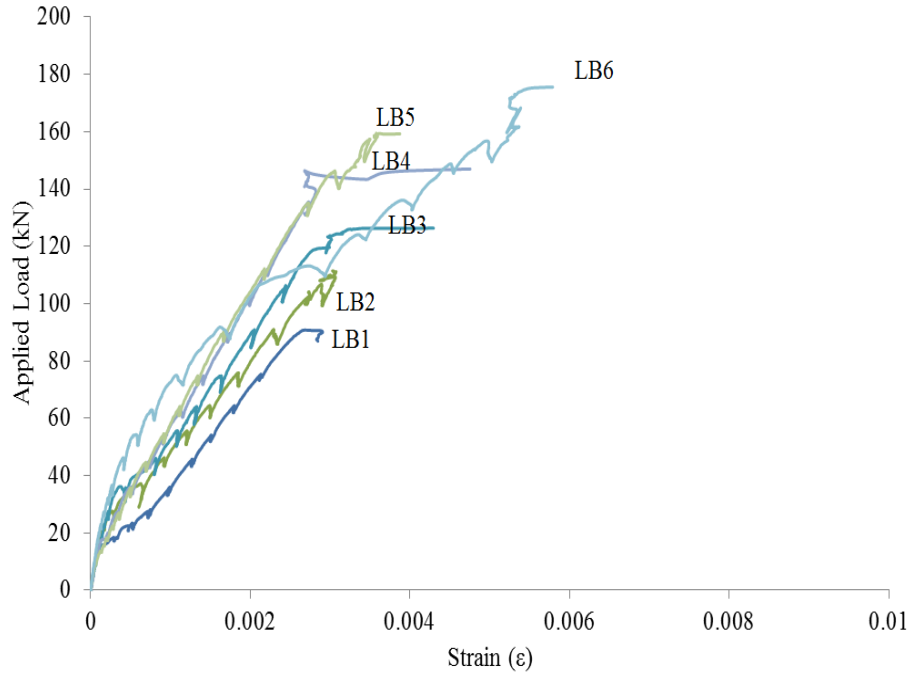

Figure 5.32: Load vs. Steel Strain for LWAC Beams.

5.6 Cracking Behaviour

5.6.1 Cracks Patterns

During all experiments, the visible cracks were marked at each load increment, and the different crack patterns were observed . Figures 5.33 and 5.34 show the crack patterns and the corresponding loads in kips for all the NWC and LWAC beams respectively. In general, the cracks developed in the pure moment zone were vertical and perpendicular to maximum tensile stress. Outside the constant moment region, the cracks propagated vertically and gradually curved afterwards due to increasing the load which had caused an increase in the shear stress. Furthermore; it can be noted that, the distribution of those cracks were almost symmetrical around the center of the beam. Smaller spacing between cracks was observed in all beams with fibres. Moreover, the trajectories of the beams containing less amount of flexural reinforcement appeared straighter than the others with higher longitudinal reinforcement ratio. The influence of the fibres on the shape of the crack pattern was not evident. On the other hand, the steel fibres had a clear iMPact on reducing the crack widths and increasing number of cracks for all beams. Moreover, the effect of steel fibres extended to slightly control the depth of cracks; where beams with no steel fibres presented a longer crack depth. Crack depth and the number of cracks at ultimate load within the constant moment zone are presented in the Table 5.6. The crack spacing is discussed in section 5.6.4 of this chapter.

Table 5.6: Maximum Crack Depth and Number of Cracks for All Beams.

Beam	Number of Crack	Max. Crack Depth	Beam	Number of Crack	Max Crack Depth

		mm			mm
NB1	7	370	LB1	8	320
NB2	8	315	LB2	11	315
NB3	9	310	LB3	11	305
NB4	8	330	LB4	11	310
NB5	9	305	LB5	13	305
NB6	10	295	LB6	15	300

In general, the crack patterns for both types of concrete were similar. However, within the serviceability limits, a higher number of cracks were developed in LWAC beams compered to corresponding NWC beams, which resulted in a decrease in the crack width and crack spacing. It was also noted that more than one crack formed beyond the service load, that was assumed and taken as 0.45 times the ultimate load. Moreover, the final number of cracks occurred within the constant moment zone which has a length of 860mm fluctuated between 8 and 15 for LWAC beams, whereas the number of cracks rated between 7 and 10 for NWC beams. Beside the noticeable impact of steel fibres on the crack spacing and crack number, the longitudinal reinforcement ratio had also an effect on the crack spacing and final crack number for both types of concrete. Beams with higher reinforcement ratio had presented less crack spacing and more crack number for both types of concrete. Moreover, the depth of the crack was also influenced by the reinforcement ratio, the depth of crack decreased as a result of increasing the ratio of longitudinal reinforcement. For both types of concrete, beams failed in flexural mode through the crushing of the concrete. In all beams, cracks initiated and propagated upwards the neutral axis reducing the compression zone. The crushing of compression concrete zone had occurred after the steel reinforcement had undergone a remarkable strain. For all beams, no horizontal cracks had been seen throughout the loading time

which indicated the absence of any bond failure. The crack spacing and crack width are discussed in details in section 5.6.4 and 5.6.7, respectively, of this chapter.

5.6.2 First Crack Initiation

For all beams, the first flexural crack developed within the constant moment zone at the tension side, where the maximum flexural tensile stress and zero shear stress occurred. As the load was increased, more cracks appeared and propagated towards the neutral axis of the beam. During the tests, the first crack was observed by the naked eye. The first crack loads and the corresponding widths of the beams are shown in Table 5.7. It seemed that steel fibre volume ratio had delayed the initiation of the first crack. Hence, the increase of steel fibres had somehow increased the load at which the first crack occurred for both high strength normal and lightweight concrete beams. The first vertical crack for the NWC beams initiated at approximately 22 kN, 27 kN, and 31 kN for beams with fibre volume ratios of 0 %, 0.375 %, and 0.75 % respectively. The difference in reinforcement ratios had negligible effect on the load at which the crack developed. However, the different types of concrete had an influence on the initiation of first crack. It was observed that the first crack loads for the high strength light weight concrete beams LWAC were lower than the corresponding once for high strength normal weight beams NWC. The first crack widths of the LWAC beams were generally wider than their corresponding NWC beams except for LB2. Three cracks occurred simultaneously in LB1. That made the first crack width of NB1 larger that in LB1. The first crack width for LB1, presented in Table 5.7, was taken as the larger reading between the three cracks.

Table 5.7: First Cracking Load and Width.

Concrete Type	Beam	Cracking Load kN	Crack width mm	Concrete Type	Beam	Cracking Load kN	Crack width mm
NWC	NB1	22.2	0.030	LWAC	LB1	18.3	0.025
	NB2	26.7	0.025		LB2	22.3	0.020
	NB3	31.1	0.025		LB3	26.6	0.040
	NB4	22.2	0.025		LB4	20.0	0.035
	NB5	26.7	0.020		LB5	21.6	0.035
	NB6	31.4	0.020		LB6	26.5	0.020

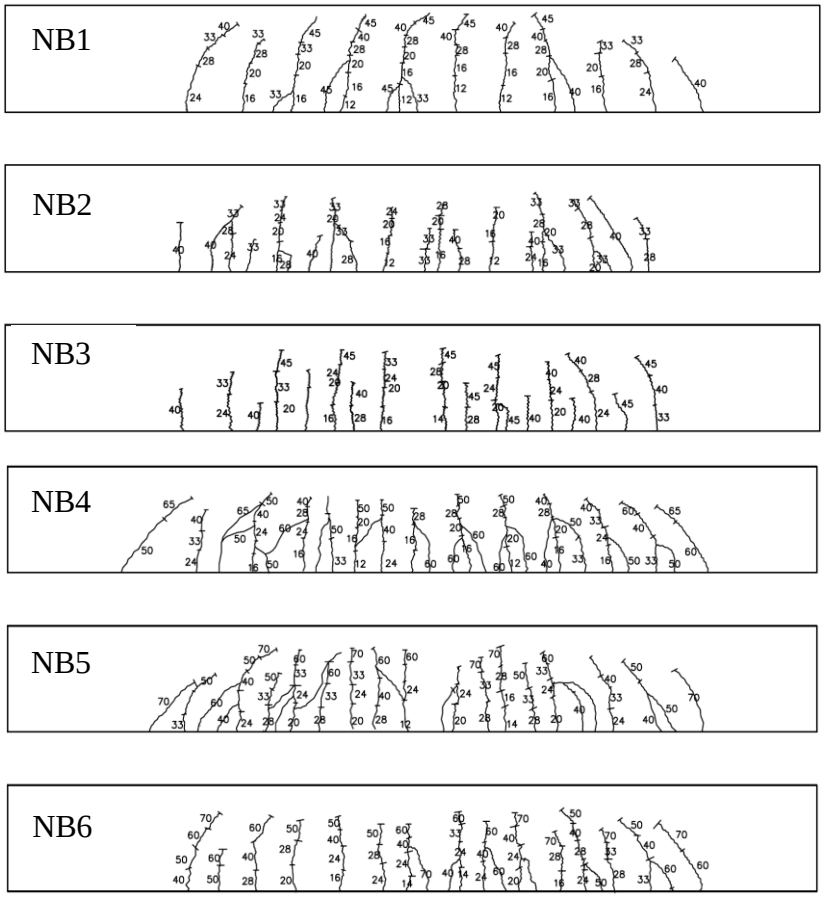

Figure 5.33: Crack Patterns for NWC Beams at Ultimate Load.

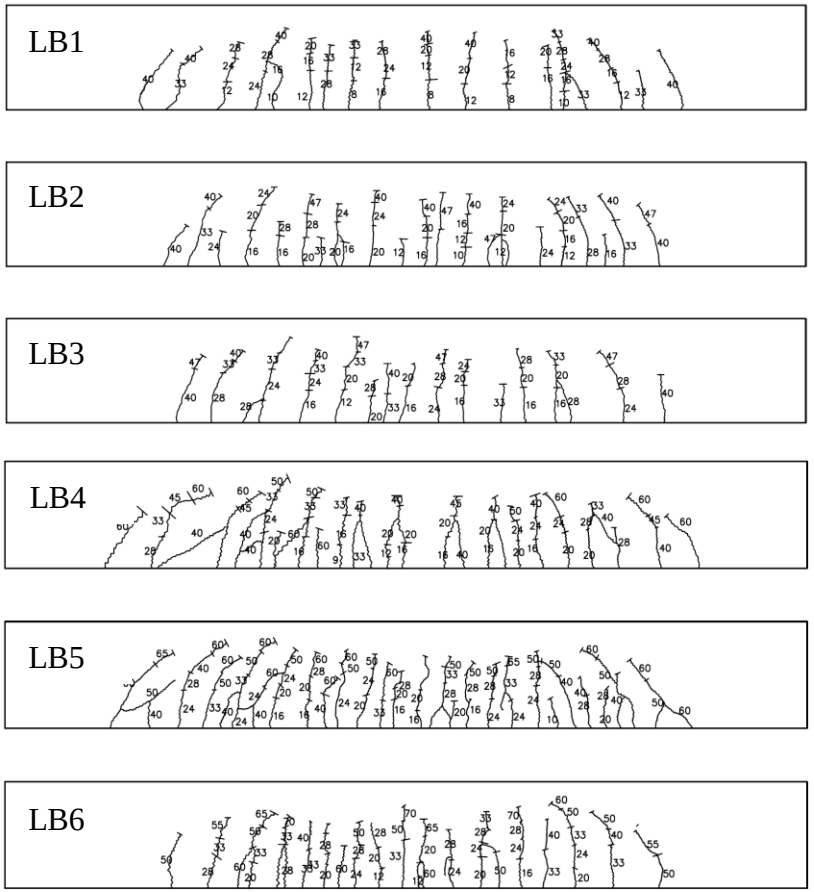

Figure 5.34: Crack Patterns for LWAC Beams at Ultimate Load.

5.6.3 Cracking Moment and Codes Predictions

The experimental cracking moments are compared with the values calculated using different codes. These code include the American Code (ACI318-14), Canadian Code (CSA A23.3-14), European (EC2-04), and the Model Code (CEB-FIP 1990). The main difference between these codes is the values of the modulus of rupture, f_r, as each code uses different expressions to calculate the modulus of rupture as shown in Table 5.8. Table 5.9 shows a coMParison between the experimental and code prediction cracking moments. It can be seen from the mean value of the ratio of experimental to code prediction that CEB-FIP1990 code and EC2-04 code overestimate the cracking moment for all LWAC and NWC beams particularly for beams without steel fibres (NB1, NB4, LB1 and LB4). ACI318-14 code and CSA A23.3-14 codes appear to give acceptable predictions for the cracking moment for steel fibre LWAC and NWC beams . However, these two codes seem to also overestimate the cracking moment for non-fibrous LWAC and NWC beams. Accordingly, all applied codes appeared to overestimate the cracking moment for non-fibrous LWAC and NWC beams. This overestimation in the cracking moment can be attributed to the shrinkage that might cause invisible micro-cracks in test beams before the load was applied. Therefore, the modulus of rupture equations which were developed for normal strength concrete have to be modified to account for the larger shrinkage of high strength concrete due to higher paste volume compared to normal strength concrete. Of the four design codes, the CSA A23.3-14 code seems to give better predications of the cracking moment for all LWAC and NWC beams with a mean value of 0.93 and 0.92 respectively.

Table 5.8: Code Recommendations for Modulus of Rupture.

Code	Cracking Moment	Modulus of Rupture, f_r
Canadian Code [CSA A23.3-14]	$M_{cr} = f_r \frac{I_g}{y_t}$	$f_r = 0.62\lambda\sqrt{f_c'}$
The American Code [ACI 318-14]	$M_{cr} = f_r \frac{I_g}{y_t}$	$f_r = 0.6\lambda\sqrt{f_c'}$
The European code [EC2-04]	$M_{cr} = f_r \frac{I_g}{y_t}$	$f_r = max\left[\left(1.6f_{ctm} - \frac{hf_{ctm}}{1000}\right), f_{ctm}\right]$ $f_{ctm} = 0.3\eta_1 2.12 \ln\left[1 + \frac{f_{ck}+8}{10}\right]$ $\eta_1 = 0.4 + 0.6\frac{w}{2200}$
Model Code [CEB-FIP 1990]	$M_{cr} = f_r \frac{I_g}{y_t}$	$f_r = \left[\frac{1+1.5(h/100)^{0.7}}{1.5(h/100)^{0.7}}\right] f_{ctm}$ $f_{ctm} = 0.3\eta_1 f_{ck}^{\frac{2}{3}}$, $\eta_1 = 0.4 + 0.6\frac{w}{2200}$

Table 5.9: Experimental and Code Prediction of Cracking Moments.

Type of Concrete	Beam	Exp. Values	Code prediction				Ratio of Experimental to Code Prediction			
		M_{cr} EXP kN.m	M_{cr} ACI318-14 kN.m	M_{cr} CSA kN.m	M_{cr} EC2-04 kN.m	M_{cr} CEB-FIP kN.m	$\frac{M_{cr,EXP}}{M_{ACI}}$	$\frac{M_{cr,EXP}}{M_{CSA}}$	$\frac{M_{cr,EXP}}{M_{EC\,2}}$	$\frac{M_{cr,EXP}}{M_{CIB-FIP}}$
NWC	NB1	22.69	29.58	28.62	32.65	34.05	0.77	0.79	0.69	0.67
	NB2	27.22	31.02	30.02	33.92	35.37	0.88	0.91	0.80	0.77
	NB3	31.76	31.37	30.36	34.22	35.69	1.01	1.05	0.93	0.89
	NB4	22.62	29.76	28.80	33.35	34.23	0.76	0.79	0.68	0.66
	NB5	27.22	31.37	30.36	34.78	35.69	0.87	0.90	0.78	0.76
	NB6	32.04	30.84	29.85	34.32	35.22	1.04	1.07	0.93	0.91
						Mean	**0.89**	**0.92**	**0.80**	**0.78**
						SD	**0.12**	**0.12**	**0.11**	**0.11**
LWAC	LB1	18.66	25.30	24.48	30.13	31.42	0.74	0.76	0.62	0.59
	LB2	22.79	25.91	25.08	30.72	32.03	0.88	0.91	0.74	0.71
	LB3	27.10	26.07	25.22	30.86	32.18	1.04	1.07	0.88	0.84
	LB4	20.40	25.14	24.33	30.87	32.19	0.81	0.84	0.66	0.63
	LB5	22.02	25.14	24.33	30.87	32.19	0.88	0.91	0.71	0.68
	LB6	27.07	25.45	24.63	31.18	32.51	1.06	1.10	0.87	0.83
						Mean	**0.90**	**0.93**	**0.75**	**0.72**
						SD	**0.13**	**0.13**	**0.11**	**0.10**

5.6.4 Crack Spacing

It was evident that the inclusion of fibres increased the number of cracks and thus reduced the average crack spacing when compared to non-fibrous beams for both types of concrete beams. The average crack spacing measured during the different load steps are presented in Table 5.10.

As mentioned earlier, the LWAC beams developed a higher number of cracks and thus smaller average crack spacing compared to the NWC beams. The average crack spacing varied from 118 mm to 58 mm in the LWAC beams and from 112 mm to 83 mm in NWC beams. Increasing the fibre volume ratio from 0.375 % to 0.75 % resulted in an increase in the number of cracks and reduced the average crack spacing in both the LWAC and NWC beams with reinforcement ratio of 1.50 %. This decrease in the average crack spacing was not apparent in beams with reinforcement ratio of 0.85 %. This could be attributed to the better distribution of the cracks in the beams with higher reinforcement ratio. Similarly a higher number of cracks in the LWAC beams compared to NWC ones developed within the serviceability limits where the load is around 45 % of the ultimate load, thus a shorter average crack spacing was obtained in the LWAC beams.

The minimum and maximum crack spacing were also measured for all beams. It was clear that the smallest spacing between the cracks always occurred in the beams with steel fibre volume ratio of 0.75 % and the maximum crack spacing was observed with non-fibrous beams. The minimum and maximum crack spacing, at different load steps, for all beams are shown in Table 5.10.

The reinforcement ratio had a noticeable effect on the crack spacing for both types of concrete. The increase of reinforcement ratio improved the cracking response, resulting

in a greater number of cracks and smaller average crack spacing for the LWAC and NWC beams.

Table 5.10: Average, Minimum, and Maximum Crack Spacing.

Beam	$\frac{M}{M_n}$	n	s_{avg}	s_{max}	s_{min}	Beam	$\frac{M}{M_n}$	n	s_{avg}	s_{max}	s_{min}
	%		mm	mm	mm				mm	mm	mm
	20	1					16	3	320	326	314
	24	4	202	220	167		20	3	320	326	314
	28	4	202	220	167		24	5	200	326	145
	33	4	202	220	167		32	6	160	202	122
NB1	41	4	202	220	167	LB1	40	6	160	202	122
	49	4	202	220	167		48	6	160	202	122
	57	4	202	220	167		56	7	134	201	41
	67	5	152	167	73		66	7	134	201	41
	100	7	112	167	41		100	8	118	195	30
	22	2		408	408		18	1			
	30	4	204	213	195		22	3	211	247	175
	37	4	204	213	195		29	5	172	271	98
	44	4	204	213	195		36	6	165	273	98
NB2	52	6	123	213	77	LB2	44	6	165	273	98
	61	7	102	155	77		51	6	165	273	98
	74	8	99	155	77		60	9	102	168	41
	100	8	99	155	77		73	9	102	168	41
							100	11	81	130	33
	24	1					20	1			
	27	3	210	247	174		27	5	223	129	268
	34	4	204	247	174		34	6	179	253	130
	41	5	181	247	110		40	7	149	243	99
NB3	48	7	121	247	74	LB3	47	7	149	243	99
	56	7	121	247	74		56	9	112	152	63
	68	8	121	247	74		67	9	112	152	63
	77	9	106	247	38		100	11	90	142	49
	100	9	106	247	38						

Table continues on next page

Beam	$\frac{M}{M_n}$ %	n	s_{avg} mm	s_{max} mm	s_{min} mm	Beam	$\frac{M}{M_n}$ %	n	s_{avg} mm	s_{max} mm	s_{min} mm
NB4	13	1	0	0	0	LB4	12	1			
	16	3	312	400	224		16	2	186	186	186
	21	4	208	241	159		21	6	149	186	62
	27	4	208	241	159		27	7	143	186	62
	32	5	156	241	110		44	8	122	170	53
	37	5	156	241	110		54	9	107	165	53
	44	6	142	241	89		81	10	95	165	53
	54	7	141	241	89		100	11	86	165	49
	67	7	141	241	89						
	100	8	109	173	51						
NB5	14	1				LB5	11	1			
	16	2	379	379	379		16	1			
	19	2	379	379	379		22	4	177	342	111
	24	4	187	193	184		27	6	126	199	164
	28	4	187	193	184		32	9	102	145	64
	33	8	113	185	61		44	10	90	122	47
	39	8	113	185	61		54	11	82	114	47
	47	9	99	140	46		71	11	82	114	47
	59	9	99	140	46		81	12	75	111	47
	71	9	99	140	46		100	13	69	111	43
	100	9	99	140	46						
NB6	17	2	192	192	192	LB6					
	19	3	221	251	192		18	2	153	153	153
	24	4	229	251	192		20	3	279	405	153
	29	6	136	192	85		25	5	195	220	153
	33	6	136	192	85		30	7	111	158	94
	39	6	136	192	85		42	9	108	158	62
	48	8	107	167	40		63	10	96	133	62
	60	8	107	167	40		69	11	86	125	34
	71	9	93	167	40		76	13	72	94	15
	83	10	83	167	40		100	15	58	94	15
	100	10	83	167	40						

s_{avg} = Average crack spacing between cracks

s_{max} = Maximum crack spacing between cracks

s_{min} = Minimum crack spacing between cracks

n = number of cracks at moment M

M_n = Ultimate moment capacity

5.6.5 Codes Prediction for Crack Spacing

The crack spacing is a significant parameter by which a better evaluation for the crack width can be obtained. The experimental average crack spacing are compared to the predicted ones obtained using different codes and proposed models. These codes are the European EC2-91 code, the Model Code CEB-FIP 1978, RIELM TC-162, and the model proposed by Jorden R. Deluce et al (2013) for beams with steel fibres. A summary of these models is shown in Table 5.11. Details of these models were presented in section 2.4 and 2.5 of the literature review.

Table 5.11: A Summary of the Equation for Average Crack Spacing.

Code	Average crack spacing
The European code [EC2-91]	$s_{rm} = 50 + 0.25 k_1 k_2 d_b / \rho_{eff}$
Model Code [CEB-FIP 1978]	$s_m = 2\left(c + \frac{s}{10}\right) + k_1 k_2 d_b / \rho_{eff}$
RILEM TC 162-TDF	$s_{rm} = \left(50 + 0.25 k_1 k_2 \frac{d_b}{\rho_{eff}}\right)\left(\frac{50}{l_f / d_f}\right)$
Jorden R. Deluce et al.(2013)	$s_m = 2\left(c + \frac{s_b}{10}\right) k_3 + \frac{k_1 k_2}{s_{mi}}$

Table 5.12 shows a comparison of the experimental to prediction crack spacing. It can be seen that EC2-91 code gives a good predication for the crack spacing of non-fibrous NWC beams. The mean value of experimental to theoretical crack spacing, s_{Exp} / s_{EC2-91}, is 0.88 and the standard deviation is 0.05. Furthermore, EC2-91 code seems to better predict the average crack spacing for non-fibrous NWC beams compared to non-

fibrous LWAC beams. A mean value of experimental to predicted crack spacing, $s_{Exp} / s_{EC\,2-91}$, of 0.81 and standard deviation of 0.11 are obtained for non-fibrous LWAC beams (LB1 and LB4). CEB-FIP 1978 crack spacing model includes more parameters compared to EC2-91 code. However, CEB-FIP 1978 mode is found to overestimate the average crack spacing for both high strength LWAC and NWC beams. For LWAC and NWC beams with steel fibres, EC2-91 code and CEB-FIP 1978 code overestimate the crack spacing. That is expected since none of those two average crack spacing models incorporate the presence of steel fibres.

The RIELM model and the Jorden model are the only ones to consider the existence of steel fibres. In the RIELM model, the steel fibres are considered through the aspect ratio of the fibres, l_f / d. Even though the model does not account for the volume ratio of the steel fibres, the model is found to better estimate the crack spacing for fibrous high strength NWC beams with a mean value of experimental to predicted average crack spacing, s_{exp} / s_{RIELM}, of 0.99 and standard deviation of 0.08.

However, less accuracy is found when applying this model to fibrous LWAC beams. The Rilem model overestimates the average crack spacing for fibrous LWAC beams with a mean value of experimental to theoretical average crack spacing, s_{exp} / s_{RIELM}, of 0.76 and standard deviation of 0.11.

The model developed by Deluce et al (2013), which was developed based on CEB-FIP1978 crack spacing model, appears to give good predictions of the average crack spacing for fibrous NWC beams with a mean value of experimental to predicated average

crack spacing, s_{exp}/s_{Jorden}, of 1.10 . Even though this model seems to give better predictions of the average crack spacing for LWAC beams compared to the RIELM model, it still overestimate the average crack spacing with a mean value of experimental to theoretical average crack spacing, s_{exp}/s_{Jorden}, of 0.85. In general, the Jorden model is found to be the best model among those applied models in this study in predicting the average crack spacing for both the fibrous NWC and LWAC beams.

Table 5.12: Experimental and Predicted Crack Spacing.

Type of Concrete	Beam	Exp. Values	Predicted Values				Ratio of Experimental to Predicted Values			
		s_{rm} EXP	s_{rm} EC2-91	s_{rm} CIB-FIP	s_{rm} RIELM	s_{rm} Jorden	$(\frac{s_{Exp}}{s_{EC\,2-91}})$	$(\frac{s_{Exp}}{s_{CIB-FIP}})$	$(\frac{s_{Exp}}{s_{RIELM}})$	$(\frac{s_{Exp}}{s_{Jorden}})$
			mm	mm	mm	mm				
NWC	NB1	112	133	160			0.84	0.70		
	NB2	99	133	160	102	96	0.74	0.62	0.97	1.03
	NB3	106	133	160	102	83	0.80	0.66	1.04	1.28
	NB4	109	120	147			0.91	0.74		
	NB5	99	120	147	93	93	0.83	0.67	1.06	1.06
	NB6	83	120	147	93	81	0.69	0.56	0.89	1.02
						Mean	0.80	0.66	0.99	1.10
						SD	0.08	0.06	0.08	0.12
LWAC	LB1	118	133	160			0.89	0.74		
	LB2	81	133	160	102	96	0.61	0.51	0.79	0.84
	LB3	90	133	160	102	83	0.68	0.56	0.88	1.08
	LB4	88	120	147			0.73	0.60		
	LB5	69	120	147	93	93	0.58	0.47	0.74	0.74
	LB6	58	120	147	93	81	0.48	0.39	0.62	0.72
						Mean	0.66	0.54	0.76	0.85
						SD	0.14	0.12	0.11	0.17

5.6.6 Crack Width and Defining Service Load Level.

Flexural cracking occurs in all reinforced concrete beams and commences at loads below the expected service loads. When a reinforced concrete beam is well designed, the cracks, in the tension side, remain fine and unnoticeable for naked eyes, so called hairline cracks. At service loads and to ascertain that crack width lie within acceptable values, different codes typically limits the maximum crack width to be between 0.3 mm to 0.4 mm depending on the surrounding environment and condition of exposure.

Even though the cracking of the concrete is a random process, it is still influenced by different parameters. One of these parameters is the stress in the longitudinal reinforcement. Gergely and Lutz (1973) showed that the crack width is proportional to f_s^n, where f_s is the reinforcement stress and n is an exponent varying between 1.0 to 1.4. When the stresses lie within the practical limits which is usually from 138 MPa to 248 MPa, the value n can be taken as 1.0. The present methods for predicting crack width take in account the stress at which the maximum crack width shall be calculated. Thus the service load is considered and implicitly included in a form of stress in these equations. The north American codes adopt the Gergely and Lutz (1973) equation. The Canadian Code CSA A23.3-14 code states that f_s may be taken as 60 % of the specified yield strength f_y, whereas the ACI318-14 code permits to assume f_s to be equal to 67 % of the specified yield strength f_y. The CSA A23.3-14 code recommended value of 0.6 f_y is assumed in the current study in order to determine the service load level. The measured flexural tensile reinforcement stress to the yielding stress , f_s / f_y, are shown in Table

5.10 at different loads. Based on the obtained results it was found that when the service load, P_s, is assumed to be 45% of the ultimate load, the stress, f_s, in the reinforcement is almost 60 % of the yielding stress f_y. Different researchers recommended different service load to ultimate load ratios to be used when evaluating the serviceability conditions. Rashid and Mansur (1999) recommended the service load to be 0.6 times the ultimate load. However, based on the results obtained herein, this assumption seems to be non-conservative as the flexural reinforcement stress at that load level is about 88% of yielding stress f_y.

Table 5.13: The Ratio of the Flexural Reinforcement Stress to Yielding Stress at Different Load Levels.

Beam	P_u	Maximum Flexural Reinforcement Stress Ratios at Different Service loads to Yielding Stress (f_s / f_y)						
	kN	$0.3P_u$	$0.35P_u$	$0.4P_u$	$0.45P_u$	$0.5P_u$	$0.55P_u$	$0.6P_u$
NB1	109.40	0.26	0.49	0.55	0.63	0.70	0.82	0.86
NB2	120.60	0.20	0.41	0.53	0.59	0.70	0.79	0.90
NB3	130.57	0.14	0.29	0.46	0.57	0.63	0.71	0.85
NB4	166.15	0.28	0.39	0.52	0.60	0.66	0.76	0.83
NB5	188.98	0.29	0.43	0.52	0.60	0.70	0.78	0.93
NB6	186.80	0.29	0.39	0.47	0.57	0.70	0.79	0.88
LB1	113.00	0.43	0.51	0.58	0.66	0.74	0.83	0.89
LB2	125.14	0.30	0.39	0.49	0.59	0.71	0.77	0.89
LB3	134.60	0.27	0.41	0.50	0.61	0.67	0.78	0.84
LB4	165.00	0.39	0.47	0.58	0.65	0.73	0.83	0.90
LB5	165.00	0.39	0.46	0.58	0.65	0.73	0.83	0.89
LB6	176.00	0.31	0.43	0.52	0.63	0.75	0.87	0.97
		Mean	0.42	0.53	0.61	0.70	0.80	0.88
		SD	0.06	0.04	0.03	0.03	0.04	0.04

5.6.7 Crack Width

The observed crack widths recorded for all beams at the assumed service loads are shown in Table 4.14. It can be seen that when all different parameters other than concrete type were held the same, the LWAC beams developed higher number of cracks compared to their identical NWC beams, which resulted in smaller crack widths at the assumed service load. The addition of fibres improved the crack response of the LWAC and NWC beams. A smaller crack width was obtained in fibrous LWAC beams compared to LWAC beams containing no fibres. For example, at the assumed service load, beam LB1 had 0.21 mm maximum crack width compared to 0.13 mm and 0.14 mm for beams LB2 and LB3 respectively.

The loads at which the serviceability limit of crack width was reached in Table 5.14. It is defined as the load, $P_{w=0.3}$, that caused 0.3 mm crack width in each beam. An increase of 14 % and 19 % in load was seen for beam LB2 and LB3 compared to beam LB4. Similarly, an improvement also occurred in the presence of fibres for beams LB5 and LB6. The addition of steel fibres to high strength normal weight concrete beams seemed to be more effective compared to high strength lightweight concrete beams in increasing the load at which the crack width of 0.3 mm was reached. This is consistently evident from the results of beams NB2, NB3, NB5, and NB6. A maximum improvement of 43 % in load was recorded for beam NB3 in coMParison to NB1.

Moreover, within the expected service load the increase of fibre volume from 0.375 % to 0.75 % appeared to slightly decrease the maximum crack width for both LWAC and NWC beams. Furthermore, in addition to increasing the number of cracks, the

increase of flexural reinforcement played a significant role in restricting the opening of cracks for all beams. Subsequently, beams with higher reinforcement ratio had less crack widths and more number of cracks. Figures 5.35 and 5.36 show the moment versus crack width for the NWC and LWAC beams, respectively.

Table 5.14: Load Corresponding to 0.3 mm Crack Width and Maximum and Average Crack Width for all Beams.

Concrete type	Beam	Reinfor. ratio	Fibre Volume	Comp. Strenth.	Service Load	Load at 0.3mm Crack width	Experimental values	
		ρ %	V %	f_c' MPa	P_s kN	$P_{0.3mm}$ kN	w_{avg} mm	w_{max} mm
NWC	NB1	0.85	0	80	49	60	0.22	0.25
	NB2	0.85	0.375	88	54	73	0.14	0.15
	NB3	0.85	0.75	90	59	89	0.09	0.16
	NB4	1.50	0	81	75	89	0.17	0.28
	NB5	1.50	0.375	90	85	126	0.11	0.17
	NB6	1.50	0.75	87	84	127	0.10	0.19
LWAC	LB1	0.85	0	81	51	78	0.14	0.21
	LB2	0.85	0.375	85	56	89	0.09	0.13
	LB3	0.85	0.75	86	61	93	0.09	0.14
	LB4	1.50	0	81	74	133	0.13	0.20
	LB5	1.50	0.375	80	74	137	0.09	0.15
	LB6	1.50	0.75	82	79	147	0.08	0.13

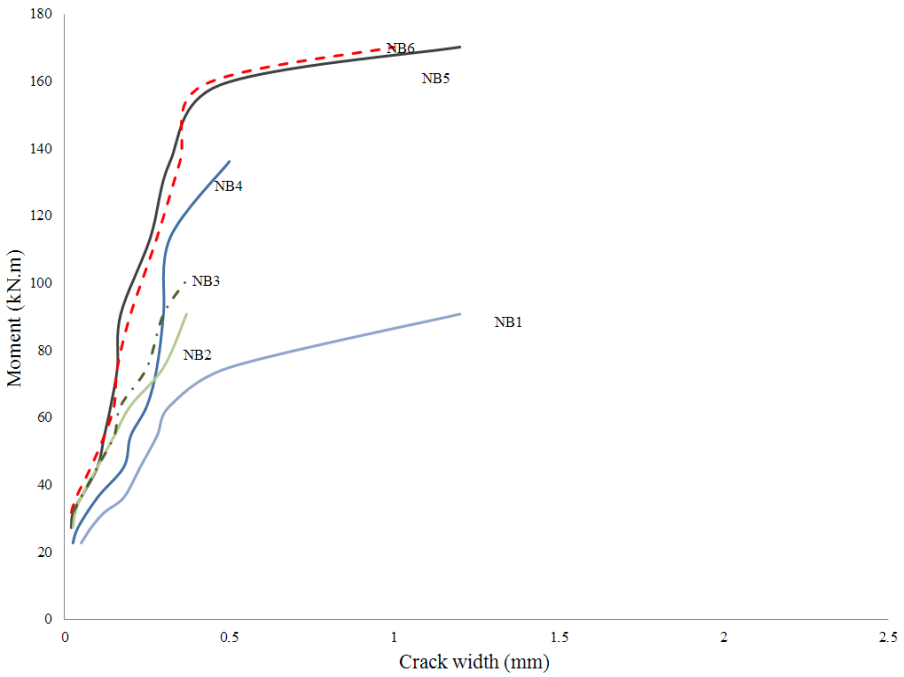

Figure 5.35: Moment vs. Maximum Crack Width for NWC Beams.

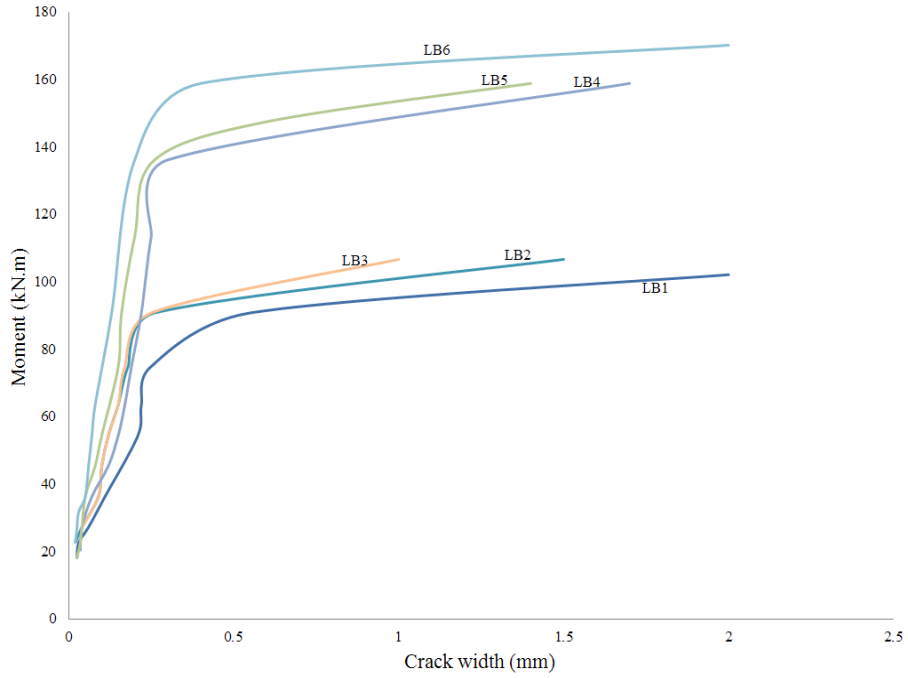

Figure 5.36: Moment vs. Maximum Crack Width for LWAC Beams.

5.6.8 Codes Prediction for Crack Width

Different models are adapted by different codes to calculate the crack width. Some codes are assessed based on the test results .The codes are the American Code (ACI318-08), the Canadian Code (CSA A23.3-14), the European (EC2-04), the European (EC2-91) and Rilem TC162-TDF. Table 5.15 shows a summary of these models. Details of the models are given in section 2.5.4. Table 5.16 reveals that for non-fibrous NWC beams, the Canadian code (CSA A23.3-14) which utilizes the well-known equation derived by Gergely and Lutz (1973) gives the best prediction for the maximum crack width with a mean value of the experimental-to-predicted ratio, w_{Exp}/w_{CSA} , of 0.98 and standard deviation (SD) of 0.02. The crack width predictions of the American Code (ACI318-08) also seem to agree with the measured results for non-fibrous NWC beams with a mean value w_{Exp}/w_{ACI318} of 1.13 and standard deviation (SD) of 0.06.

The other two codes, EC2-04 and EC2-91, appear to underestimate the maximum crack width for non-fibrous NWC beams with mean values of the experimental-to-predicted ratio of 1.39, and 1.57, and with standard deviation of 0.11, and 0.14, respectively. Contrary to non-fibrous NWC beams, EC2-04 code and EC2-91 code are found to be fairly satisfactory for predicting the maximum crack width for non-fibrous LWAC beams with mean values of the experimental-to-predicted ratio of 1.00 and 1.08, and with standard deviation of 0.0 and 0.12 respectively. Table 5.15 shows that the CSA A23.3-14 and ACI318-08 codes gave mean values of the experimental-to-predicted ratio of 0.72 and 0.81 respectively for non-fibrous LWAC beams. Therefore, both CSA A23.3-

14 and ACI318-08 codes are conservative in predicting the maximum crack width for non-fibrous LWAC beams.

Table 5.15: A Summary of Average Crack Width Models.

Canadian Code [CSA A23.3-14]	$w = 11 \text{ x} 10^{-6} \beta f_s \sqrt[3]{d_c A}$
The American Code [ACI 318-08]	$w = 2 \frac{f_s}{E_s} \beta + \sqrt{d_c^2 + \left(\frac{s}{2}\right)^2}$
The European code [EC2-04]	$w = s_{rm,max} \left(\varepsilon_{sm} - \varepsilon_{cm}\right)$ $s_{rm,max} = 3.4c + 0.425 k_1 k_2 d_b / \rho_{eff}$ $\varepsilon_{sm} - \varepsilon_{cm} = \frac{\sigma_s}{E_s} - \frac{k_t f_{ctm} \left(1 + n\rho_{eff}\right)}{E_s \rho_{eff}} \geq 0.6 \frac{f_s}{E_s}$
The European code [EC2-91]	$w_k = \beta \cdot s_{rm} \cdot \varepsilon_{sm}$ $s_{rm} = 50 + 0.25 k_1 k_2 d_b / \rho_{eff}$ $\varepsilon_{sm} = \frac{\sigma_s}{E_s} \left(1 - \beta_1 \beta_2 \left(\frac{\sigma_{sr}}{\sigma_s}\right)^2\right)$
RILEM TC 162-TDF	$w_m = \beta \cdot s_{rm} . \varepsilon_{sm}$ $s_{rm} = \left(50 + 0.25 k_1 k_2 \frac{d_b}{\rho_{eff}}\right)\left(\frac{50}{l_f / d_f}\right)$ $\varepsilon_{sm} = \frac{\sigma_s}{E_s} \left(1 - \beta_1 \beta_2 \left(\frac{\sigma_{sr}}{\sigma_s}\right)^2\right)$

All methods except the Rilem TC162-TDF do not incorporate the effect of the steel fibres in the parameters used in the crack width equations. This results in an overestimation of the maximum crack width. According to the results presented in Table 5.17 for beams with steel fibres, the Rilem model, which takes in account the presence of steel fibres, gives good predictions of the crack width for the NWC beams containing steel fibres with a mean value of the experimental-to-predicted ratio, $w_{\text{Exp}} / w_{\text{RIELM}}$, of

1.08 and standard deviation (SD) of 0.07. However, the model seems to be conservative when predicting the crack widths for LWAC beams. This model overestimates the crack widths for LWAC beams with a mean value of the experimental-to-predicted ratio , $w_{\text{Exp}}/w_{\text{RIELM}}$, of 0.82 and standard deviation (SD) of 0.08.

Table 5.16: Comparison of Experimental and Predicted Crack Width for Non-Fibrous Beams.

Beam	w_{exp} mm	Code Values (mm)				Ratio of Maximum Experimental to Code Predictions			
		w_{CSA}	w_{ACI}	$w_{EC\,2-04}$	$w_{EC\,2-91}$	$\frac{w_{exp}}{w_{CSA}}$	$\frac{w_{exp}}{w_{ACI}}$	$\frac{w_{exp}}{w_{EC\,2-04}}$	$\frac{w_{exp}}{w_{EC\,2-91}}$
NB1	0.25	0.25	0.23	0.19	0.15	1.00	1.09	1.32	1.67
NB4	0.28	0.29	0.24	0.19	0.19	0.97	1.17	1.47	1.47
					Mean	0.98	1.13	1.39	1.57
					SD	0.02	0.06	0.11	0.14
LB1	0.21	0.26	0.24	0.21	0.18	0.81	0.88	1.00	1.17
LB4	0.20	0.32	0.27	0.20	0.20	0.63	0.74	1.00	1.00
					Mean	0.72	0.81	1.00	1.08
					SD	0.13	0.09	0.00	0.12

Table 5.17: Comparison of Experimental and Predicted Maximum Crack Width for Fibrous Beams.

Conc. Type	Beam	w_{exp} mm	Predicted values					Ratio of Maximum Experimental to Predicted Values				
			w_{CSA}	w_{ACI}	$w_{EC\,2-04}$	$w_{EC\,2-91}$	w_{RIELM}	$\frac{w_{exp}}{w_{CSA}}$	$\frac{w_{exp}}{w_{ACI}}$	$\frac{w_{exp}}{w_{EC\,2-91}}$	$\frac{w_{exp}}{w_{EC\,2-04}}$	$\frac{w_{exp}}{w_{RIELM}}$
NWC	NB2	0.15	0.23	0.22	0.21	0.17	0.13	0.65	0.68	0.71	0.88	1.15
	NB3	0.16	0.22	0.21	0.23	0.20	0.15	0.73	0.76	0.70	0.80	1.07
	NB5	0.17	0.29	0.24	0.22	0.22	0.17	0.59	0.71	0.77	0.77	1.00
	NB6	0.19	0.28	0.23	0.22	0.22	0.17	0.68	0.83	0.86	0.86	1.12
							Mean	0.66	0.74	0.76	0.83	1.08
							SD	0.06	0.06	0.08	0.05	0.07
LWAC	LB2	0.13	0.23	0.22	0.23	0.21	0.16	0.57	0.59	0.57	0.62	0.81
	LB3	0.14	0.24	0.23	0.25	0.23	0.18	0.58	0.61	0.56	0.61	0.78
	LB5	0.15	0.32	0.27	0.20	0.20	0.16	0.47	0.56	0.75	0.75	0.94
	LB6	0.13	0.31	0.26	0.22	0.22	0.17	0.42	0.50	0.59	0.59	0.76
							Mean	0.51	0.56	0.62	0.64	0.82
							SD	0.08	0.05	0.09	0.07	0.08

5.7 Moment Capacity

All beams failed in flexure as designed. The failure was due to the yielding of the longitudinal reinforcement and crushing of the concrete in the compression zone. For beams containing no steel fibres, the crushing of the concrete was accompanied by a sudden drop in the applied load. For the fibrous LWAC and NWC beams, the contribution of steel fibre made the load gradually decrease after the ultimate load was attained.

In this section, the experimental ultimate strength, expressed as the moment capacity M_{Exp} was compared to that calculated using different code predictions as shown in Table 5.17. It can be seen that both the ACI318-14 and CSA A23.3-14 codes were conservative in predicting the moment capacity for the LWAC and NWC beams with no steel fibres as both codes underestimated the moment capacity. The ratio of the experimental to theoretical moment, M_{Exp} / M_{Theo}, was almost the same for LWAC and NWC beams and ranged from 1.26 to 1.30. The slight differences in the results between NWC beams and their identical LWAC beams can be attributed to the different compressive strength of each beam. These two codes were also used to predicate the ultimate moment capacity for the fibrous NWC and LWAC beams. Both codes underestimated the moment capacity of all fibrous beams with a considerable margin. This was expected due to the fact that these codes do not include the effect of steel fibre.

For fibrous beams, three different models were used to predict the theoretical moment. These models were Oh.(1992) model, Imam et al.(1995) model, and ACI544.1

R-96 model. The results obtained for the LWAC beams showed that Oh model and ACI 544 model underestimated the moment capacity with mean values of the ratio of the experimental to theoretical moment, $M_{Exp} / M_{Oh,ACI}$, of 1.27 and 1.34 respectively. Similar results were obtained for NWC beams. A percentage of this underestimation can be attributed to the fact that those two models were developed for normal strength concrete where the used fibre bond stress, τ_f, taken as 2.3 MPa, is less than the bond stress for high strength concrete. The Imam model, though it was developed to account for high strength concrete, was found to underestimate the ultimate moment for fibrous LWAC and NWC beams with means value of the ratio of the experimental to theoretical moment, $M_{Exp} / M_{\mathrm{Im}am}$, of 1.29 and 1.26 and standard deviation (SD) of 0.02 and 0.09, respectively.

It is important to mention that due to the improved ductility of the beams with fibres, the longitudinal reinforcement underwent strain hardening. Consequently, the steel stresses exceeded the yielding stress and almost reached the ultimate stress, leading to rupture of the longitudinal reinforcement in some beams as shown in Figure 5.37. Hence, using the yielding stress in the models to predict the moment capacity resulted in an increase in an underestimation of the predicted moments as evidenced by the results presented in Table 5.14.

Table 5.18 shows the calculated moment capacity using the ultimate steel stress, f_u, for all fibrous NWC and LWAC beams. The measured ultimate stress of the used steel bars were approximately 575 MPa. The obtained calculations suggest that the

predictions of all three employed models (Oh model, Imam Model, and ACI544) appear to be in good agreement with the experimental values for both fibrous NWC and LWAC beams.

Table 5.18: Comparison between Experimental and Theoretical Moment Capacity Using Reinforcement Stress of $f_s = f_y$ = 430MPa.

Beam	M_{exp} kN.m	Theoretical values (M_{Theo}) kN.m					Ratio of Experimental to theoretical Calculation (M_{Exp} / M_{Theo})				
		Oh	Imam	ACI 544	ACI 318	CSA 23-14	Oh	Imam	ACI 544	ACI 318	CSA 23-14
NB1	112				89	89				1.25	1.25
NB2	123	98	96	92	90	90	1.25	1.28	1.34	1.37	1.37
NB3	133	107	103	96	90	90	1.24	1.29	1.39	1.48	1.48
NB4	170				134	134				1.26	1.26
NB5	193	145	145	143	135	135	1.33	1.33	1.35	1.43	1.43
NB6	191	153	151	147	135	135	1.25	1.26	1.30	1.41	1.41
						Mean	1.27	1.29	1.34	1.39	1.39
						SD	0.04	0.02	0.03	0.07	0.07
LB1	115				89	89				1.30	1.30
LB2	128	98	96	92	90	90	1.30	1.33	1.39	1.42	1.42
LB3	137	106	103	96	90	90	1.29	1.33	1.43	1.53	1.53
LB4	168				134	134				1.26	1.26
LB5	168	143	144	142	134	134	1.17	1.17	1.19	1.26	1.26
LB6	180	152	150	146	135	134	1.18	1.20	1.23	1.33	1.34
						Mean	1.24	1.26	1.31	1.36	1.36
						SD	0.07	0.09	0.12	0.12	0.12

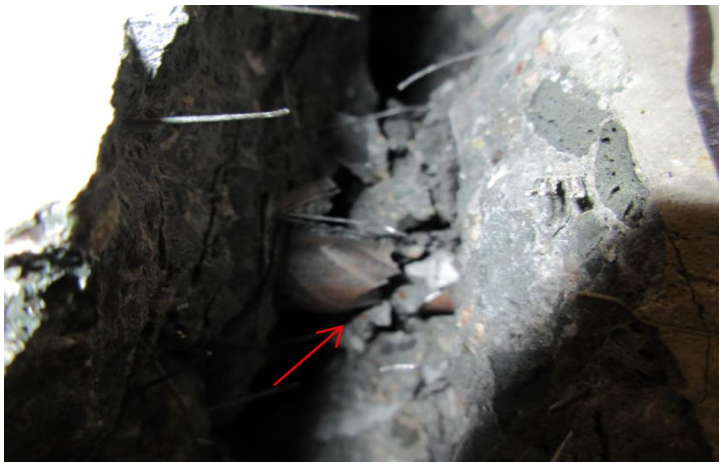

Figure 5.37: Steel Bar Rupture in Beam NB3.

Table 5.19: Comparison between Experimental and Theoretical Moment Capacity Using Reinforcement Stress of $f_s = f_u$ = 575MPa.

Beam	M_{Exp} kN.m	Theoretical values (M_{Theo}) kN.m			Ratio of experimental to theoretical calculation (M_{Exp} / M_{Theo})		
		Oh	Imam	ACI544	Oh	Imam	ACI544
NB2	123	126	125	121	0.98	0.98	1.02
NB3	133	134	131	125	0.99	1.02	1.07
NB5	193	187	188	186	1.03	1.03	1.04
NB6	191	195	194	188	0.98	0.98	1.01
				Mean	0.99	1.00	1.03
				SD	0.02	0.02	0.02
LB2	128	125	125	121	1.02	1.02	1.05
LB3	137	134	132	124	1.02	1.04	1.11
LB5	168	184	187	184	0.91	0.90	0.91
LB6	180	193	193	188	0.93	0.93	0.95
				Mean	0.97	0.97	1.01
				SD	0.06	0.07	0.09

5.8 Crack Localization

Excluding the number of cracks and final crack spacing, the high strength LWAC beams exhibited similar behaviour to the corresponding high strength NWC beams in terms of development of cracks and the crack widening behaviour. Within the constant moment zone and for all beams, the cracks developed and almost widened uniformly throughout the loading stages until roughly 85 % of the ultimate load which is higher than the assumed service load. After exceeding that percentage of loading, both types of concrete with fibre volume of 0.75 % and different reinforcement ratios of 0.85 % and 1.50 % showed a different crack widening behaviour compared to other beams. While crack widening of the control beams and 0.375 % fibrous beams were to some extent uniform, localization of strains and cracking occurred in the 0.75 % fibrous beams. It was noticed that a single crack widened distinctly in beams LB3 and NB3 which had 0.75 % fibre volume and 0.85 % reinforcement ratio leading to the shortening of the plastic hinge region and ultimately to the rupture of the steel after exceeding the ultimate loads of the beams. For both beams, the reinforcement ruptured at the same section at which the concrete was crushed, as shown in Figures 5.38 and 5.39. Furthermore, it seemed that at the location of localization, and when the steel ruptured, the LWAC beam LB3 had less final crack width compared to NWC beam NB2 and possibly the strain localization in reinforcement of NWC beam NB3 had started before the LWAC beam LB3. The final crack width of beams LB3 and NB3 were about 33 mm and 40 mm and the crack numbers were 11 and 9 respectively. Localization of cracking developed at two different locations in beams LB6 and NB6 which contained 0.75 % fibre volume with reinforcement ratio of 1.50% as shown in Figure 5.40 and 5.41.

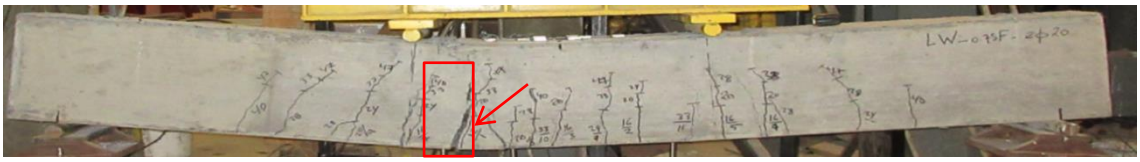

Figure 5.38: Beam LB3 at Failure.

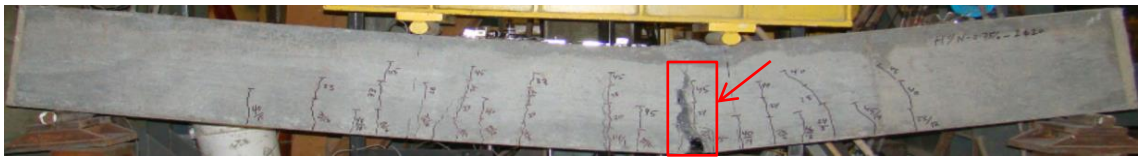

Figure 5.39: Beam NB3 at Failure.

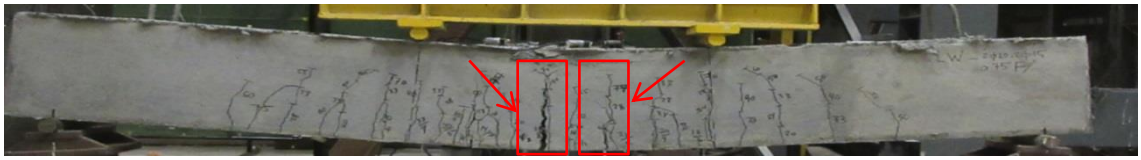

Figure 5.40: Beam LB6 at Failure.

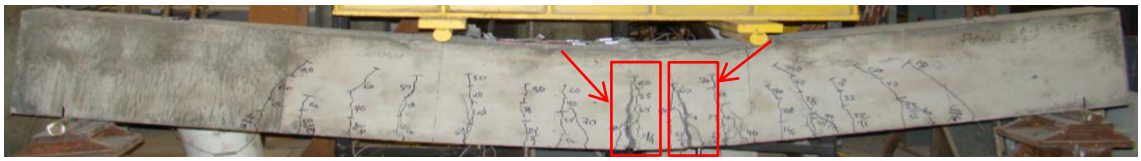

Figure 5.41: Beam NB6 at Failure.

Chapter 6

Summary & Conclusions

The effect of adding steel fibre on the flexural behaviour of reinforced concrete beams was experimentally investigated. In total, Twelve beams with dimensions of 200 mm × 400 mm × 3200 mm and with constant shear ratio of 2.9 were tested in this study. The main parameters applied in this study are the concrete type, the percentage of the longitudinal reinforcement and the steel fibre volume ratio. Material investigation was also conducted by testing twenty four prisms and one hundred and twenty cylinders to study the effect of steel fibre on the mechanical properties of both high strength normal and lightweight concrete.

The following conclusion can be drawn based on the current study:

1. The addition of steel fibres to either high strength normal or lightweight concrete resulted in an improvement in the splitting tensile strength, modulus of rupture and the compressive strength. Also, adding steel fibres to both type of concrete significantly enhanced the flexural toughness of the concrete.
2. For almost the same compressive strength and the same steel fibre volume ratio, high strength normal weight concrete had higher splitting tensile strength, modulus of rupture and flexural toughness compared to high strength lightweight concrete.
3. Increasing the fibre volume ratio from 0.375 % to 0.75 % increased splitting tensile strength, modulus of rupture and flexural toughness values for both type of

concrete. However, no clear trend was found in terms of compressive strength values for both type of concrete.

4. High strength lightweight concrete LWAC beams had lower un-cracked stiffness and lower first cracking load compared to their identical high strength normal weight concrete NWC beams, regardless of the content of steel fibres. Also, the addition of steel fibres to both type of concrete increased the cracked stiffness and first cracking load.
5. Increasing the longitudinal reinforcement ratio resulted in increasing both un-cracked and cracked stiffness for both high strength normal and lightweight concrete.
6. The addition of steel fibres improved the cracking behaviour for both types of concrete beams. The implantation of steel fibres led to decrease both crack width and crack spacing for both type of concrete beams. However, LWAC beams exhibited better performance in terms of maximum crack width and average crack spacing compared to NWC beams.
7. Both high strength normal and lightweight concrete beams exhibited similar behaviour in terms of the mode of failure. The yielding of the longitudinal reinforcement happened prior to the crushing of the compression concrete in the constant moment zone. Also, the flexural capacity of the LWAC beams are quite similar to NWC beams regardless of the existence of steel fibres.
8. The addition of steel fibres was found to cause a gradual transition in the load-deflection curve for both LWAC and NWC beams when concrete cover spalled

off. In contrast, a sudden drop in the load carrying capacity occurred in all beams containing no steel fibres.

9. An increase in the flexural capacity was observed as a result of adding steel fibres to both LWAC and NWC beams. Also, increasing the fibre volume ratio from 0.375 % to 0.75 % resulted in increasing the flexural capacity for almost all beams.
10. The measured ductility indexes calculated based on the two definitions introduced in Chapter 5 showed that the addition of steel fibres to both NWC and LWAC beams improved the ductility displacement indexes. The measured values also indicated that LWAC beams had less ductility compared to their identical NWC beams.
11. Like NWC beams, the opening of cracks in LWAC beams containing no steel fibre or LWAC beams with 0.375 % steel fibre volume ratio was similar and uniform. However, one crack distinctly opened in beams with steel fibre ratio of 0.75 % and longitudinal reinforcement ratio of 0.85 % starting at roughly 85 % of the ultimate capacity. This distinct widening of one crack caused a strain localization in reinforcing bars leading finally to the rupture of the bars at that position.
12. Increasing the longitudinal reinforcement ratio seemed to limit the phenomenon of the localizing strain by increasing the number of cracks widening distinctly. Two cracks widened distinctly in beams with longitudinal reinforcement ratio of 1.50 % and steel fibre volume ratio of 0.75 %.

13. The predictions of the Canadian Code CSA A23.3-14 for the maximum crack width of non-fibrous NWC beams width are the best among the applied model with a mean value of the experimental to predicted ratio, w_{Exp}/w_{CSA} , of 0.98 and standard deviation (SD) of 0.02. However, For LWAC beams without steel fibres, EC2-04 and EC2-91 codes are more accurate at predicating the maximum crack width compared to CSA A23.3-14 and ACI 318-14 codes that appeared to be more conservative.
14. The RILEM TC-162-TDF crack width model is the only model in the literature to consider the inclusion of steel fibre in predicting the crack width. The model was found to fairly give an acceptable prediction for the crack width for fibrous high strength normal weight reinforced concrete beams. The model is however overestimating the crack width for fibrous high strength lightweight reinforced concrete beams.
15. CSA A23.3-14 and ACI318-14 codes appeared to be conservative at predicating the ultimate moment capacity for both NWC and LWAC beams without steel fibres. The results obtained using those two codes were almost identical. For fibrous NWC and LWAC beams, all the applied models used in this study (Oh model, Imam Model, and ACI544) which account for the existence of the steel fibre underestimated the ultimate moment capacity.

References

ACI Committee 318M-14, "Building Code Requirements for Structural Concrete (ACI 318-14) and Commentary," American Concrete Institute, Farmington Hills, MI, 2014

ACI Committee 318-08, "Building code requirements for structural concrete (ACI 318-08) and commentary (ACI 318M-08)," ACI318-08, American Concrete Institute, Farmington Hills, Michigan, 2008.

ACI Committee 318M-95, "Building code requirements for structural concrete (ACI 318-95) and commentary," ACI318-05, American Concrete Institute, Farmington Hills, Michigan, 1995.

ACI Committee 544, "Design Consideration for Steel Fibre Reinforced Concrete (ACI544. 1R-96)," American Concrete Institute, Farmington Hills, 1997.

ACI Committee 211 (ACI 211.4R-93) (1993), "Guide for Selecting Proportions for High Strength Concrete With Portland Cement and Fly Ash," American Concrete Institute, Detroit, Michigan, 13 pp.

ASTM C39 / C39M-17b (2017) "Standard Test Method for Compressive Strength of Cylindrical Concrete Specimens," ASTM International, West Conshohocken, Pa

ASTM C78 / C78M-16 (2016). "Standard Test Method for Flexural Strength of Concrete (Using Simple Beam with Third-Point Loading)," ASTM International, West Conshohocken, Pa

ASTM C127-15 (2015). "Standard Test Method for Relative Density (Specific Gravity) and Absorption of Coarse Aggregate," ASTM International, West Conshohocken, Pa

ASTM C469 / C469M-14 (2014). "Standard Test Method for Static Modulus of Elasticity and Poisson's Ratio of Concrete in Compression," ASTM International, West Conshohocken, Pa

ASTM C496 / C496M-17 (2017), "Standard Test Method for Splitting Tensile Strength of Cylindrical Concrete Specimens," ASTM International, West Conshohocken, Pa

Altun, Fatih, and Bekir Aktaş., "Investigation of reinforced concrete beams behaviour of steel fibre added lightweight concrete," Construction and Building Materials, Vol. 38, 2013, pp. 575-581.

Ahmad, Shuaib H., and Roy Barker., "Flexural behaviour of reinforced high-strength lightweight concrete beams," Structural Journal, Vol. 88, NO. 1, 1991, pp. 69-77.

Ahmad, Shuaib H., and Jaime Batts., "Flexural behaviour of doubly reinforced high-strength lightweight concrete beams with web reinforcement," Structural Journal, Vol. 88, NO. 3, 1991, pp. 351-358.

Almousawi, Ahmed Naamah., "Flexural and shear performance of high strength lightweight reinforced concrete beams," Vol. 72. No. 11. 2011.

Ashour, Samir A., "Effect of compressive strength and tensile reinforcement ratio on flexural behaviour of high-strength concrete beams," Engineering Structures, Vol. 22, NO. 5, 2000, pp. 413-423.

Balendran, R. V., et al., "Influence of steel fibre on strength and ductility of normal and lightweight high strength concrete," Building and environment, Vol. 37, NO. 12, 2002, pp. 1361-1367.

Branson, Dan Earle, and Gene Alan Metz., "Instantaneous and time-dependent deflections of simple and continuous reinforced concrete beams," Department of Civil Engineering and Auburn Research Foundation, Auburn University, 1963.

Broms, Bengt B., "Crack width and crack spacing in reinforced concrete members," Journal Proceedings. Vol. 62. No. 10. 1965.

BS EN 1992-1-1, "Eurocode 2: Design of Concrete Structures-Part 1: General rules and rules for buildings," Brussels, Belgium, 2004.

Carmo, R. N. F., et al., "Influence of both concrete strength and transverse confinement on bending behaviour of reinforced LWAC beams," Engineering structures, Vol. 48, 2013, pp. 329-341.

CEB-FIP model code 1990, "Design code," London, Thomas Telford Service Ltd, 1993.

Chunxiang, Qian, and Indubhushan Patnaikuni., "Properties of high-strength steel fibre-reinforced concrete beams in bending," Cement and Concrete Composites, Vol. 21, NO. 1, 1999, pp. 73-81.

CSA A23.3-14, "Design of Concrete Structures for Buildings," Canadian Standards Association, Rexdale, ON, Canada, 2014.

Deluce, Jordon R., and Frank J. Vecchio, "Cracking behaviour of steel fibre-reinforced concrete members containing conventional reinforcement," ACI Structural Journal, Vol. 110, NO. 3, 2013, 481p.

DD ENV 1992-1-1, "Eurocode 2: Design of Concrete Structures-Part 1: General Rules and Rules for Buildings," Brussels, Belgium, 1992.

Frosch, Robert J., "Another look at cracking and crack control in reinforced concrete," Structural Journal, Vol. 96, NO. 3, 1999, pp. 437-442.

Gao, Jianming, Wei Sun, and Keiji Morino., "Mechanical properties of steel fibre-reinforced, high-strength, lightweight concrete," Cement and Concrete Composites, Vol. 19, NO. 4, 1997, pp. 307-313.

Hamrat, M., et al., "Flexural cracking behaviour of normal strength, high strength and high strength fibre concrete beams, using Digital Image Correlation technique," Construction and Building Materials, Vol. 106, 2016, pp. 678-692.

Imam, Mahmoud, Lucie Vandewalle, and Fernand Mortelmans., "Shear–moment analysis of reinforced high strength concrete beams containing steel fibre," Canadian Journal of Civil Engineering, Vol. 22, NO. 3, 1995, pp. 462-470.

Jun Li, Jing, et al., "Investigation on mechanical properties and microstructure of high performance polypropylene fibre reinforced lightweight aggregate concrete," Construction and Building Materials, Vol. 118, 2016, pp. 27-35.

Kayali, O., M. N. Haque, and B. Zhu., "Some characteristics of high strength fibre reinforced lightweight aggregate concrete," Cement and Concrete Composites, Vol. 25, NO. 2, 2003, pp. 207-213.

Khuntia, Madhusudan, Bozidar Stojadinovic, and Subhash C. Goel., "Shear strength of normal and high-strength fibre reinforced concrete beams without stirrups," Structural Journal. Vol. 96, NO. 2, 1999, pp. 282-289.

Wang, H. T., and L. C. Wang., "Experimental study on static and dynamic mechanical properties of steel fibre reinforced lightweight aggregate concrete," Construction and Building Materials, Vol. 38, 2013, pp. 1146-1151.

Wu, Chung-Hao, et al., "Flexural behaviour and size effect of full scale reinforced lightweight concrete beam," Journal of Marine Science and Technology, Vol. 19, NO. 2, 2011, pp. 132-140.

L. Vandewalle., "Cracking behaviour of concrete beams reinforced with a combination of ordinary reinforcement and steel fibres", Materials and Structures, Vol. 33, 1999, pp 164–170.

Meda, Alberto, Fausto Minelli, and Giovanni A. Plizzari., "Flexural behaviour of RC beams in fibre reinforced concrete," Composites Part B: Engineering, Vol. 43, NO. 8, 2012, pp. 2930-2937.

Oh, Byung Hwan., "Flexural analysis of reinforced concrete beams containing steel fibres," Journal of structural engineering, Vol. 118, NO. 10, 1992, pp. 2821-2835.

Rashid, Mohammad Abdur, and Mohammad Abul Mansur., "Considerations in producing high strength concrete," Journal of civil engineering, Vol. 37, NO. 1, 2009, pp. 53-63.

Rashid, M. A., and M. A. Mansur., "Reinforced high-strength concrete beams in flexure," Structural Journal, Vol. 102, NO. 3, 2005, pp. 462-471.

Shah, Surendra P., "Do fibres increase the tensile strength of cement-based matrix?," Materials Journal, Vol. 88, NO. 6, 1992, pp. 595-602.

Sahoo, Dipti Ranjan, and Abhimanyu Sharma., "Effect of steel fibre content on behaviour of concrete beams with and without stirrups," ACI Structural Journal, Vol. 111, NO. 5, 2014, pp. 1157.

Sin, Lim Hwee, et al., “Reinforced lightweight concrete beams in flexure,” ACI Structural Journal, Vol. 108, NO. 1, 2011, 3p.

Song, P. S., and S. Hwang., “Mechanical properties of high-strength steel fibre-reinforced concrete,” Construction and Building Materials, Vol. 18, NO. 9, 2004, pp. 669-673.

Song, P. S., and S. Hwang., “Mechanical properties of high-strength steel fibre-reinforced concrete,’ Construction and Building Materials, Vol. 18, NO. 9, 2004, pp. 669-673.

Swamy, F. N., and A. Sa'ad.,”Deformation and Ultimate Strength in Flexure of Reinforced,” ACI journal, 1981.

Palmquist, Shane M., and Daniel C. Jansen., “Postpeak strain-stress relationship for concrete in compression,” Materials Journal, Vol. 98, NO. 3, 2001, pp. 213-219.

T.C. Rilem, 162-TDF. Final recommendation of RILEM TC 162-TDF., “Test and Design Methods for Steel Fibre Reinforced Concrete,” Materials and Structures, Vol. 36, 2003, pp. 560–567.

Wang, H. T., and L. C. Wang., “Experimental study on static and dynamic mechanical properties of steel fibre reinforced lightweight aggregate concrete,” Construction and Building Materials, Vol. 38, 2013, pp. 1146-1151.

Wu, Chung-Hao, et al., “Flexural behaviour and size effect of full scale reinforced lightweight concrete beam,” Journal of Marine Science and Technology, Vol. 19, NO. 2, 2011, pp. 132-140.

Appendix A

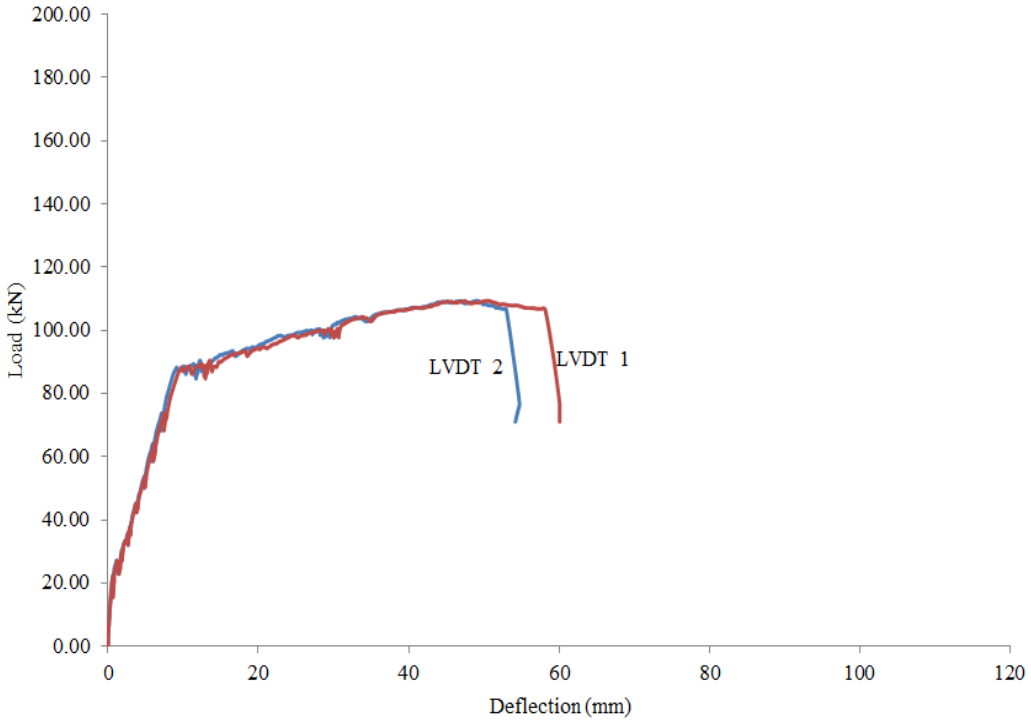

Figure A.1: Load vs. Deflection at the Two Ends of the Constant Moment Zone for Beam NB1.

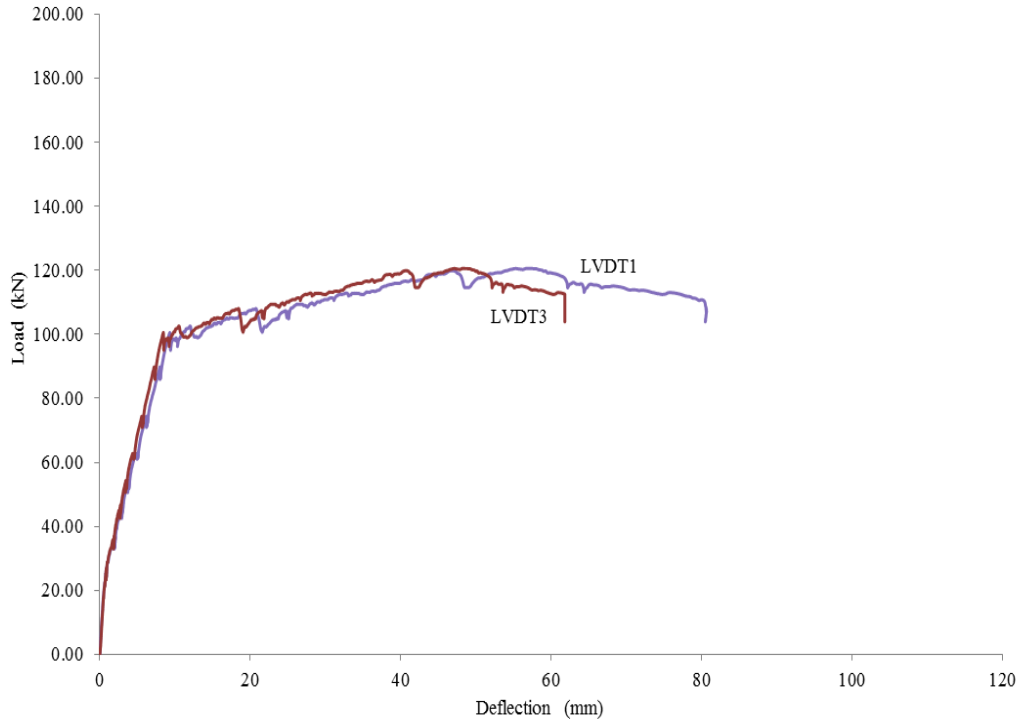

Figure A.2: Load vs. Deflection at the Two Ends of the Constant Moment Zone for Beam NB2.

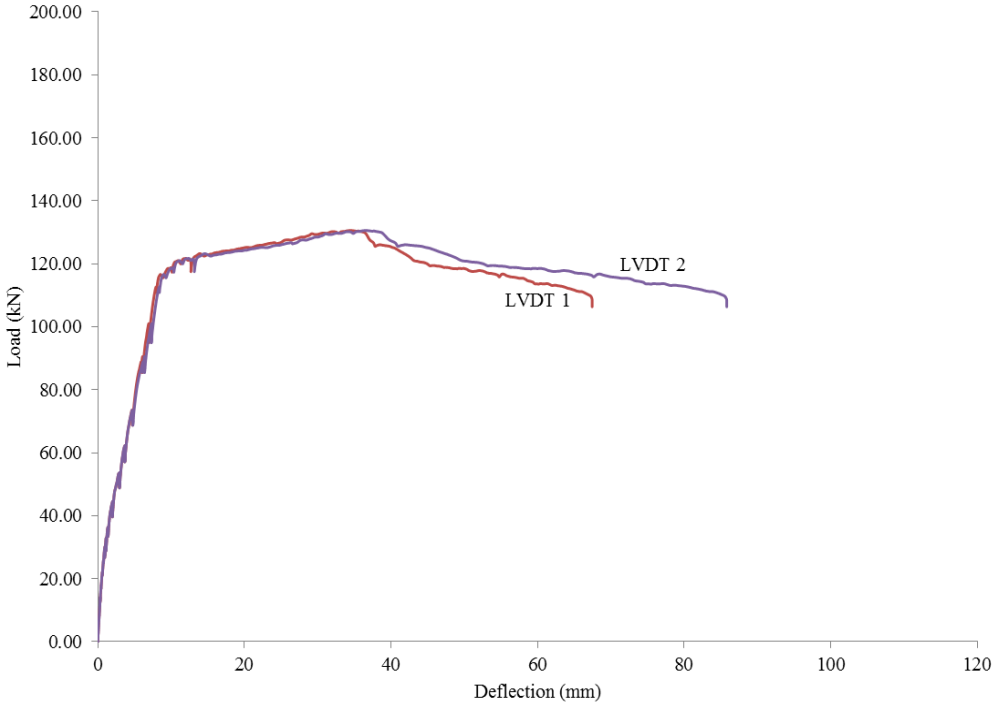

Figure A.3: Load vs. Deflection at the Two Ends of the Constant Moment Zone for Beam NB3.

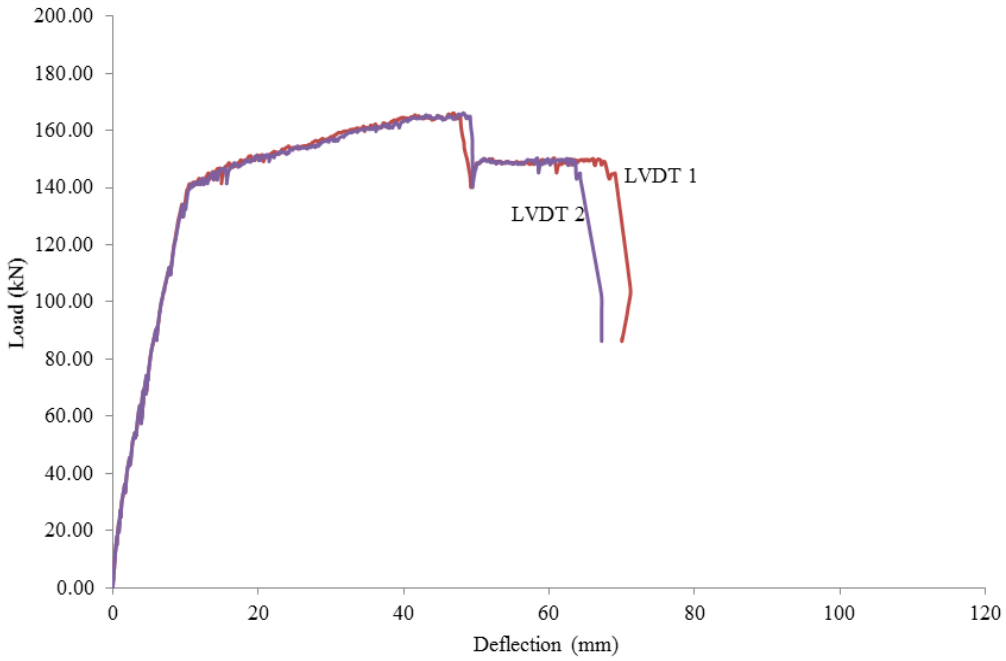

Figure A.4: Load vs. Deflection at the Two Ends of the Constant Moment Zone for Beam NB4.

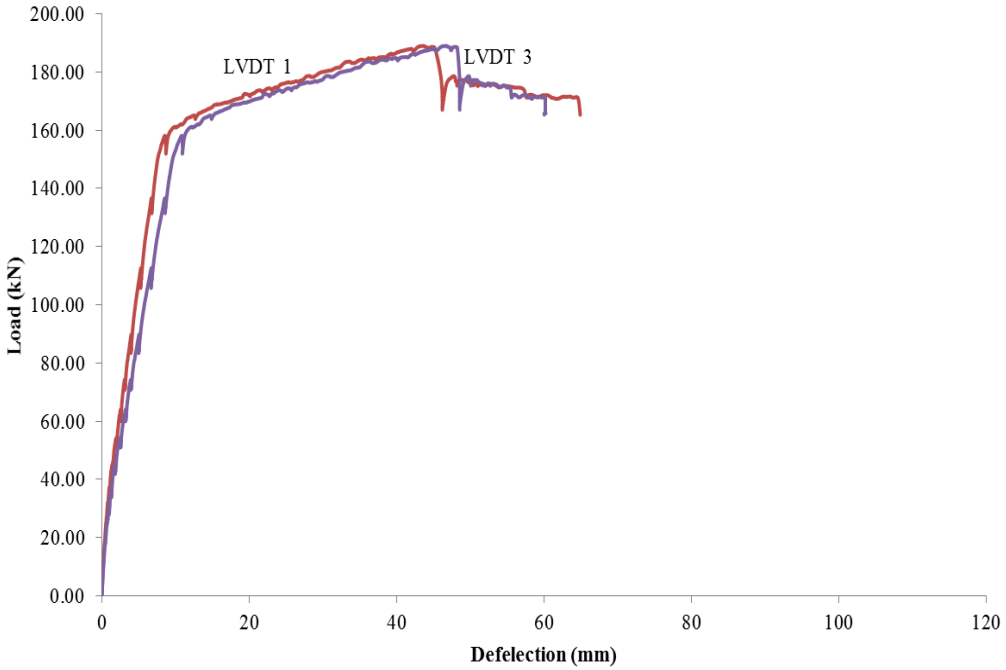

Figure A.42: Load vs. Deflection at the Two Ends of the Constant Moment Zone for Beam NB5.

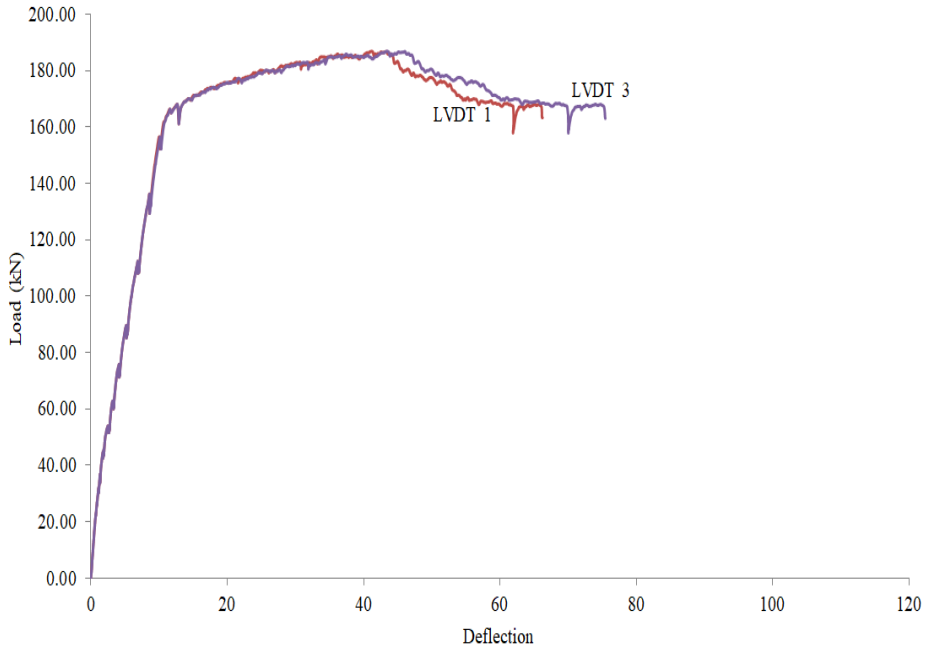

Figure A.6: Load vs. Deflection at the Two Ends of the Constant Moment Zone for Beam NB6.

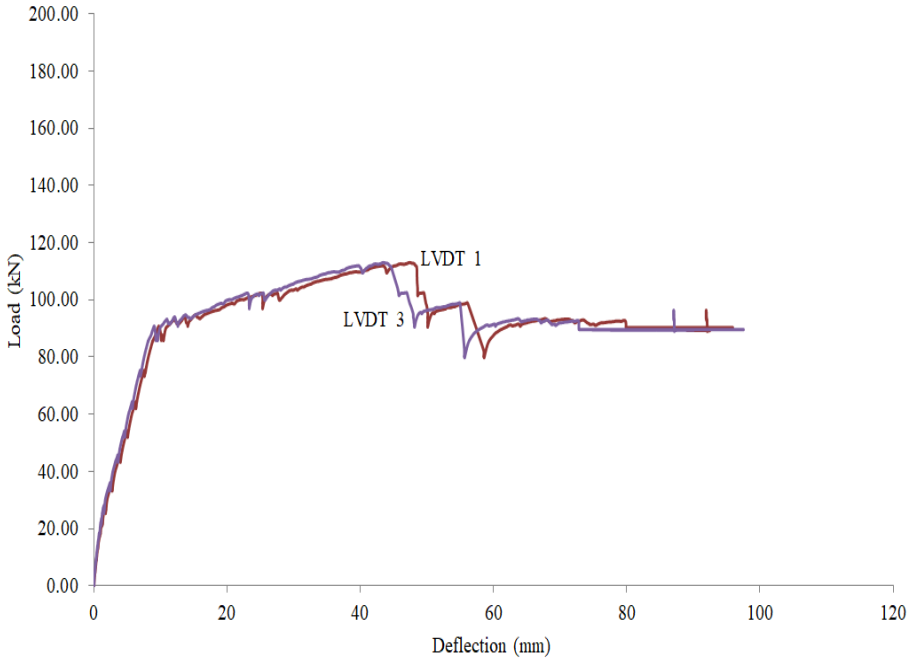

Figure A.**7**: Load vs. Deflection at the Two Ends of the Constant Moment Zone for Beam LB1.

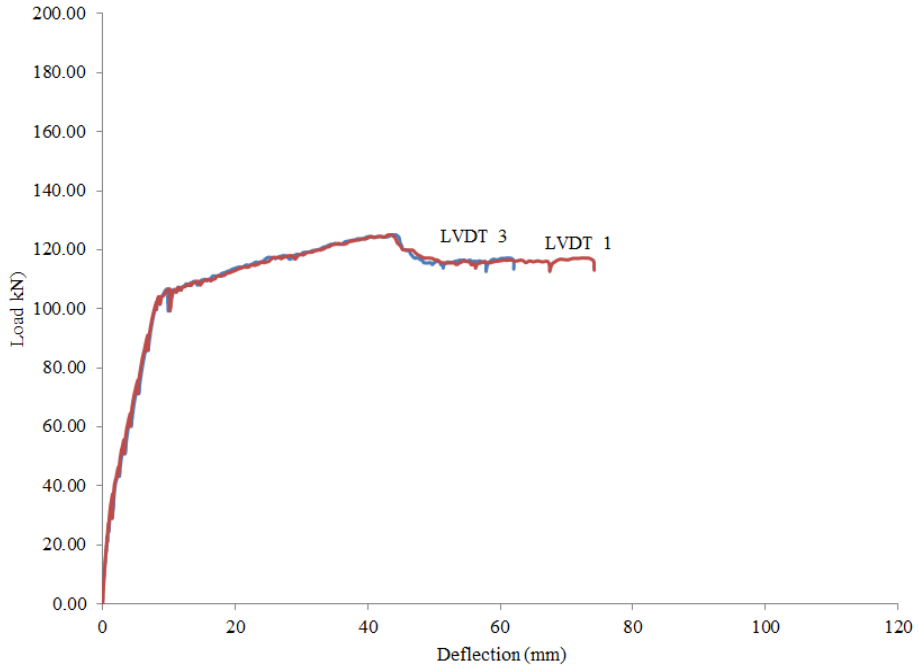

Figure A.8: Load vs. Deflection at the Two Ends of the Constant Moment Zone for Beam LB2.

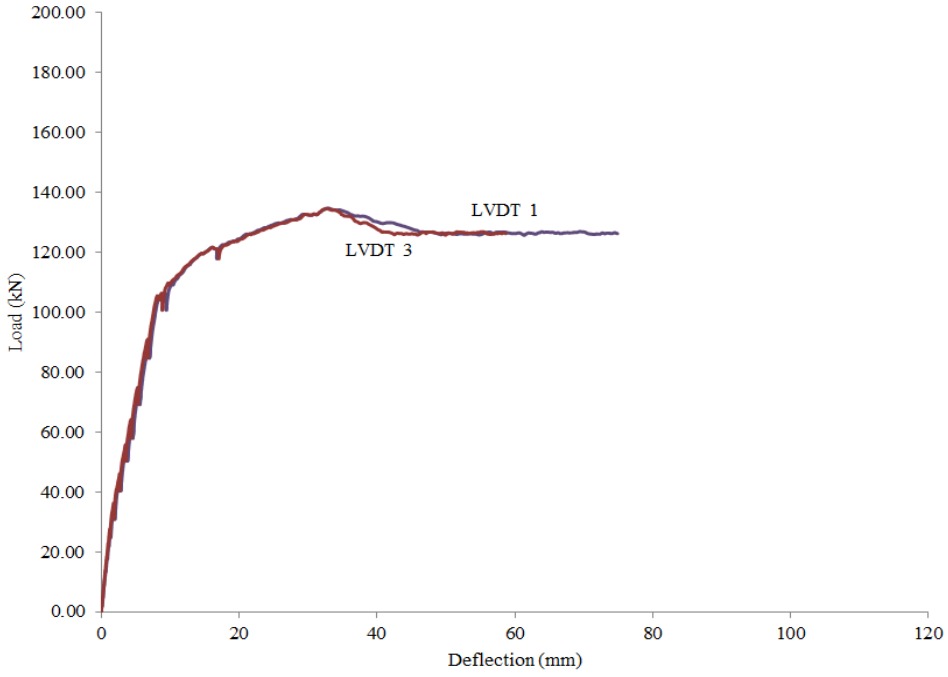

Figure A.9: Load vs. Deflection at the Two Ends of the Constant Moment Zone for Beam LB3.

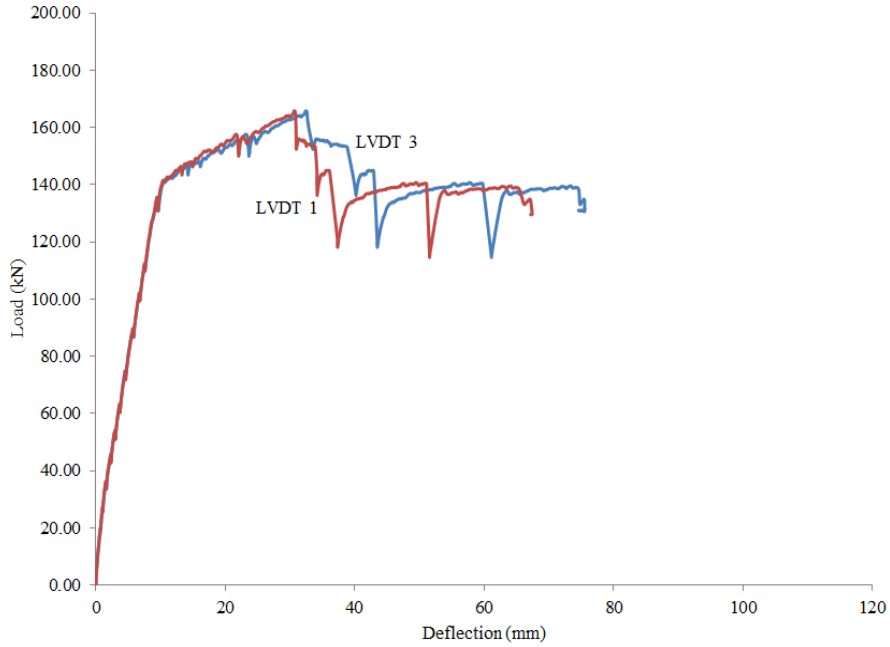

Figure A.10 : Load vs. Deflection at the Two Ends of the Constant Moment Zone for Beam LB4.

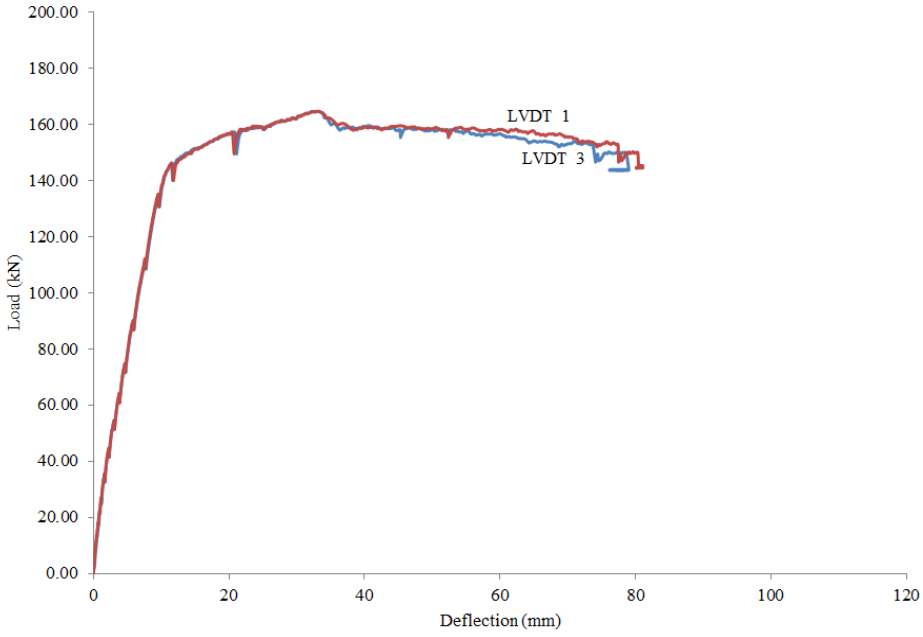

Figure A.11: Load vs. Deflection at the Two Ends of the Constant Moment Zone for Beam LB5.

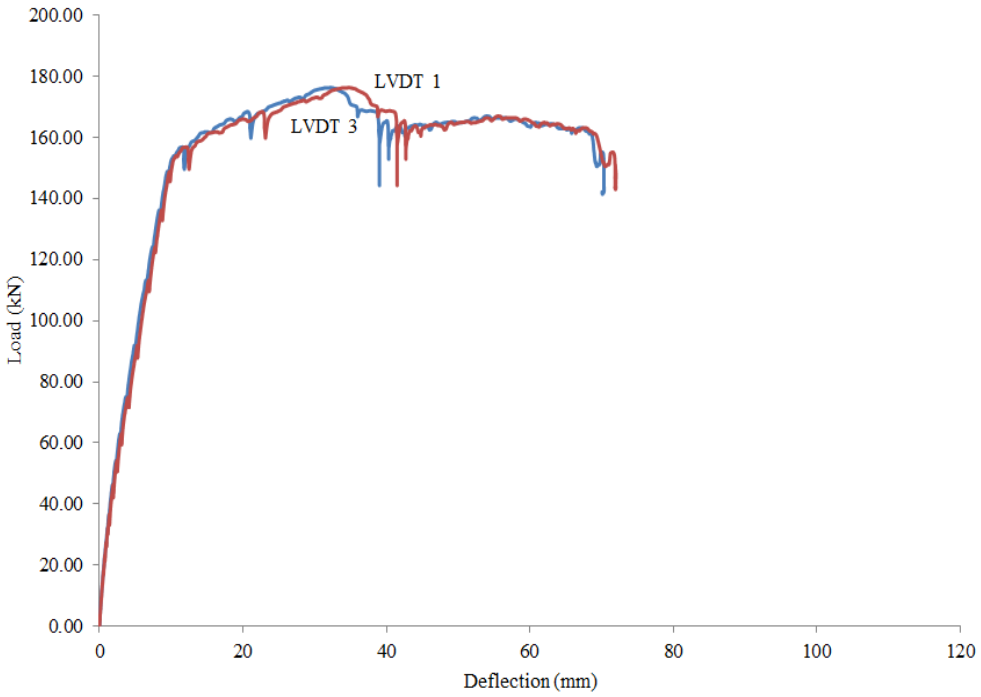

Figure A.12: Load vs. Deflection at the Two Ends of the Constant Moment Zone for Beam LB6.